Automated Classification of Human Epileptic Spikes for the Purpose of Modelling BOLD Changes Using Simultaneous Intracranial EEG-fMRI

Niraj K. Sharma

Institute of Neurology
Department of Clinical and Experimental Epilepsy
University College London

Thesis submitted for the degree of Doctor of Philosophy

To my Family

Declaration

I, Niraj K. Sharma, confirm that the work presented in this thesis is my own. Where information has been derived from other sources, I confirm that this has been indicated in the thesis.

Niraj K. Sharma

Table of Contents

Abstract

Mapping the BOLD correlates of interictal epileptiform discharges (IEDs) using EEG-fMRI can provide a unique insight into the region(s) responsible for their generation. Scalp EEG-fMRI studies have shown to provide added clinical value in the localisation of the epileptogenic zone in patients with pharmacoresistant epilepsy undergoing presurgical evaluation. However, scalp EEG has limited sensitivity in detecting IEDs as only a small percentage of the underlying electrical activity is recorded. Intracranial EEG (icEEG) provides a higher sensitivity of detecting underlying IEDs compared to scalp EEG due to the electrodes being closer to their generators. Recent safety and feasibility studies have allowed the acquisition of simultaneous icEEG-fMRI circumventing the lack of whole brain coverage of icEEG. Therefore, icEEG-fMRI has the potential to provide unprecedented insight in the relationship between the region(s) generating IEDs and the epileptogenic zone. However, one of the main challenges associated with icEEG-fMRI data is the difficulty of forming a parsimonious model of potential BOLD changes from the complex spatio-temporal dynamics of icEEG IEDs. The aim of this thesis is to provide a solution for a more consistent and less biased marking of icEEG IEDs using an automated neuronal spike classification algorithm, Wave_clus (WC), for the purpose of producing more biological meaningful IED-related BOLD maps. Adapting the icEEG IED dataset to Wave_clus was the first problem tackled which involved developing a new algorithm that identified the peak of the spiky component of an IED and defining an optimal IED classification epoch time-window. The two chapters that followed involved assessing the performance of WC as an icEEG IED classifier. First, I assessed the performance by comparing WC IED classification to the classification of multiple EEG reviewers using a novel validation scheme. This was determined by analysing whether WC-human agreement variability falls within inter-reviewer agreement variability and comparing the individual IED class labels visually and quantitatively. In this regard WC performance was found to be indistinguishable to that of EEG reviewers. Second I assessed the performance of WC by comparing the IED-related BOLD maps obtained using WC to those obtained using the visual/conventional approach. I found that WC was able to produce more biologically meaningful IED-related BOLD maps indicating that this approach can be used to further explore the region(s) responsible for generating IEDs in patients that have undergone icEEG-fMRI.

Acknowledgements

I sincerely thank my supervisors Professor Louis Lemieux, Dr Beate Diehl and Dr Carlos Pedreira for their time, dedication, guidance and support throughout my PhD.

I would like to thank everyone in the EEG-fMRI group past and present for their input and friendship at various stages of my PhD: Dr Maria Centeno, Dr Umair Chaudhary, Dr David Carmichael, Dr Teresa Murta, Dr Marco Leite, Hassan Hawsawi, Lucas Franca, Dr Don Yadee, Dr Jacopo Fantini, Dr Anna Vaudano, Dr Irene Pappalardo and Francesca Talami.

I would like to thank everyone in the MRI unit at Chalfont Centre for Epilepsy and all my colleagues at Queen Square past and present for creating a nice atmosphere in the lab: Professor John Duncan, Professor Matthias Koepp, Phillipa Bartlett, Jane Burdett, Andrea Hill, Peter Guilford, Dr Lorenzo Caciagli, Dr Marian Galovic, Dr Britta Wandschneider, Luke Allen, Dr Sam Angwafor, Dr Sjoerd Vos, Vejay Vakharia, Dr Tim Wehner, Dr Fenglai Xiao, Dr Karin Trimmel, Bianca De Blasi, Kristin Hegelli, Jane de Tisi, Dr Simona Balestrini, Mark Nowell, Michelle Rizzi, Dr Roman Rodionov and Dr Ana Bartmann.

I would also like to thank Professor Karl Friston for his help during the latter stages of my PhD.

Finally I would like to thank my family for their encouragement and support for the entire PhD.

List of Abbreviations

BOLD	Blood Oxygen Level Dependent
C	Concordant
C+	Concordant Plus
CBF	Cerebral Blood Fluid
CED	Continuous Epileptiform Discharge
$CMRO_2$	Cerebral Metabolic Rate of Oxygen
D	Discordant
DMN	Default Mode Network
EC	Entirely Concordant
ECoG	Electrocorticography
EEG	Electroencephalography/ Electroencephalogram
EPI	Echo Planar Imaging
EPSP	Excitatory Post-synaptic Potential
ERP	Event Related Potential
EZ	Epileptogenic Zone
FCD	Focal Cortical Dysplasia
FLE	Frontal Lobe Epilepsy
FN	False Negative
FP	False Positive
FPLE	Fronto-parietal Lobe Epilepsy
FMRI	Functional Magnetic Resonance Imaging
FWHM	Full Width Half Maximum
GA	Gradient Artefact
GFP	Global Field Power
GLM	General Linear Model
GM	Global Maximum
GNT	Glioneuronal Tumour
H	Human
H1	Human EEG Reviewer 1
H2	Human EEG Reviewer 2
H3	Human EEG Reviewer 3
H4	Human EEG Reviewer 4
HRF	Haemodynamic Response Function
Hz	Hertz

IcEEG	Intracranial EEG
ICN	Intrinsic Connectivity Network
IED	Interictal Epileptiform Discharge/epileptic spike
ILAE	International League Against Epilepsy
IZ	Irritative Zone
LFP	Local Field Potential
MRI	Magnetic Resonance Imaging
MUA	Multi Unit Activity
NA	Resective surgery not considered
OLE	Occipital Lobe Epilepsy
PA	Pulse Artefact
PFA	Paroxysmal Fast Activity
PLE	Parietal Lobe Epilepsy
PQE	Posterior Quadrant Epilepsy
PSP	Post-synaptic Potential
SC	Some Concordance
SD	Standard Deviation
SED	Single Epileptiform Discharge
SEEG	Stereo Electroencephalography
SOZ	Seizure Onset Zone
SPM	Statistical Parametric Mapping
SPM [F]	Statistical Parametric Mapping F Contrast
TOLE	Temporo-occiptial Lobe Epilepsy
TLE	Temporal Lobe Epilepsy
TN	True Negative
TP	True Positive
VI	Variation of Information
WC	Wave Clus

List of Figures

List of Tables

List of Publications and Software Developed for this Thesis

Publications

Sharma, N.K., Pedreira, C., Chaudhary, U.J., Centeno, M., Carmichael, D.W., Yadee, T., Murta, T., Diehl, B., Lemieux, L., 2017. BOLD mapping of human epileptic spikes recorded during simultaneous intracranial EEG-fMRI: the impact of automated spike classification. *Neuroimage. In submission*

Sharma, N.K., Pedreira, C., Centeno, M., Chaudhary, U.J., Wehner, T., França, L.G., Yadee, T., Murta, T., Leite, M., Vos, S.B., Ourselin, S., Diehl, B. and Lemieux, L., 2017. A novel scheme for the validation of an automated classification method for epileptic spikes by comparison with multiple observers. *Clinical Neurophysiology*, *128*(7), pp.1246-1254.

Software

Tyclus. https://github.com/nirajsharma1/tyclus. *Last updated: 02/08/2016*[*]

[*] This code is related to the algorithm described in Chapter 4 and 5

Conference Posters and Invited Talks Related to This Thesis

Conference Posters

Automated Classification of Human Epileptic Spikes for the Purpose of Modelling Simultaneous Intracranial EEG-fMRI, Society for Neuroscience 2017, Washington DC, USA.

Automated Classification of Epileptic Spikes in icEEG Recorded During Simultaneous fMRI Acquisition, Organisation for Human Brain Mapping 2017, Vancouver, Canada.

A Novel Scheme for the Validation of an Automated Classification Method for Epileptic Spikes by Comparison with Multiple Observers and the use of Information Theory, Computational Neurology 2017, Newcastle upon Tyne, UK.

A Statistical Framework for the Validation of Automated Spike Classification Methods, British International League against Epilepsy Congress 2016, Dublin, Republic of Ireland.

Automated Classification of Epileptic Spikes in icEEG Recorded during fMRI Acquisition for Improved BOLD Modelling, 13th European Congress on Epileptology 2016, Prague, Czech Republic.†

Invited Talks

Mapping Epileptic Generators Using Intracranial EEG-fMRI, Automated Spike Classification and Quantitative EEG based Modelling, Division of Neuroradiology and Neurophysics Annual Meeting 2017, Institute of Neurology, UCL Queen Square, London, UK.

EEG-fMRI: A Brief Overview and Clinical Value, Chalfont Centre for Epilepsy Journal Club 2014, National Epilepsy Society, Buckinghamshire, UK

† Awarded best poster certificate

CHAPTER 1: INTRODUCTION

1.1 Preface

This thesis fits in the general framework of improved pre-surgical characterisation of the generators of interictal epileptiform discharges, also known as epileptic spikes, in patients with refractory focal epilepsy, using advanced imaging techniques.

Epilepsy is a neurological disorder affecting roughly 50 per 100,000 people per year in developed countries with a likely higher incidence in resource poor countries (Sander, 2003). Patients with epilepsy have seizures, which are *'transient occurrence of signs and/or symptoms due to abnormal excessive or synchronous neuronal activity in the brain'* (Fisher et al., 2005). Seizures can be defined into two categories; generalised seizures, involving a bilateral distributed network and focal seizures that can be localised to a specific region of the brain (Berg et al., 2010).

The work in this thesis is focused on patients with focal epilepsy that are refractory to anti-epileptic medication and are considered for surgery. Anti-epileptic medication is the first line of treatment for patients with focal epilepsy. Approximately 60% of patients enter remission with the first antiepileptic drug they receive and 10-15% are successfully treated after the administration of a second AED (Duncan, 2010). In the rest 30-40% of patients, seizures cannot be controlled with anti-epileptic medication (Kwan et al., 2004). Further assessment of these patients is required and surgical removal of the region generating the seizures can be a valuable intervention. Patients in which surgery is considered undergo pre-surgical evaluation to localise the *'minimum amount of cortical tissue that must be resected to produce seizure freedom'* (Lüders et al., 2006); the epileptogenic zone (EZ). The EZ is a hypothetical area and can only be reliably determined once the patient is seizure free after surgery (Lüders et al., 2006). Hence, clinicians commonly use the seizure onset zone (SOZ); *"the area of cortex that initiates clinical seizures"* (Lüders et al., 2006) and the irritative zone (IZ); *"the area of cortex capable of generating interictal epileptiform discharges (IED)"* (Lüders et al., 2006) as a guide to infer the extent of the EZ.

Electroencephalography (EEG) is considered the "gold-standard" for localising the SOZ and IZ (Rosenow et al., 2015). EEG uses electrodes to measure the aggregated electrical activity generated by the neurons in a region of the brain with a high temporal resolution. Clinical neurophysiologists use EEG to monitor epileptiform discharges during seizures (ictal) to determine the extent of the SOZ and in between seizures (interictal) to determine the potential region of the IZ. This can be carried out non-

invasively (scalp EEG) and invasively (intracranial EEG) with most centres considering the invasively defined SOZ as the gold standard for localising the EZ.

Significant interest exists in understanding the relationship between the region responsible for generating IEDs (the IZ) and the EZ. Clinical neurophysiologists are able to detect IEDs on EEG based on their temporal characteristics; they can be distinguished from background EEG and usually have a high amplitude spiky component lasting approximately 40-100ms, occasionally followed by a slow wave) (De Curtis & Avanzini, 2001). Following this, the IEDs are classified by assessing the IED waveform across multiple channels (the spatial distribution of the IED), which can highlight the potential boundary of the IZ (Gotman, 1999, James et al., 1999).

The IZ is a theoretical concept and has been shown in most patients to be more extensive than the EZ; IEDs have been seen to originate from the EZ (so called "red-spikes") and areas outside the EZ (so-called "green-spikes") (Lüders et al. 2006). Scalp EEG is the most commonly used tool to detect IEDs in clinical practice. Clinical neurophysiologists often use the spatial distribution of the IEDs to aid them in the localisation of the EZ. Indeed there is evidence to suggest that IEDs contralateral to the presumed EZ is associated with a poor outcome and IEDs focal to the presumed EZ have been associated with a good postsurgical outcome (Chung et al., 1991, Radhakrishnan et al., 1998, Bautista et al., 1998, Schulz et al., 2000, Holmes et al., 2000, Rosenow and Lüders, 2001, Vadlamudi et al., 2004). Scalp EEG can provide adequate whole brain coverage however, it has low spatial resolution. The simultaneous acquisition of scalp EEG during functional MRI (fMRI) has the potential to circumvent this limitation.

FMRI is an imaging technique that is used to map regional changes in the brain's haemodynamic activity in relation to neuronal activity using the Blood Oxygenated Level Dependent (BOLD) effect. During an fMRI scan, multiple volumes of the whole brain are acquired over time, providing high spatial resolution images of brain activity. By combining fMRI with scalp EEG, one can map the BOLD response associated with IEDs and circumvent the low spatial resolution of scalp EEG (Graan et al., 2013). A general linear model (GLM) is often used to map the BOLD changes associated with IEDs detected on the EEG. This involves identifying and noting the time the IED occurs on the EEG (events of interest) and incorporating this as a regressor of interest in the GLM. The correlation of the events of interest are statistically analysed across all voxels in the fMRI time series and presented as statistical parametric maps. A statistical parametric map will sometimes show BOLD changes correlated to the IED (Chaudhary et al., 2013,

Graan et al., 2013). As a result, simultaneous EEG-fMRI can provide a unique insight into the IZ because of its high spatio-temporal resolution.

Interictal scalp EEG-fMRI studies have demonstrated the added clinical value IED-related BOLD maps can have during presurgical evaluation (Zijlmans et al., 2007, Thornton et al., 2010, Thornton et al., 2011, An et al., 2013, Coan et al., 2016, Khoo et al., 2017). In one study IED-related BOLD maps resulted in some patients being reconsidered for surgery (Zijlmans et al., 2007). IED-related BOLD maps were also shown to provide more contributory information than scalp EEG alone in the localisation of the EZ (Pittau et al., 2012) and in other studies they have shown to be concordant with the invasively defined SOZ (Thornton et al., 2011, Khoo et al., 2017) and potentially useful in predicting postsurgical outcome (Thornton et al., 2010, An et al., 2013, Coan et al., 2016). However, the ability of scalp EEG to detect underlying IEDs is limited since up to $10cm^2$ of synchronous neuronal activity has to occur for an IED to be detected on a scalp EEG electrode (Tao et al., 2005).

In contrast to scalp EEG, intracranial EEG has greater sensitivity and spatial specificity for detecting IEDs as patients are implanted with multiple electrodes targeting deep areas of the brain or directly on the cortex (Fernández and Loddenkemper, 2013). Therefore, there is less volume of synchronous neuronal activity required for a voltage signal to be detected on the intracranial electrodes (Fernández & Loddenkemper, 2013). However, a limitation of icEEG is a lack of whole brain coverage. Recent safety and feasibility studies have allowed the acquisition of simultaneous intracranial EEG-fMRI (icEEG-fMRI) (Carmichael et al., 2010, Carmichael et al., 2012, Boucousis et al., 2012) circumventing this limitation. Therefore, icEEG-fMRI has the potential to provide unprecedented insight in the relationship between the IZ and the EZ compared to scalp EEG-fMRI. However, the high local sensitivity of icEEG can result in more abundant and varied IEDs compared to scalp EEG. Indeed the marking of IEDs by clinical neurophysiologists can be highly time consuming and has shown to be highly subjective between EEG reviewers for IEDs detected on icEEG (Dümpelmann and Elger, 1999, Barkmeier et al., 2012, Gaspard et al., 2014). Furthermore, the incorrect and inconsistent markings of IEDs has shown to result in less biologically meaningful BOLD maps due to the presence of false positive and false negative BOLD clusters (Flanagan et al., 2009).

Therefore, the aim of this thesis was to provide a solution for a more consistent and less biased marking of icEEG IEDs using an automated neuronal spike classification

algorithm, Wave_clus, for the purpose of producing more biologically meaningful IED-related BOLD maps.

1.2 Thesis outline

The remainder of this thesis is structured as follows:

CHAPTER 2: Overview of the Literature

In this chapter I discuss the localising value of IEDs, detected on scalp EEG and icEEG, to the EZ. I also summarise the limitations of scalp EEG and icEEG and how simultaneous EEG-fMRI may provide additional, or complementary localising information. I present an overview of the added clinical value mapping the BOLD correlates of scalp IEDs has and the unique insight it provides regarding the relationship between the IZ and EZ. I also review the studies that have mapped the BOLD correlates of IEDs on icEEG and how the subjectivity of icEEG IED marking between EEG reviewers can be a limitation for icEEG-fMRI studies. I provide a summary of how automated algorithms used to reduce this subjectivity of icEEG IED marking and current limitations of these algorithms. Finally, I discuss how automated icEEG IED marking can be improved using an automated neuronal spike classification algorithm, Wave_clus, and how this can be implemented for the purpose of BOLD modelling.

CHAPTER 3: Summary of icEEG-fMRI data

In this chapter I summarise the icEEG-fMRI data acquired to date with emphasis on the IED marking carried out by Dr Umair Chaudhary (EEG reviewer 'H1'), which will be used for the remainder of this thesis).

CHATPER 4: Data preparation for application of Wave_clus to icEEG IED classification

A number of pre-processing steps are necessary to adapt an IED dataset to produce an input to the Wave_clus algorithm. These include: 1- Consistent and precise time marking for each event, in contrast with the approximate marking obtained from the human observer; and 2- Determination of the informative IED classification epoch to feed to the WC classification algorithm. In this Chapter, I present the results of the pilot study that optimised these pre-processing steps.

CHAPTER 5: Validating Wave_clus by comparison with multiple EEG reviewers

In this chapter I provide a validation framework for the application of Wave_clus to our icEEG dataset by comparing the automated classification to that of multiple EEG

reviewers on a sample of icEEG IEDs using a novel validation scheme. First, I determined whether Wave_clus-human agreement variability falls within inter-reviewer agreement variability by calculating the variation of information for each classifier pair and quantifying the overlap between all Wave_clus-reviewer and all reviewer-reviewer pairs. Second, I compared Wave_clus and EEG reviewers' IED identification and individual IED class labels visually and quantitatively.

CHAPTER 6: BOLD mapping of icEEG IEDs recorded during simultaneous fMRI acquisition using Wave_clus

In this chapter I applied Wave_clus, to all the IEDs marked visually on icEEG that was acquired during simultaneous fMRI acquisition in eight patients that had a good postsurgical outcome. The motivation of this work was to determine whether using Wave_clus can produce more biologically meaningful BOLD patterns with the epileptogenic zone (EZ) compared to the BOLD patterns obtained based on the conventional, visual classification carried out by EEG reviewer H1.

CHAPTER 7: Conclusion and future work

In this chapter I provide a summary of our findings from the previous chapters and suggest possible future directions.

CHAPTER 2: OVERVIEW OF THE LITERATURE

This chapter is divided into four sections. In the first section (2.1) I describe the neural basis of the EEG signal and how it can be used to record electrical activity of the brain non-invasively (scalp EEG) and invasively (icEEG). Section (2.2) summarises the morphological characteristics of IEDs and their localising value to the EZ. In the third section (2.3) I review the unique insight the BOLD mapping of IEDs has in the characterisation of the IZ in patients that have undergone scalp EEG-fMRI and icEEG-fMRI. In the fourth section (2.4), I review the automated algorithms used to reduce the subjectivity of icEEG IED marking and how they can be further improved for the purpose of BOLD modelling.

2.1 Recording electrical activity from the brain using EEG

The electroencephalogram (EEG) was initially developed by Hans Berger in the late 1920s and is the most commonly used tool for detecting IEDs[3] (Noachtar and Remi, 2009). Within the EEG setup, the electrodes measure the aggregated electrical activity generated by neurons in a region of the brain at a high temporal resolution. In this section, I describe the neural basis of the EEG signal (Section 2.1.1) and how EEG electrodes capture electrical activity of the brain non-invasively (Section 2.1.2.1) and invasively (Section 2.1.2.2).

2.1.1 Neural basis of EEG signal

EEG electrodes are sensitive to the electrical voltage fluctuations that arise as a result of the activity from multiple pyramidal neurons that align perpendicular with the cortex or from pyramidal neurons found in deep brain structures such as the hippocampus (icEEG – see Section 2.1.2.2). The apical dendrite of pyramidal neurons can form multiple synapses with presynaptic neurons (Figure 2-1 shows a synapse between one presynaptic axon and an apical dendrite). The presynaptic axon can release a chemical neurotransmitter that can lead to a postsynaptic potential; these can be inhibitory neurotransmitters (resulting in an inhibitory PSP) or excitatory neurotransmitters (resulting in an excitatory PSP). For example, when a neuronal stimulus occurs, an excitatory neurotransmitter causes the influx of positively charged sodium ions (Na^+) into the postsynaptic apical dendrite resulting in an excitatory postsynaptic action potential (EPSP). This causes the local extracellular environment near the apical dendrite to take on a negative charge (sink) (see Figure 2-1). The EPSP initiates the movement of the positively charged ions to the cell body of the pyramidal cell where they are released. This causes the local extracellular environment near the cell body to take on a positive charge (source) (see Figure 2-1), effectively creating a dipole. It is the summation of the multiple dipoles that thus arise transiently that forms the neural basis of the EEG signal (Niedermeyer and da Silva, 2005); the EEG electrodes detect this change in extracellular electrical potential and the signal is filtered, amplified and digitised on to a computer screen as a voltage potential.

[3] Magnetoencephalography (MEG) can also be used to detect IEDs

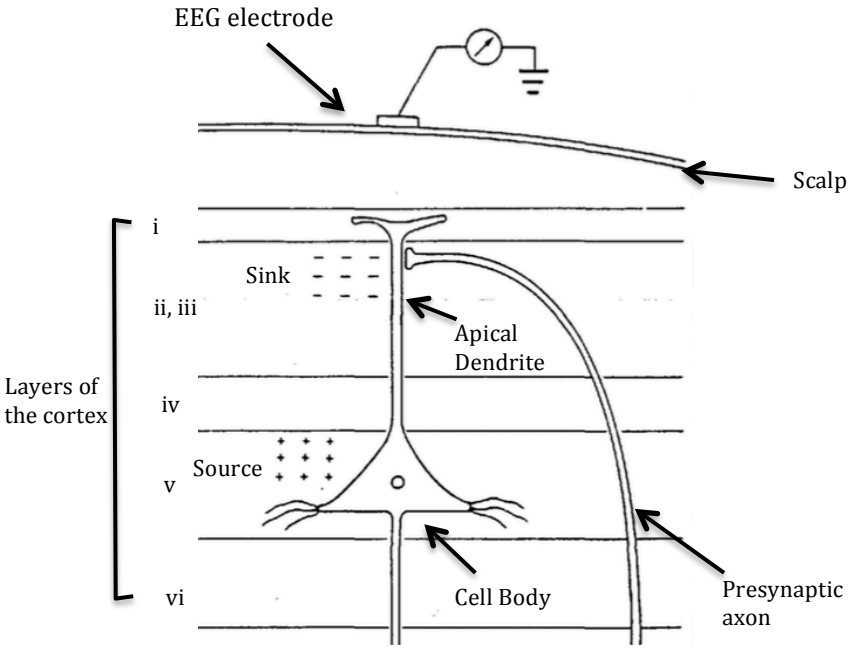

Figure 2- 1| Neural basis of EEG signal. The presynaptic axon releases an excitatory neurotransmitter, which causes an influx of positively charged ions in the postsynaptic apical dendrite causing an EPSP resulting in an extracellular sink. The EPSP initiates movement of the positively charged ions to the cell body of the apical dendrite where they are released resulting in an extracellular source effectively creating a dipole. Image adapted from Olejniczak (2006)

2.1.2 Scalp EEG and Intracranial EEG

As mentioned previously, the electrical activity of the brain can be monitored by placing EEG electrodes non-invasively on the scalp (Section 2.1.2.1) or invasively implanted in the brain (Section 2.1.2.2) as part of an EEG system. In the next two sections I introduce both techniques and outline their differences and similarities.

2.1.2.1 Scalp EEG

Scalp EEG is the most commonly used technique to record electrical activity of the brain during presurgical evaluation in patients with epilepsy (Rosenow et al., 2015). A typical layout of scalp EEG is the international 10-20 system (see Figure 2-2), which can provide a general overview of the entire brain. The electrical activity recorded using scalp EEG is from pyramidal neurons that align perpendicular to the cortex (see Figure 2-1). However, scalp EEG has low spatial resolution. Furthermore, due to the layers of the scalp and skull (see Figure 2-3), which introduce attenuation and distortion of the electrical signal, only a small percentage of the underlying electrical activity is recorded. Indeed a study carried out by Tao et al. (2005) showed that for IEDs to be detected on scalp EEG, up to 10cm^2 of synchronous neuronal activity is required (Tao et al., 2005).

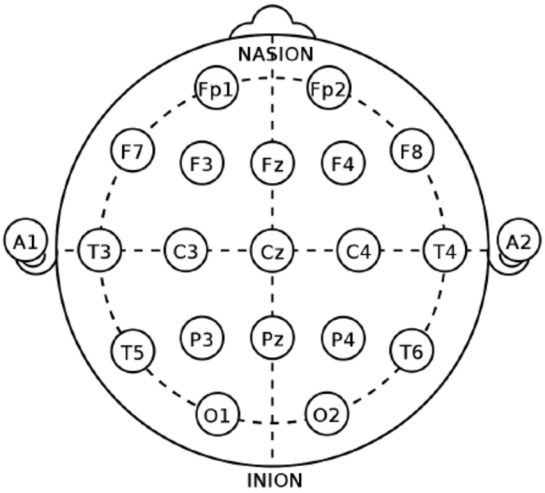

Figure 2- 2| The standard 10-20 scalp EEG electrode placement system

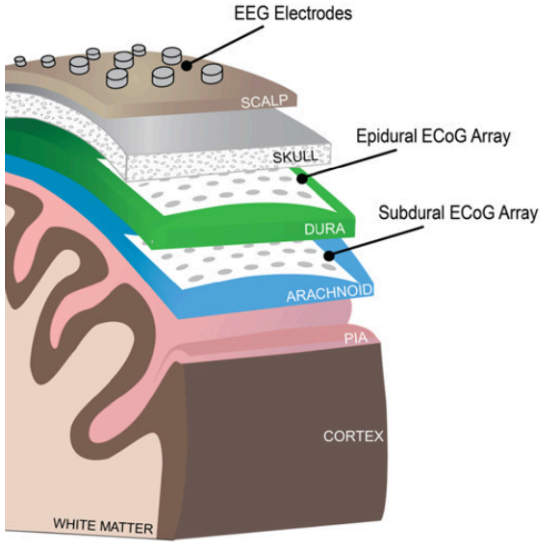

Figure 2- 3| The placement of scalp EEG and icEEG electrodes and the layer of tissues between the cortex and the scalp. Image taken from Jorfi et al. (2015)

2.1.2.2 Intracranial EEG

In patients with epilepsy, where there is strong evidence of an epileptogenic focus but not enough information to define a resectable area, multiple intracranial EEG electrodes can be inserted to perform an icEEG study[4] (Fernández & Loddenkemper, 2013). The aim of these studies is to sample all regions that could potentially form part of the EZ and to sample the sensory, motor and language areas (these are critical areas commonly

[4] IcEEG study can also be referred to as ECoG

known as the eloquent cortex and are localised so as to avoid resecting them during surgery) (Spencer et al., 2015). There are two main techniques used for invasive recordings (Spencer et al., 2015):

1) Subdural grid (and/or strip) electrodes, depth electrodes or a combination of both (see Figure 2-4)
2) Stereoelectroencephalography (SEEG) (see Figure 2-4)

Subdural grids and strips are inserted on to a layer of the cortex (see Figure 2-3 and Figure 2-4) and require open craniotomy. A grid implantation may be used if the presumed EZ potentially overlaps with the eloquent cortex (Spencer et al., 2015). Depth electrodes may be inserted to record from deep brain structures such as the hippocampus, amygdala, orbitofrontal cortex and insula (see Figure 2-4) (Spencer et al., 2015). Due to the direct sampling from the cortex and deep brain structures, icEEG has higher sensitivity and greater spatial specificity compared to scalp EEG, as there is less volume of synchronous neuronal activity required for a voltage signal to be detected on the intracranial electrodes (Fernández & Loddenkemper, 2013). However, one of the main drawbacks of an icEEG study is the lack of whole brain coverage, which can result in a lack of information from other regions of the brain that may be involved in the generation of IEDs (Carreño and Lüders, 2001).

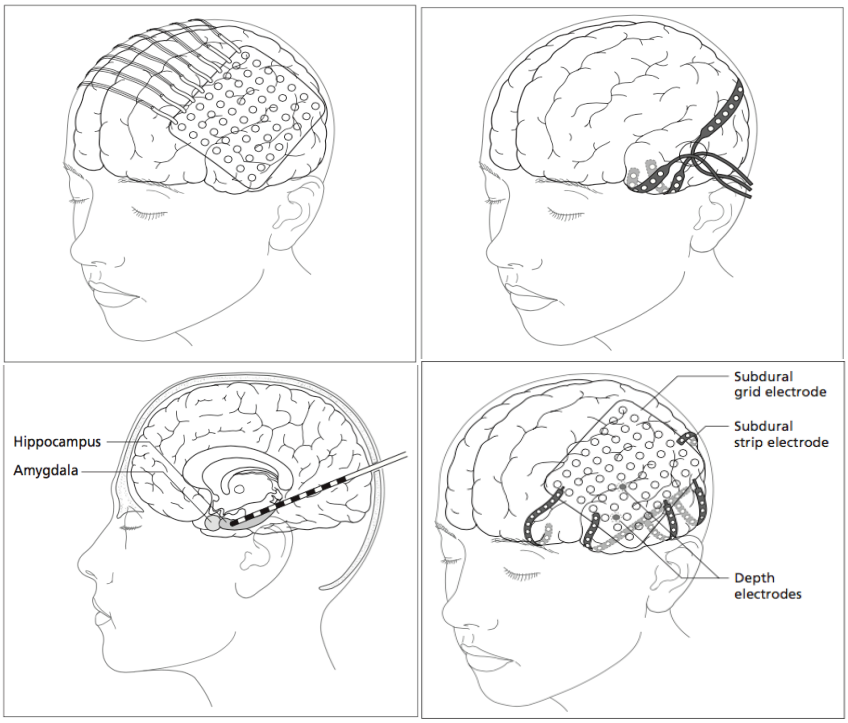

Figure 2- 4| IcEEG implantation. Top left: Subdural grid implantation, Top right: Subdural strip implantation, Bottom left: Depth electrode implantation, Bottom right: Combination of subdural grid, strip and depth implantation. Adapted from Spencer et al. (2009)

2.2 Interictal Epileptiform Discharges

As mentioned in Chapter 1, the region responsible for generating IEDs is known as the IZ (Lüders et al., 2006). The IZ is a theoretical concept and therefore, IEDs detected on scalp EEG and icEEG only provide an approximation of the region that could be responsible for the generation of IEDs. In this section I summarise the morphological characteristics of IEDs (Section 2.2.1) observed on EEG and the localising value of IEDs detected on scalp EEG (Section 2.2.2) and icEEG (Section 2.2.3) to the EZ.

2.2.1 IED morphology, detection and classification

There is no gold-standard as to what constitutes an IED however, a common morphological characteristic is a high amplitude spiky component (lasting approximately 40-100ms for spikes or 50-200ms for sharp waves), that can be distinguished from the background EEG, occasionally followed by a slow wave (De Curtis & Avanzini, 2001) (these can also be referred to as individual IEDs) (see Figure 2-5). Repetitive IEDs, commonly referred to as polyspikes, can also be observed on EEG. In clinical practice, clinical neurophysiologists are able to detect IEDs based on characteristics of the waveform (i.e. the high amplitude spiky component etc.). They then classify the IEDs by assessing the IED field distribution (also known as the spatial distribution of the IED), which can highlight the potential boundary of the region responsible for generating them (the IZ) (Gotman, 1999, James et al., 1999). In the next section I discuss studies that investigate the contribution the detection and classification of IEDs have in localising the EZ for IEDs that have been detected on scalp EEG and icEEG.

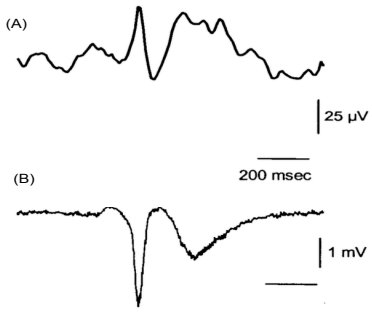

Figure 2- 5| Interictal epileptiform discharge. (A) Spike (B) Sharp wave. Figure taken from De Curtis and Avanzini, 2001

2.2.2 IEDs detected on Scalp EEG

In patients with TLE, scalp IEDs are commonly detected in electrodes overlapping both temporal lobes (bilateral IED focus) or from one temporal lobe (unilateral IED focus) (Rosati et al., 2003, Janszky et al., 2005). Extra-TLE patients consist of patients that have

frontal lobe epilepsy (FLE) and posterior quadrant epilepsy (PQE) (parietal lobe epilepsy (PLE)/occipital lobe epilepsy (OLE)) (Fahoum et al., 2012). In contrast to TLE, IEDs detected in patients with extra-TLE are less localisable. For example, in patients with FLE, IEDs can be observed in multiple lobes, bilateral and can also be generalised (Laskowitz et al., 1995). The majority of patients with PQE have shown to have IEDs distant to the posterior quadrant (Boesebeck et al., 2002). In the next section I will provide a summary of studies that have investigated the localising value of scalp EEG IEDs to the EZ in patients with TLE and extra-TLE.

2.2.2.1 Localising value

2.2.2.1.3 TLE

The correlation between IED distribution and postsurgical outcome has been assessed by many studies in patients with TLE (Chung et al., 1991, Radhakrishnan et al., 1998, Schulz et al., 2000, Sirven et al., 1997, Hardy et al., 2003, Krendl et al., 2008). Some studies have shown that a unitemporal IED focus can be a good indicator of the EZ (Chung et al., 1991, Radhakrishnan et al., 1998, Schulz et al., 2000). These studies demonstrate that if >90% of the IEDs can be lateralised to a unitemporal region then the patient is likely to have a good postsurgical outcome (Chung et al., 1991, Radhakrishnan et al., 1998, Schulz et al., 2000). However, other studies did not find a significant correlation between spike distribution and postsurgical outcome (Sirven et al., 1997, Hardy et al., 2003, Krendl et al., 2008). Indeed, Krendl et al. (2008) discovered that IED frequency and not IED distribution was associated with postsurgical outcome; patients with a high frequency of IEDs were likely to have postsurgical seizures.

2.2.2.1.4 Extra-TLE

The number of studies investigating the localising value of IEDs detected in patients with extra-temporal lobe epilepsy is fewer due to the heterogeneity of the group.

In patients with FLE, IEDs have shown to have more of a localising value if the EZ is located in the dorsolateral frontal lobe compared to the medial frontal lobe (Bautista et al., 1998, Vadlamudi et al., 2004). Bautista et al. (1998) demonstrated that in patients with a presumed EZ in the dorsolateral frontal lobe, the IEDs were concordant to that region whereas in patients with a presumed EZ in the medial frontal lobe, no IEDs were detected or the IEDs were multifocal (Bautista et al., 1998). Vadlamudi et al. (2004) investigated patients that had frontal lobe resections and good postsurgical outcome. They discovered that in patients where the EZ was in the dorsolateral frontal region, 72% of the IEDs detected were also found to be concordant to the same region. In contrast, only 33% of patients with medial FLE had concordant IEDs (Vadlamudi et al.,

2004). Since resective surgery in the posterior quadrant is relatively rare the number of studies investigating the localising value of IEDs to the EZ is low for this group of patients. In a study by Boesebeck et al. (2002), they investigated 42 patients that underwent resective surgery in the posterior quadrant. They discovered that 90% of patients had IEDs found in the temporal region (53%) as well as the frontal region (34%). However, they found no significant relationship between location of IEDs and postsurgical outcome (Boesebeck et al., 2002). Another study investigated the scalp EEG of a heterogeneous group of patients that underwent extratemporal lobe resections (Holmes et al., 2000). They discovered that on scalp EEG, only 21% of the patients showed focal spike discharges. However, of these patients, 77% were seizure free and had a unilateral seizure onset indicating that focal IEDs can be a good indicator of good postsurgical outcome (Holmes et al., 2000).

The studies described in this section indicate the potential localising value of IEDs detected on scalp EEG to the EZ in patients with TLE and extra-TLE. In patients with TLE, unitemporal IEDs have been shown to potentially be a good indicator of the EZ (Chung et al., 1991, Radhakrishnan et al., 1998, Schulz et al., 2000) and focal IEDs in extra-TLE patients have shown to be a potential indicator of the EZ (Bautista et al., 1998, Holmes et al., 2000, Vadlamudi et al., 2004). However, as mentioned in Section 2.2.2, scalp EEG has a low spatial resolution and records only a small percentage of underlying electrical activity. Indeed, Tao et al. (2005) carried out a study in patients that underwent simultaneous scalp and icEEG and discovered that icEEG IEDs with an area of 10cm^2 were necessary for scalp IEDs to be detected (Tao et al., 2005). Due to the greater sensitivity and spatial specificity of icEEG compared to scalp EEG, IEDs detected on icEEG may be able to provide a more reliable representation of the IZ since the intracranial electrodes are closer to the generators of IEDs. In the next section, I will summarise the studies that have explored the localising value of IEDs detected on icEEG to the EZ.

2.2.3 IEDs detected on icEEG

Due to the direct sampling from the cortex and deep brain structures, the IEDs observed on icEEG can be more abundant and differ in morphology (such as size of amplitude and duration of the discharge) as well as having a more widespread spatial distribution compared to scalp EEG (Spencer et al., 2015). For example, patients with mesial TLE have shown to have bitemporal IEDs even when seizures were identified to originate prominently from one temporal lobe (So et al., 1989, Hirsch et al., 1991). So et al. (1989) demonstrated bitemporal IEDs were present in 77% of TLE patients that had seizures originating from a one temporal lobe. Similarly Hirsch et al. (1991) also discovered that 56% of TLE patients that had seizures arising from one temporal lobe had bitemporal

IEDs (Hirsch et al., 1991). Lesions such as focal cortical dysplasia (FCD) and glioneuronal tumours (GNT) are commonly associated with refractory extrahippocampal focal epilepsies. In these patients, a variety of discharges, some of which are focal and others widespread, can be observed during interictal examination of the EEG. These can be broadly classified into single isolated epileptiform discharges (SED) (spikes/ sharp waves and polyspikes) (Turkdogan et al., 2005), continuous epileptiform discharges (CED) (continuous rhythmic spikes and/or polyspikes – 1-10Hz) and paroxysmal fast activity (>10Hz) (Palmini et al., 1995, Ferrier et al., 2001, Turkdogan et al., 2005, Widdess-Walsh et al., 2007). Due to icEEG IEDs being highly abundant and having a more widespread distribution, some studies have used previously validated automated algorithms[5] to determine whether a quantitative approach can be useful in understanding the relationship between IEDs and the EZ (Hufnagel et al., 2000, Asano et al., 2003, Marsh et al., 2010, Barkmeier et al., 2012, Gaspard et al., 2014).

2.2.3.1 Localising value

The studies carried out using these automated algorithms were performed on data from a heterogeneous cohort of TLE and extralTLE patients. They have focused on the frequency (Hufnagel et al., 2000, Asano et al., 2003, Marsh et al., 2010), latency (Hufnagel et al., 2000, Asano et al., 2003) as well as other features, such as the amplitude (Hufnagel et al., 2000, Asano et al., 2003) or prominence (Gaspard et al., 2014) of the IEDs, to determine whether these features can be informative of the invasively defined SOZ (considered the gold standard in localising the EZ in most centres).

Asano et al. (2003) showed that channels with the highest frequency of IEDs overlapped with the SOZ in all of the patients studied. However, Hufnagel et al. (2000) and Marsh et al. (2010) discovered that channels showing the highest frequency of IEDs only overlapped with the SOZ in just over half of the cases (53% and 57% respectively).

As well as the frequency of the IEDs, Hufnagel et al. (2000) and Asano et al. (2003) also determined whether the latency of the IEDs contributed to the localisation of the SOZ. A strong correlation was found between the channels showing the leading IED and the SOZ; the channels showing the leading IED overlapped with the SOZ in 84% and 77% of patients investigated in the studies carried out Hufnagel et al. (2000) and Asano et al. (2003) respectively. These two studies (Hufnagel et al., 2000, Asano et al., 2003) as well as Gaspard et al. (2014) also investigated the relationship between the morphological characteristics of the IED and the SOZ. Hufnagel et al. (2000) and Asano et al. (2003) measured the amplitude of the IEDs and Gaspard et al. (2014) were able to identify IEDs

[5] These algorithms will be further discussed in Section 2.4

that were the most prominent. The contacts showing the highest amplitude IED overlapped with the SOZ in 75% and 92% of the patients investigated in the studies carried out by Hufnagel et al. (2000) and Asano et al. (2003) respectively. Gaspard et al. (2014) showed that IEDs that were more prominent were found close to the seizure onset zone (approximately 2cm).

These results suggest that perhaps the morphological characteristics of the IED (such as high amplitude) can provide valuable information with regards to the invasively defined SOZ. However, due to the lack of algorithms for the automated detection of IEDs recorded on icEEG, the number of studies is relatively low. It is also important to note that IEDs observed on icEEG are more abundant and widespread and can also occur outside the EZ, (similar to IEDs detected on scalp EEG). Therefore, since icEEG studies have limited sampling of the whole brain (Section 2.1.2.2) there may be regions of the brain that are involved in the generation of IEDs that are not sampled.

In summary, the studies described in this section show that the IZ as characterised by the detection of IEDs on scalp and icEEG can potentially localise the EZ. However, as mentioned previously one of the main limitations of scalp EEG is the low spatial resolution and limited recording of electrical activity from deep brain structures whereas the main limitation of icEEG is the lack of whole brain coverage. The simultaneous acquisition of fMRI during scalp EEG and icEEG recordings has provided the potential means to circumvent these limitations. In the next section I will review how the IZ can be further characterised using simultaneous EEG-fMRI and how it could contribute to the localisation of the EZ.

2.3 BOLD Correlates of Interictal Epileptiform Discharges

Simultaneous EEG-fMRI is a multimodal imaging technique that combines EEG with fMRI acquisition. Its development was initially driven by epileptologists to further characterise the generators of IEDs detected on scalp EEG (Laufs, 2012a). Conventionally, fMRI acquisition allows the mapping of haemodynamic changes linked to a neuronal stimulus, by exploiting the blood oxygenated level dependent (BOLD) effect. As mentioned in Section 2.1, scalp EEG has a high temporal resolution but low spatial resolution. FMRI has relatively good spatial resolution but low temporal resolution (further explained in Section 2.3.1) therefore, the combination of scalp EEG with fMRI results in an imaging technique with a high spatio-temporal resolution. Recent safety and feasibility studies (Carmichael et al., 2012, Boucousis et al., 2012) have also allowed the acquisition of simultaneous icEEG-fMRI providing a unique opportunity to characterise the generators of IEDs at a fundamental level. In this section, I describe the nature of the BOLD signal (Section 2.3.1) and how the BOLD correlates of IEDs detected during simultaneous EEG recordings can be mapped using the general

linear model (GLM) framework (Section 2.3.2). I also summarise the contribution the BOLD mapping of scalp IEDs can have in the localisation of the EZ as well as the current limitations of this technique (Section 2.3.3). Finally, I will review the studies that have mapped the IED-related BOLD in patients that have undergone icEEG-fMRI (Section 2.3.4).

2.3.1 Functional MRI

Functional Magnetic Resonance Imaging (fMRI) is a non-invasive imaging technique that involves acquiring multiple volumes of the whole brain across a time series. It can provide high spatial resolution whole-brain maps of changes in blood oxygenation levels during a neuronal stimulus as measured by the BOLD signal. In this section I will describe the nature of the BOLD signal and its basic characteristics.

2.3.1.1 Nature of the BOLD signal

The mechanism of the BOLD effect is based on the haemodynamic response to a neuronal stimulus. In regions of the brain where there is a large amount of neuronal activation, the cerebral blood flow (CBF) exceeds the cerebral metabolic rate of oxygen ($CMRO_2$) (Fox and Raichle, 1986) resulting in an increase in oxy-Hb and a decrease in deoxy-Hb. Ogawa et al. (1990) demonstrated that an MR signal, recorded during a functional MRI scan, can measure the levels of oxy-Hb and deoxy-Hb in the blood due to their different magnetic properties; oxy-Hb is diamagnetic and deoxy-Hb is paramagnetic (Ogawa et al., 1990). They showed that during rest there is more deoxy-Hb in the blood and that the paramagnetic properties of the deoxy-Hb result in a decrease in the intensity of the MR signal. However, when the levels of the oxy-Hb increase, the diamagnetic properties of oxy-Hb increase the intensity of the MR signal (Ogawa et al., 1990). It is this coupling of neuronal activation and the haemodynamic response that is captured in the most commonly cited models of the biophysical basis of the BOLD signal (Buxton, 2012). The type of neuronal activation that best correlates with the BOLD signal was investigated by Logothetis et al. (2001). They determined whether the local field potential (LFP) and/or multi unit activity (MUA) correlated with the BOLD signal in the visual cortex of monkeys. The LFP captures was a measurement of the extracellular current around hundreds of neurons, reflecting synaptic activity (i.e. a postsynaptic potential (PSP); this is also what is measured by the EEG electrodes – see Section 2.1.1), whereas MUA reflects action potentials (caused by the depolarisation of the membrane when an excitatory chemical neurotransmitter binds to the postsynaptic axon) of small number of neurons (Logothetis et al., 2001). The authors showed that neural activation measured by the LFP and MUA significantly correlated with the amplitude of the BOLD signal with the LFP showing the strongest correlation

(Logothetis et al., 2001). Therefore, these findings suggest that the BOLD signal shows a strong association between the haemodynamic changes and neuronal stimulus.

2.3.1.2 Haemodynamic response function

The BOLD response to a brief neuronal stimulus has been described as a mathematical function called the haemodynamic response function (HRF). Studies have shown that after a short and sharp neuronal stimulus (i.e. a stimulus which increases neuronal activity in a region of the brain), the BOLD signal starts to increase and reaches its peak 5-7 seconds post stimulus (see Figure 2-5). Once the neuronal activity stops, the BOLD signal starts to decrease and reaches baseline approximately 10 seconds post stimulus. There is then a small undershoot which then returns to baseline 30 seconds post stimulus (see Figure 2-6) (Glover, 1999, Friston et al., 1998, Logothetis et al., 1999, Buxton, 2012). The mathematical representation of this time course is known as the canonical HRF and is the most commonly used in fMRI studies (Friston et al., 1998). The haemodynamic response to a neuronal stimulus can also be characterised by Glover HRF or a Gamma HRF (see Figure 2-6) (Lu et al., 2006).. These two HRF models also have a similar shape to the canonical HRF; they have a similar shape up to the peak of the BOLD response (see Figure 2-6).

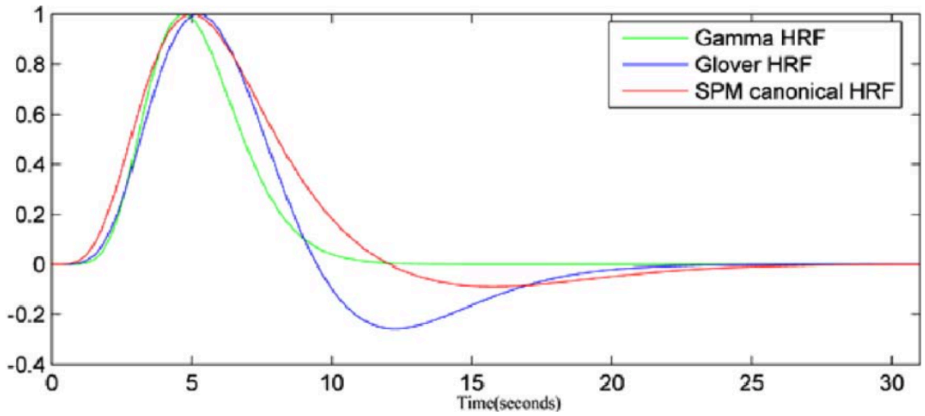

Figure 2- 6| HRF: Gamma, Glover and canonical. Image taken from Lu et al. (2006)

Although fMRI provides a high spatial resolution, the haemodynamic delay to a neuronal stimulus as characterised by these three HRF models (see Figure 2-6) highlight the low temporal resolution. During an EEG recording, underlying neuronal activity is detected across a time series with a high temporal resolution. Therefore, the simultaneous acquisition of EEG during fMRI scanning can provide a unique dataset that has the potential to combine the two time series and provide a high spatio-temporal resolution of underlying neuronal activity. Indeed, in patients with epilepsy, simultaneous EEG-fMRI has been used to map the BOLD correlates with IEDs detected on scalp and icEEG

to further characterise the IZ. In the next section, I provide a summary of how the BOLD correlates of IEDs can be mapped using a general linear model.

2.3.2 Mapping the BOLD correlates of IEDs: methodology

A general linear model (GLM) is a mathematical linear model commonly used to map the BOLD changes associated with IEDs detected on EEG. It is a predictive model and is derived from the interpretation of the EEG; it is the time of the IEDs (detected by an EEG reviewer(s)) that is used to predict the BOLD changes across each scanned voxel from the functional MR images (see Figure 2-7) (Chaudhary et al., 2013, Graan et al., 2013). However, since the EEG is recorded whilst acquiring functional MRI images[6] there are artefacts that can obscure the interpretation of the EEG. Furthermore, there are also artefacts that can degrade the quality of fMRI images. Therefore, prior to implementing a GLM, it is important to reduce any EEG and fMRI related artefacts. In this section, I provide a summary as to how EEG-fMRI data is acquired (Section 2.3.2.1). Then I explain how the artefacts observed on EEG (Section 2.3.2.2) and fMRI data (Section 2.3.3.3) can be reduced. I then provide a summary as to how a GLM can be used to map the BOLD changes associated with IEDs (Section 2.3.3.4).

2.3.2.1 EEG-fMRI data acquisition

During simultaneous EEG-fMRI acquisition, the subject is placed inside the scanner bore and vacuum cushions are placed beside the head to reduce motion. The electrical activity detected by the electrodes is relayed to an MR-compatible amplifier that is in the scanner room. This amplifier amplifies and digitises the signal, which is then transmitted, using fibre optic cables, to the recording equipment placed outside the scanner room. The EEG clock is synchronised to the fMRI acquisition clock resulting in simultaneous EEG-fMRI acquisition (Laufs et al., 2008). Since the EEG is acquired inside the scanner, there are a number of artefacts that can obscure the interpretation of the EEG. In the next section, I describe the artefacts observed on EEG and how they can be reduced for the interpretation of the EEG reviewer.

2.3.2.2 EEG artefact reduction and interpretation

The two main artefacts observed on scalp EEG are; gradient (scanner related) artefact (GA) and pulse (heartbeat related) artefact (PA). GA is caused by the rapid gradient switching during the fMRI scan (Allen et al., 2000) and pulsatile movement of the head linked to the cardiac cycle causes the PA. The most commonly applied method to reduce these artefacts is averaged template subtraction, which can be done offline (Allen et al., 1998, Allen et al., 2000). Regarding icEEG-fMRI, GA also obscures icEEG interpretation,

[6] Often using a T2*-weighted single shot echo-planar imaging gradient sequence

however, PA is not large enough to significantly distort the icEEG quality (Carmichael et al., 2012). Once the EEG artefacts have been corrected, an expert EEG reviewer(s) often interprets the EEG and the epileptiform events are marked on the EEG as an event of interest (see Figure 2-7). In order to create an optimal fMRI model for IEDs, IEDs with similar spatial distribution and morphological characteristics are often classified in the same group based on the assumption that they arise from the same generator. For example, IEDs from the left temporal lobe will be classified separately to IEDs from the right temporal lobe in the GLM (Liston et al., 2006b).

2.3.2.2 FMRI artefact reduction

Artefacts caused by head movement and physiological noise can degrade the quality of images acquired during the fMRI scan. In order to reduce this artefact during the scan, vacuum cushions can be used to restrict movement of the head however, it has been shown that head movement even at the millimetre scale is sufficient to make the images acquired during the scan unusable (Friston et al., 1995). Therefore, another way to reduce this artefact is to use offline motion correction algorithms (Friston et al., 1995, Wilke, 2012, Tierney et al., 2016) that can be used to explain the head motion movement and can be included in the design matrix of the GLM (as explained in the next section) (see Figure 2-7). Physiological noise such as the pulse changes caused by the cardiac cycle (Glover et al., 2000, Liston et al., 2006a) as well as swallowing and eye blinks (Chaudhary et al., 2012) can also degrade the quality of the resulting fMRI images. Similar to head motion movement, accounting for physiological noise in the design matrix of the GLM can improve the quality of the data (Glover et al., 2000, Liston et al., 2006a, Chaudhary et al., 2012) (see Figure 2-7).

2.3.2.3 EEG-fMRI data analysis: general linear model

Once the EEG artefacts are removed and interpreted by the EEG reviewer, the time point at which the events of interest occur are noted and represented as a mathematical function (see Figure 2-7). The mathematical representation of these events can be boxcar functions, as commonly used for polyspikes, or zero-duration stick functions, commonly incorporated for individual IEDs. The events of interest are then convolved with an appropriate haemodynamic response function (HRF) (described in Section 2.3.1.2; see Figure 2-7) and incorporated into the design matrix of the GLM as an effect of interest (see Figure 2-7).

It is also important to regress out the influence of potential sources of noise that can cause signal variation on the fMRI data in order to reduce their effect when observing BOLD changes correlated to IEDs. As mentioned in Section 2.3.1.2, there are algorithms that can account for noise caused by head motion artefacts and these are added into the design matrix as an effect of no interest (see Figure 2-7). Other potential sources of

noise related to the cardiac cycle (see Section 2.3.1.2) and eye blinks can be derived from the EEG and also incorporated in the design matrix as an effect of no interest (see Figure 2-7).

The correlation of each effect of interest (each IED class) can then be statistically analysed across all voxels (using a mass univariate voxel by voxel approach) to determine which voxels show significant BOLD fluctuations associated with the effect of interest (see Figure 2-7) (Chaudhary et al., 2013, Murta et al., 2015). The results are then presented as statistical parametric maps which will sometimes show BOLD changes correlated to the effect of interest. These BOLD changes can then be overlaid to coregistered structural scans to determine the region of the BOLD changes (Chaudhary et al., 2013).

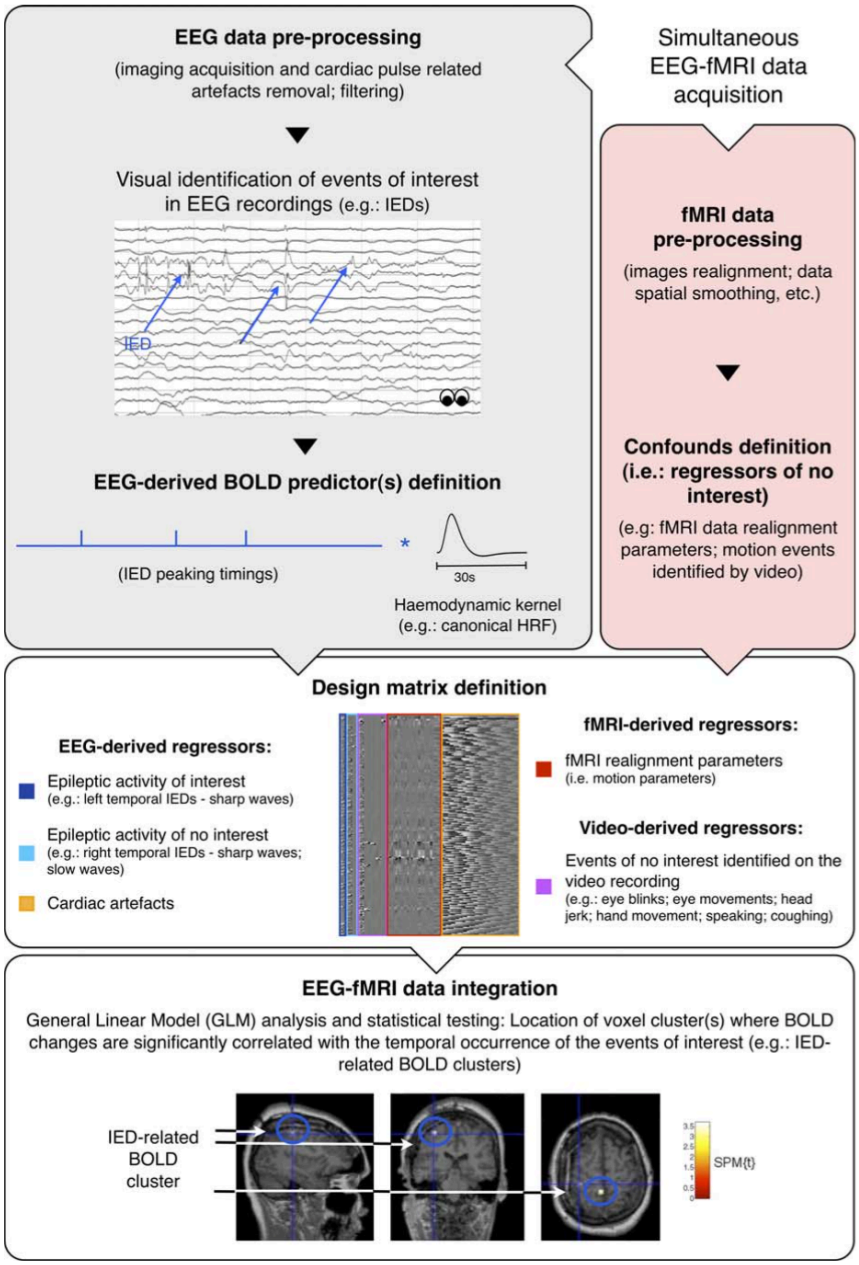

Figure 2- 7| Pipeline of EEG-fMRI analysis using a GLM. Top left: IEDs are detected by an EEG reviewer (after EEG artefact removal), represented as a mathematical function (zero duration stick function is the example shown in this figure) and convolved with a HRF resulting in regressor of interest. Top right: Pre-processing of fMRI images and movement related regressors of no interest are determined. Middle: Regressors of interest and movement regressors of no interest as well as regressors of no interest regarding physiological noise are added to the GLM design matrix. Bottom: Statistical analysis of IED-correlated BOLD response is carried out sometimes resulting in a statistical parametric map. Image taken from Murta et al. (2015).

2.3.3 BOLD mapping of IEDs detected on Scalp EEG

Characterising the IZ using scalp EEG-fMRI has provided a unique insight into the relationship it has with the EZ. In this section, I will review the studies that have assessed the clinical value of scalp IED-related BOLD maps as well as the limitations involved in mapping the BOLD correlated of scalp IEDs.

2.3.3.1 Clinical Value

The clinical value and contribution of scalp EEG-fMRI in the localisation of the EZ in patients with focal epilepsy has been assessed by comparing the IED-related BOLD maps to non-invasive methods used during presurgical evaluation (Zijlmans et al., 2007, Moeller et al., 2009, Pittau et al., 2012), as well as the invasively defined SOZ (Thornton et al., 2011, Khoo et al., 2017) and in some studies the area of resection (Thornton et al., 2010, An et al., 2013, Coan et al., 2016).

2.3.3.1.1 Comparison with non-invasive studies

Zijlmans et al. (2007) carried out an EEG-fMRI study on patients that were initially rejected for surgical resection due to an unclear focus or if focus was presumed to be multifocal. Eight out of fifteen patients showed an IED-related BOLD cluster concordant to the field of the IED and in four of these patients, EEG-fMRI results were shown to improve the localisation of the EZ. In these four patients, non-invasive presurgical evaluation tools indicated an unclear focus in three and presumed multifocality in the other. However, EEG-fMRI results showed a circumscribed focus in all four patients and these patients were reconsidered for surgery. Two out of these four patients subsequently underwent icEEG and the invasively defined SOZ validated the findings of the EEG-fMRI results (Zijlmans et al., 2007). These findings suggest that scalp EEG-fMRI can improve the localisation of the presumed EZ in patients considered for surgery. Moeller et al. (2009) also investigated a cohort of nine patients that had an unclear focus (non-lesional FLE). In eight out of nine patients, they found the most statistically significant BOLD cluster (the global maximum (GM)) to be concordant to the field of the IED and to the corresponding PET and SPECT results. Furthermore, two of these patients underwent postoperative histological analysis revealing FCD and microdygenesis; the GM IED-related BOLD clusters were found to be adjacent or overlapping these regions (Moeller et al., 2009). A larger study by Pittau et al. (2012), determined whether the IED-related BOLD maps added any further information than scalp EEG to the presumed region of the EZ. Similar to Moeller et al. (2009), they discovered that in the majority of patients (29 out of 33 patients; 88%), the GM BOLD cluster was concordant to the field of the IED. Furthermore, the GM BOLD cluster for 21 of the 33 patients was found to be more contributory in the localisation of the presumed region of the EZ compared to scalp EEG alone (the GM BOLD cluster was deemed contributory if it more accurately localizes the region responsible for generating the spike (i.e. anterior or posterior region of a lobe) or if it identified a deep brain structure such as the hippocampus) (Pittau et al., 2012). In 12/14 patients the GM BOLD was validated in as the region of the EZ using the information obtained from icEEG and/or lesions detected on MRI (Pittau et al., 2012).

These results indicate that IED-related BOLD clusters show good concordance with the field of the IED and can contribute more to the localisation of the EZ compared to current non-invasive presurgical studies (Zijlmans et al., 2007) and scalp EEG (Moeller et al., 2009, Pittau et al., 2012) during presurgical evaluation. However, as mentioned in Chapter 1, most centres use the invasively defined SOZ as the gold standard in localising the EZ. Two of the three studies discussed above used the invasively defined SOZ to validate their findings however, this was in a few patients within a cohort (Zijlmans et al., 2007, Pittau et al., 2012).

2.3.3.1.2 Comparison with invasive studies

Two studies have compared scalp IED related BOLD maps only to the invasively defined SOZ (Thornton et al., 2011, Khoo et al., 2017).

Thornton et al. (2011) carried out a study in patients with FCD and discovered that in 9 out of 11 patients, there was at least one IED-related BOLD cluster concordant to the same region as the invasively defined SOZ. This study also showed that scalp EEG-fMRI is good at delineating the area of resection in FCD patients. For example, in those patients in whom all the IED-related BOLD clusters were in the same lobe as the invasively defined SOZ, they had a good postsurgical outcome. In those patients in whom the IED-related BOLD clusters were more widespread (in other lobes to the invasively defined SOZ) they were likely to have a poor postsurgical outcome or a SOZ that was widespread (Thornton et al., 2011). Khoo et al. (2017) carried out a larger study in 37 patients with mixed aetiology and hypothesised that the GM IED-related BOLD cluster is the region of the IZ that also delineates the invasively defined SOZ. They discovered that the GM BOLD cluster could predict the invasively defined SOZ with high confidence in 68% of the IED-related BOLD maps (Khoo et al., 2017) and concluded that the GM BOLD clusters could contribute and guide icEEG electrode placement. However, in contrast to Thornton et al. (2011), Khoo and her colleagues did not include details as to whether these patients had surgical resection and their postsurgical outcome. Therefore, they were unable to determine whether the location of the GM BOLD cluster is also indicative of the EZ as the EZ can only reliably determined once the patient has had surgery since it is *'the minimum amount of cortical tissue that must be resected to produce seizure freedom'* (Lüders et al., 2006). There are only three studies that use the area of resection to determine how well scalp EEG-fMRI localises the EZ and potentially predict postsurgical outcome (Thornton et al., 2010, An et al., 2013, Coan et al., 2016).

2.3.3.1.3 Comparison with area of resection

The three studies that have aimed to determine whether IED-related BOLD maps can be predictive of good postsurgical outcome have compared the BOLD maps to the area of

resection between good and poor postsurgical outcome patients (Thornton et al., 2010, An et al., 2013, Coan et al., 2016). Thornton et al. (2010) showed that in the 7 out of 10 patients that were seizure free after surgery, six patients had the GM BOLD cluster present in the area of resection. In the other poor postsurgical outcome patients, BOLD clusters were found remote from the area of resection. A larger study by An et al. (2013) showed that 70% of the patients that had the GM BOLD cluster resected had a good postsurgical outcome whereas 90% of the patients that had no BOLD cluster in the area of resection had a poor postsurgical outcome. Therefore, similar to some of the previous studies mentioned (Moeller et al., 2009, Pittau et al., 2012, Khoo et al., 2017), these two studies also indicate that the GM BOLD cluster is a good indicator of the EZ. However, it is important to note that although An et al. (2013) showed that the resection of the GM BOLD cluster increases the likelihood of a good postsurgical outcome, the sensitivity of a BOLD cluster being in the area of resection for a good postsurgical outcome patient was 47% (An et al., 2013). Indeed an investigation carried out by Coan et al. (2016) concluded that any significant BOLD cluster in the area of resection is a good predictor of postsurgical outcome whereas, the absence of a significant BOLD cluster in the area of resection is good predictor of poor post surgical outcome (Coan et al., 2016).

The studies described in this section show that the IZ mapped using scalp EEG-fMRI show good concordance to the field of the scalp IED (Zijlmans et al., 2007, Moeller et al., 2009, Pittau et al., 2012) and has been able to contribute more to the localisation of the EZ compared to scalp EEG alone (Pittau et al., 2012). IED-related BOLD maps have also shown good concordance to the invasively defined SOZ (Thornton et al., 2011, Khoo et al., 2017) and have the potential to predict good postsurgical outcome (Thornton et al., 2010, An et al., 2013, Coan et al., 2016). A common feature amongst these maps is that they show BOLD clusters in multiple regions indicating that the region responsible for generating IEDs are widespread, further reinforcing the epilepsy network hypothesis (Laufs, 2012b). Some of the studies above have described the GM BOLD cluster as the marker of the IZ that best represents the EZ (Moeller et al., 2009, Thornton et al., 2010, Pittau et al., 2012, Khoo et al., 2017) whereas other studies have shown the GM to be remote from the EZ (Thornton et al., 2011, An et al., 2013). This indicates that the GM as a marker of the EZ is still controversial however, a common finding amongst these studies is that the absence of BOLD clusters in the area of resection predicts poor postsurgical outcome (Thornton et al., 2010, An et al., 2013, Coan et al., 2016).

2.3.3.2 Limitations

The limited sensitivity of scalp EEG-fMRI emphasised by the lack of IEDs detected inside the scanner (Salek-Haddadi et al., 2006, Aghakhani et al., 2006) as well as the relatively low number of IED-related BOLD maps of IEDs detected inside the scanner (Salek-

Haddadi et al., 2006) provides a challenging limitation for the interpretation of the generators of IEDs.

This can be significantly improved by a correlation-based technique, based on IED recorded outside the scanner (Grouiller et al., 2011). Grouiller and his colleagues used scalp voltage topographic map of IEDs recorded outside the scanner, which were correlated with the scalp voltage topographic map of corrected intra-MRI EEG at each time point in the time series. The time point at which there is high correlation is then convolved with a canonical HRF resulting in a regressor of interest for fMRI analysis (Grouiller et al., 2011). This technique has been shown to increase sensitivity of identifying BOLD changes of epileptic activity by 80% (Grouiller et al., 2011).

However, the lack of sensitivity of scalp EEG not being able to detect underlying IEDs still remains (Tao et al., 2005). As mentioned in Section 2.1.2.2, icEEG studies are able to record closer to the generators of IEDs due to their invasiveness, resulting in greater sensitivity and spatial specificity than scalp EEG. However, icEEG studies also have limited whole brain coverage. Recent safety and feasibility studies (Carmichael et al., 2010, Carmichael et al., 2012, Boucousis et al., 2012) have allowed the acquisition of simultaneous icEEG-fMRI mitigating the lack of whole brain coverage of icEEG. In the following section I will describe the studies that have mapped the IZ using icEEG-fMRI across the whole brain.

2.3.4 BOLD mapping of IEDs detected on icEEG

To date there are only three studies that have mapped BOLD changes associated with IEDs recorded intracranially in humans over the whole brain (Vulliemoz et al., 2011, Cunningham et al., 2012, Aghakhani et al., 2015)[7]. In the first ever demonstration of icEEG-fMRI in humans, Vulliemoz et al. (2011) investigated two patients, one with FLE and the other with TLE. In the FLE patient significant IED-related BOLD changes were revealed close to the spiking contacts (lateral frontal cortex) and also in the region that was not sampled by icEEG (medial frontal cortex); this finding was concordant to the results from MEG recordings. However, the resection was only limited to the lateral pre and post central cortex and did not cover the medial frontal cortex. Furthermore, this patient continued to have seizures, which could indicate a key role of the medial frontal cortex region in the epileptic network (Vulliemoz et al., 2011).

Cunningham et al. (2012) investigated two TLE patients; in one patient, BOLD changes were found in the region of the spiking contacts however, in the other patient all of the BOLD clusters were found in remote regions to the spiking contact. Both patients

[7] In addition there have been two studies examining the relationship between electrophysiology and BOLD at a local level (Murta et al., 2016, Murta et al., 2017)

showed widespread BOLD activation/deactivation for focal IEDs indicating that a widespread network is involved even in the generation of very focal IEDs. Indeed, in the patient where the BOLD clusters were in remote regions from the spiking contact deactivation was observed in the default mode network (DMN); a network that usually shows activation in control subjects at rest (Raichle et al., 2001, Smith et al., 2009). This is also commonly found in scalp EEG-fMRI studies that have analysed IED-related BOLD maps in patients with focal IEDs (Fahoum et al., 2012) indicating that even very focal IEDs observed on icEEG have important consequences on brain function (Cunningham et al., 2012).

Aghakhani et al. (2015) carried out the largest study on nine patients in whom the IEDs were recorded in the temporal region (7 patients) and the extratemporal regions (2 patients). They found the BOLD cluster containing the maximum statistical score (the global maximum: GM) to be present close (<1cm) to the most active electrode contact (the contact that showed recorded an IED with the highest amplitude) in 6 out of 7 TLE patients whereas the GM BOLD cluster was remote from the most active electrode contact in the two extra-TLE patients. Four patients underwent surgery (3 TLE and 1 extra-TLE) with two patients having a good postsurgical outcome (ILAE 1) (2 TLE) and the other two having a poor postsurgical outcome (ILAE 4) (1 TLE and 1 extra-TLE). Notably in the 2 patients that had a good postsurgical outcome, the GM was close to the most active electrode contact (which was also in the region that was resected) whereas in the two poor postsurgical outcome patients there was no BOLD cluster (GM and non-GM) concordant to the most active electrode contact. Although this was a small subset of patients with regards to postsurgical outcome, these findings are similar to previous scalp EEG-fMRI studies (Thornton et al., 2010, Thornton et al., 2011, An et al., 2013, Coan et al., 2016) that indicate that the resection of the GM BOLD cluster results in a good postsurgical outcome (Thornton et al., 2010, Thornton et al., 2011, An et al., 2013) and that a resection that doesn't include any BOLD cluster in the area of resection results in a poor postsurgical outcome (Thornton et al., 2010, Thornton et al., 2011, An et al., 2013, Coan et al., 2016).

The results of these three studies indicate that even very focal IEDs can be correlated with BOLD changes remote from the intracranial electrodes showing IED activity, in addition to the local changes, even at 1.5T. Similar to scalp EEG-fMRI studies, these results suggest that the regions responsible for the generation of IEDs are not only localised to a specific region but potentially involve a widespread network (Vulliemoz et al., 2011, Cunningham et al., 2012, Aghakhani et al., 2015). The IED-related BOLD clusters have shown to complement non-invasive findings (i.e. MEG – Vulliemoz et al., 2011) and show preliminary results in complementing similar results from EEG-fMRI findings that have assessed IED-related BOLD vs postsurgical outcome (Aghakhani et al.,

2015). Therefore, icEEG-fMRI can provide unprecedented insight into the networks associated with focal IEDs that could be used to complement non-invasive clinical (and non-clinical studies) studies used to localise the potential region of the EZ (such as scalp EEG-fMRI, MEG, EEG, ESI) and provide a further understanding of the seizure network.

2.3.4.1 Limitations

A limitation of icEEG-fMRI studies is the gradient induced signal dropout (susceptibility artefacts), which is present around the electrode. Images acquired on a 1.5T scanner have shown a signal dropout of being approximately 5mm around the electrode (Carmichael et al., 2012) whereas the signal dropout on a 3T has shown to be greater; approximately 1.5cm (Boucousis et al., 2012). However, it is important to note that IED-related BOLD changes have been found in regions immediate to the most spiking contact in all three icEEG-fMRI studies (Vulliemoz et al., 2011, Cunningham et al., 2012, Aghakhani et al., 2015). Furthermore, a recent study was able to identify BOLD signal in the immediate vicinity of the intracranial electrode and managed to find a significant correlation between the width of the IED and the amplitude of the BOLD signal (Murta et al., 2016). Although icEEG has increased sensitivity in detecting IEDs compared to scalp EEG, one of the main challenges associated with icEEG-fMRI data is the difficulty of forming a parsimonious model of potential BOLD changes from the complex spatio-temporal dynamics of icEEG IEDs. Therefore, the detection and classification of icEEG IEDs by EEG reviewers can be inconsistent and inaccurate potentially resulting in false positive and false negative IED-related BOLD clusters (Flanagan et al., 2009). In the next section I will describe how IED markings on icEEG can be improved for the purpose of BOLD modelling in patients that have undergone simultaneous icEEG-fMRI.

2.4 Improving icEEG IED interpretation for the purpose of BOLD modelling

As mentioned in Section 2.2.1, EEG reviewers detect IEDs based on their temporal characteristics and classify them into various IED classes by assessing the EEG waveform, which often takes into account their spatial distribution field (Gotman, 1999, James et al., 1999). For the purpose of BOLD modelling, each class is then added as a regressor of interest in the GLM (see Figure 2-6). However, due to the highly abundant and complex IEDs observed on icEEG, this can be very time consuming and highly subjective (Dümpelmann and Elger, 1999, Brown et al., 2007, Barkmeier et al., 2012, Gaspard et al., 2014). Indeed, the detection of IEDs on icEEG has shown a low level of agreement (<50%) for both intra-rater (Brown et al., 2007) and the inter-rater comparisons between clinical neurophysiologists (Dümpelmann and Elger, 1999, Barkmeier et al., 2012, Gaspard et al., 2014). In this section I will provide a summary of the automated algorithms that have been designed to minimise subjectivity for IED

interpretation in icEEG (Section 2.4.1). I will also discuss how the automated marking of IEDs can be improved for the purpose of BOLD modelling in patients that have undergone icEEG-fMRI (Section 2.4.1).

2.4.1 Current automated algorithms used in the marking of icEEG IEDs

In order to reduce subjectivity between EEG reviewers, a variety of automated algorithms have been developed specifically for marking IEDs on icEEG (Dümpelmann and Elger, 1999, Hufnagel et al., 2000, Bourien et al., 2005, Valenti et al., 2006, Brown et al., 2007, Barkmeier et al., 2012, Gaspard et al., 2014, Janca et al., 2015). In general, these algorithms are designed to automatically detect IEDs by exploiting their temporal characteristics (Dümpelmann and Elger, 1999, Hufnagel et al., 2000, Bourien et al., 2005, Valenti et al., 2006, Brown et al., 2007, Barkmeier et al., 2012, Gaspard et al., 2014, Janca et al., 2015) with two algorithms also classifying IEDs by exploiting their activity across channels (Hufnagel et al., 2000, Bourien et al., 2005).

2.4.1.1 Automated IED detection

The majority of automated IED detection algorithms for icEEG are designed to temporally detect IEDs in any channel of an icEEG recording and mark them as distinct events (Dümpelmann and Elger, 1999, Valenti et al., 2006, Brown et al., 2007, Barkmeier et al., 2012, Gaspard et al., 2014, Janca et al., 2015). They attempt to detect events in the EEG signal based on specific features of the IED and if they stand out from background activity. For example Barkmeier et al. (2012) developed an automated algorithm that detects an IED based on the duration and amplitude of the peak of the spiky component of the IED (Barkmeier et al., 2012). Similarly Brown et al. (2007) designed an algorithm that detected IEDs based on the amplitude (did it stand out from the background activity), the width of the spiky component and the presence of a slow wave (Brown et al., 2007). Gaspard et al. (2014) developed an automated algorithm that is able to distinguish IEDs with regards to amplitude of the spiky component; the high amplitude ones were labelled as being the most prominent. However, these algorithms do not incorporate the spatial characteristics of the IEDs; an important step in the human ability to distinguish between different IED types (James et al., 1999, Gotman, 1999).

2.4.1.2 Automated IED classification

Two algorithms incorporated a second classification step after the automated detection of the IEDs (Hufnagel et al., 2000, Bourien et al., 2005). These algorithms cluster IEDs based on whether the IEDs occur over a similar temporal interval. For example, if multiple IEDs were detected in different channels but occurred within +/- 150ms (Bourien et al., 2005) or +/- 100ms (Hufnagel et al., 2000) of each other, the IEDs were classified in the same group (Hufnagel et al., 2000, Bourien et al., 2005). However, these

two algorithms do not take into account the waveform of the IEDs that occur over multiple channels.

In contrast, some automated detection algorithms for IEDs seen on scalp EEG have been designed to detect and classify spikes based on the waveform and spatial characteristics of the IED using source localisation (Flanagan et al., 2002; Ossadtchi et al., 2004; Van Hese et al., 2008, Scherg et al., 2012). Source localisation techniques vary but the concept remains the same throughout. As mentioned previously in this chapter (Section 2.1.1), the EEG electrodes detect electrical activity caused by a dipole from the presynaptic activity at the synapses of multiple pyramidal neurons and display this as a voltage potential. A number of signal processing methods have been designed to analyse this voltage potential at various locations on the scalp and as a result identify the potential source of that electrical activity (see Grech et al., 2008 for a review). These algorithms rely on the geometry of the electrodes, which may be problematic in patients that have undergone icEEG since the implantation can vary between patients.

However, recently Pedreira et al. (2014) has shown that it is possible to automatically classify scalp IEDs based only on the shape of the waveform across multiple EEG channels. They adapted an algorithm originally designed for electrophysiological processes (extracellular neuronal spikes), called Wave_clus, to classify IEDs for the purpose of modelling the concurrently acquired fMRI in patients that have undergone scalp EEG-fMRI (Pedreira et al., 2014). Therefore, as Wave_clus does not make assumptions of the geometry or spatial distribution of the electrodes, this algorithm could also be used to automatically classify IEDs detected on icEEG. In the next two sections I will provide an overview of, Wave_clus, and how it was used by Pedreira et al. (2014) for the automated classification of scalp IEDs.

2.4.2 The Wave_clus automated neuronal spike classification algorithm

Electrophysiologists have been classifying neuronal action potentials, recorded using invasive electrodes, since the 80's based on amplitude and waveform of the signal. Neuronal spike classification algorithms are machine learning algorithms that use the differences in shape of waveform of extracellular action potentials (commonly referred to as *neuronal spikes*), produced by neurons close to the recording microelectrode (Gold et al., 2006), to classify the recorded events into putative separate sources (see Figure 2-8). To summarise, once the neuronal signal is detected by the microwire, it is filtered (to eliminate slow activity and noise) (see Figure 2-8a) and neuronal spikes are detected (usually by applying an amplitude threshold) (see Figure 2-8b). The neuronal spikes are then processed through a neuronal spike classification algorithm that extracts features of the waveform (see Figure 2-8d) and clusters them into putative separate sources based on the difference in waveform (see Figure 2-8e).

Wave_clus (Quian Quiroga et al., 2004) is one of the many neuronal spike classification algorithms (Harris et al., 2000 (Klustakwik), Rutihauser et al., 2006 (OSort) – see Rey et al., 2015 for a review), which has led to the discovery of concept cells in humans (Quian Quiroga et al., 2005). These algorithms also have the potential to be incorporated in the latest applications using brain computer interfaces such as neuroprosthetic devices (Todorova et al., 2014). Wave_clus is an unsupervised machine-learning algorithm[8] that extracts features of the waveform and clusters these features in the following way:

1) **Feature extraction:** Once the neuronal spikes are detected, the features of the waveform are extracted. Wave_clus does this by applying a wavelet transform by applying a linear transformation to extract the time-frequency components of the signal according to the base selected. The resulting wavelet coefficients correspond to the feature of the waveform at a specific time and frequency range (Mallat, 1989, Quian Quiroga et al., 2004).
2) **Coefficient Selection:** A Kolmogorov-Smirnov test of normality is performed in the wavelet coefficients obtained in step 1. The algorithm then selects a reduced number of wavelet coefficients (a parameter defined by the user) that deviate most from normality and are processed through a clustering algorithm (Quian Quiroga et al., 2004).
3) **Clustering:** The clustering step involves processing the selected coefficients through an unsupervised superparamagnetic clustering algorithm (derived from statistical physics) that clusters the features as a function of a parameter designated *temperature* (Quian Quiroga et al., 2004). As a result this clustering step groups (classifies) neuronal spikes of similar shape (see Figure 2-8e).
4) **Forcing:** In the final step, Wave_clus attempts to match any unclassified event to the produced cluster from the previous step.

[8] Therefore, WC is a machine-learning algorithm that attempts to find a structure/patterns on unlabeled data. This is in contrast to supervised machine learning algorithms where the algorithms are trained on data that has been previously labelled and that can be used on new similar data.

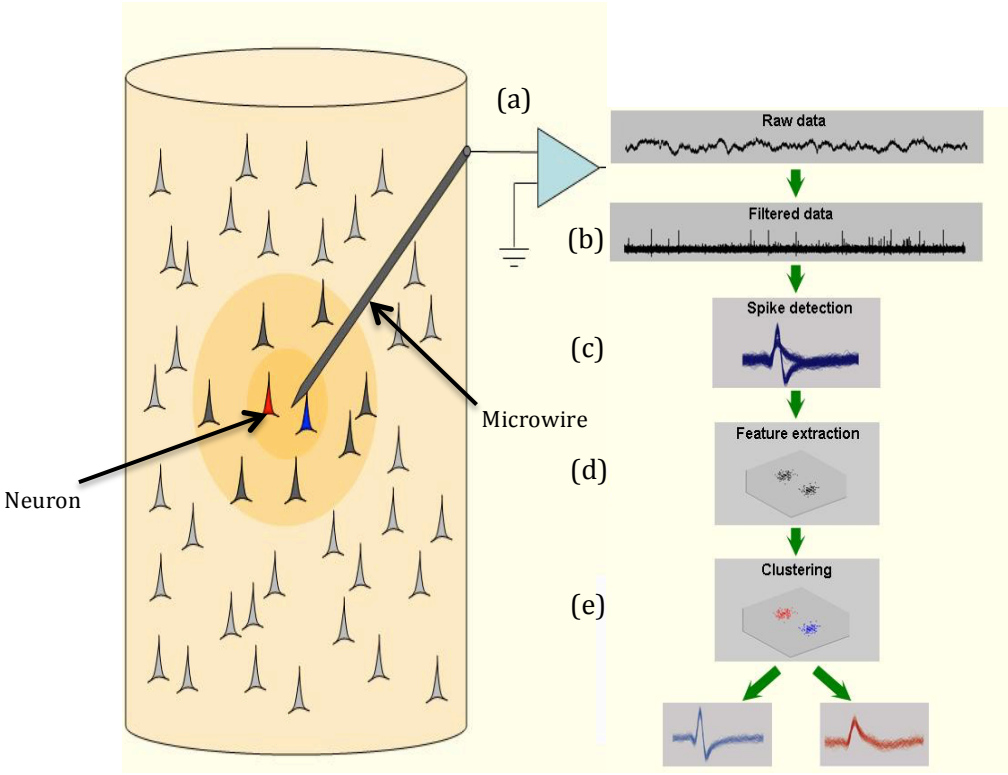

Figure 2- 8| Automated neuronal spike classification. Microwire is inserted in the brain and records ERPs from a population of neurons. The (a) raw data is (b) filtered and (c) ERPS are automatically detected. The (d) features of the waveform of the ERPs are extracted and (e) clustered resulting in the classification of ERPs of a similar shape. Image adapted from Quiroga (2007)

2.4.2.1 Application of Wave_clus for the automated classification of IEDs detected on scalp EEG

As mentioned in Section 2.4.1.2, Pedreira et al. (2014) were able to use Wave_clus for the classification of IEDs detected on multi channel scalp EEG. An expert EEG reviewer temporally detected (and marked using a single point marker) and spatially classified the IEDs (resulting in a different label for each class) (Pedreira et al., 2014). For the purpose of automated classification, the classification labels by the EEG reviewer were discarded and kept for the subsequent comparison between EEG reviewer classification and Wave_clus classification. Therefore, temporal IED detection markings of the EEG reviewer were then processed through a number of pre-processing steps designed for automated IED classification (Pedreira et al., 2014):

1) First, 8-12 channels of interest were selected based on channels in which the IEDs were noted in the clinical EEG report as being the most prominent and frequent.
2) Then the temporal IED markings were adjusted to the peak of the spiky component (see Figure 2-9a). This step is important as Wave_clus, performs a time-frequency decomposition of the waveform (see Section 2.4.2.1 – step 1)

therefore, the resulting coefficients are time bounded. As a result, it is important to have the waveforms represented across a common marker as misalignment can result in different coefficients of waveforms that are of a similar shape. The peak of the spiky component of the IED was selected, as it is a common marker across all IEDs.

3) An IED classification epoch time window of 300ms (80ms before the peak of the spiky component and 220ms after the peak) was used to segment around the single point marker representing the peak of the spiky component of the visually identified IED for each channel of interest (selected from step 1). The IED classification epoch time window length is important and should be selected to incorporate the maximum information of the IEDs with the smallest possible time span to minimise the impact of noise.
4) The selected channels were then concatenated across the channels of interest to form meta-IEDs (see Figure 2-9b).

Once these pre-processing steps were carried out, the meta-IEDs were then processed through WC in the following way:

1. As mentioned in the section 2.4.1.3, Wave_clus extracts features of the waveform using wavelet decomposition. Pedreira et al. (2014) selected eight wavelet coefficients that deviate most from normality for each channel of interest in the meta-IED. For example, if there were 7 channels of interest in the meta-IED then there would be 56 wavelet coefficients selected.
2. The selected coefficients were then processed through the superparamagnetic clustering algorithm resulting in the automated classification of the IEDs (see Figure 2-9c). Then, the user performed a visual verification of the final classes obtained; including some events that are labelled as a 'non-IED'.

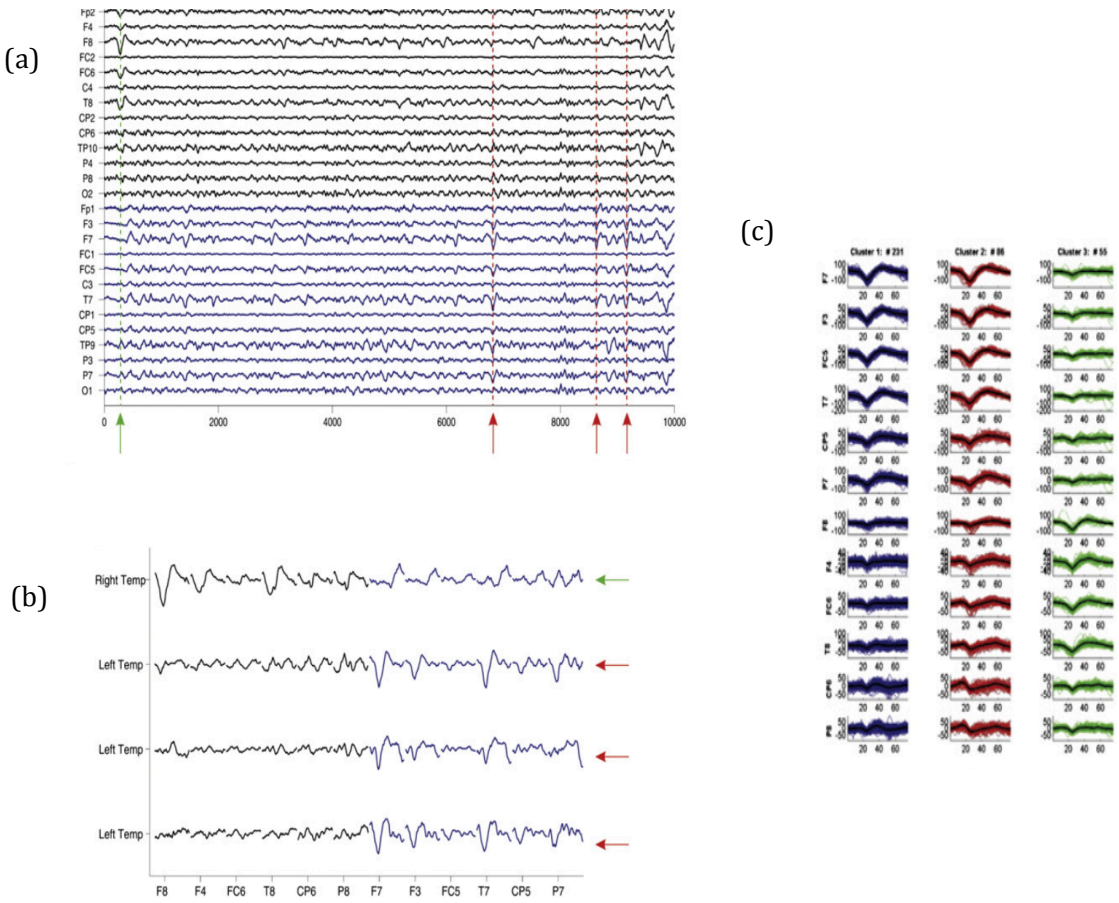

Figure 2- 9| Wave_clus for automated classification of scalp IEDs. (a) The IED marker is adjusted to the peak of the spiky component. (b) The IEDs are segmented around the peak of the spiky component and concatenated across the channels of interest resulting in meta-IEDs. The meta-IEDs are processed through Wave_clus resulting in (c) the automated classification of IEDs

Since the IEDs in this study were detected on scalp EEG during simultaneous fMRI acquisition, Pedreira et al. (2014) assessed the performance of Wave_clus classified IEDs by 1) comparing the EEG pattern of the IED classification between Wave_clus and the EEG reviewer and 2) comparing the IED-related BOLD maps obtained by the Wave_clus classification vs visual classification.

The EEG pattern of the IED classification between Wave_clus and the EEG reviewer was compared based on the topography of the IED on the scalp EEG. For example, if the EEG reviewer and/or Wave_clus detected and classified IEDs that occurred in the electrodes covering the left temporal (LT) lobe then this class would be classified as LT. Pedreira et al. (2014) discovered that there was a full match in IED classes between Wave_clus and the EEG reviewer in two out of eight patients. In another two patients, Wave_clus had the same IED classes as the EEG reviewer and also provided additional classes. In total the classes of IEDs obtained by Wave_clus overlapped in the same areas as the EEG reviewer classes in seven out of eight patients (Pedreira et al., 2014).

With regards to assessing the performance of Wave_clus by comparing IED-related BOLD maps, two different fMRI analyses were performed; one for the visually classified IEDs (GLM1) and another for the Wave_clus classified IEDs (GLM2). Each IED class was added as a regressor of interest into the GLM and the concordance of the IED-related BOLD maps for each class to the presumed IZ was determined[9]. An IED-related BOLD map was labelled as concordant if there was a significant BOLD cluster in the presumed IZ. Across all patients, there were more IED-related BOLD maps that were concordant to the presumed IZ for GLM2 (72%) compared to GLM1 (50%). This shows that Wave_clus classified IEDs produce IED-related BOLD clusters in regions that are consistent with electro clinical evidence (Pittau et al., 2012).

This study suggests that a solution based on Wave_clus could help minimise the subjectivity of IED classification on scalp EEG by exploiting the statistical properties of the waveform of the IED across multiple channels (Pedreira et al., 2014). Since this algorithm does not require the geometry of the EEG contacts, this could also be incorporated for the automated classification of IEDs detected on icEEG. Although the IED-related BOLD maps showed that Wave_clus classification showed more concordance to the presumed IZ, the IED classification of WC was not compared across multiple EEG reviewers. Indeed, validating automated algorithms often requires a gold standard to which one can compare its performance. In the next section, I will provide a summary as to how automated algorithms for icEEG IED markings are validated.

2.4.3 Validating automated algorithms for icEEG IED markings

Due to the lack of a gold standard as to what constitutes an IED, the combined opinions (e.g. consensus or majority) of a group of expert EEG reviewers can be used (Brown et al., 2007, Barkmeier et al., 2012, Halford et al., 2013, Gaspard et al., 2014, Janca et al., 2015), allowing the calculation of sensitivity and other performance metrics such as the precision of the algorithm (Brown et al., 2007, Barkmeier et al., 2012, Gaspard et al., 2014, Janca et al., 2015). For example, the most recent automated icEEG IED detection algorithms have validated the performance of the algorithm to that of three EEG reviewers (Barkmeier et al., 2012, Gaspard et al., 2014, Janca et al., 2015). All three EEG reviewers marked the IEDs on the icEEG independently and if two or more identified marked the same event as an IED then this event would be considered as a gold standard IED. If the automated algorithm also detected the same event, then the detection would be labelled as a true positive (TP). If the algorithm detected an IED that was not labelled as an IED by the majority opinion then this detection would be labelled a false positive (FP). A false negative (FN) detection was when the algorithm did not detect an IED that was labelled as an IED by the majority opinion. As a result, the

[9] This was based on scalp topography and IZ defined using icEEG

sensitivity of the algorithm can be calculated as: TP/(TP+FN) and precision: TP/(TP+FP).

However, to our knowledge, no formal comparison of automated vs multiple human EEG reviewer classification of icEEG IEDs has been carried out. As mentioned previously, Pedreira et al. (2014) compared the scalp IED classification of Wave_clus to the EEG reviewer by comparing the IED topography but this was not compared to multiple EEG reviewers. Furthermore, due to the highly abundant and complex spatio-temporal patterns of IEDs detected on icEEG (see Section 2.2.3), as well as the high spatial specificity of the implanted electrodes, comparing IED topography may not be feasible.

The studies described in this section highlight the highly subjective nature of IED marking between EEG reviewers for IEDs detected on icEEG. Automated algorithms have been designed to reduce this subjectivity however, most only detect IEDs based on their temporal characteristics (Dümpelmann and Elger, 1999, Valenti et al., 2006, Brown et al., 2007, Barkmeier et al., 2012, Gaspard et al., 2014, Janca et al., 2015). Few algorithms incorporate the spatial characteristics of the IED but this is only based on whether they occur in a similar temporal interval (Hufnagel et al., 2000, Bourien et al., 2005) and not on their waveform; an important aspect of IED classification (James et al., 1999, Gotman, 1999). Wave_clus has been shown to classify scalp IEDs based on their waveform irrespective of EEG channel location. Since IED classification distinguishes different IED types based on the assumption that they arise from different generators, applying Wave_clus to icEEG IEDs detected during simultaneous icEEG-fMRI acquisition can potentially result in more biologically meaningful IED-related BOLD maps.

2.5 Summary

The BOLD correlates of IEDs provide a unique insight into the generators of IEDs because of its 3D tomographic whole brain coverage. Scalp EEG-fMRI studies have shown the potential IED-related BOLD maps have in providing added clinical value to the localisation of the EZ. The acquisition of simultaneous icEEG-fMRI has provided us with a unique dataset that can allow the study of the generators of very focal IEDs and further understand their relationship to the EZ at a fundamental level. However, in comparison to scalp EEG, there are more abundant and complex IEDs observed on icEEG, which can make the marking of icEEG IEDs highly subjective (Dümpelmann and Elger, 1999, Brown et al., 2007, Barkmeier et al., 2012, Gaspard et al., 2014). Automated icEEG IED detection algorithms can reduce the subjectivity of IED marking however, most of these algorithms do not exploit activity across channels; a common method used by clinicians to classify IEDs. Wave_clus has shown to be effective in scalp IED classification (Pedreira et al., 2014). The performance of this algorithm was validated in a previous scalp EEG-fMRI study (Pedreira et al., 2014) by 1) comparing the scalp EEG

IED topography of WC and one EEG reviewer 2) comparing the scalp IED-related BOLD maps obtained using WC marking and those obtained using visual marking. Since Wave_clus, does not make assumptions of the geometry or spatial distribution of the electrodes, it can potentially be used in the classification of icEEG IEDs.

Therefore, in this thesis I determine if Wave_clus can provide a solution for more consistent and less biased classification of icEEG IEDs, with the aim of producing more biologically meaningful IED-related BOLD maps. I start with a pilot investigation aimed at optimising the pre-processing pipeline (see Section 2.4.2.1) for the application of WC to our dataset (Chapter 4). As mentioned previously, Pedreira et al. (2014) compared WC scalp IED classification to IED classification to that of only one EEG reviewer by comparing IED topography. However, due to the highly abundant and complex spatio-temporal patterns of IEDs detected on icEEG, comparing IED topography may not be feasible for icEEG IEDs. To our knowledge no formal comparison of automated vs multiple human observer classification of IEDs of IEDs on icEEG has been published to date. Therefore in Chapter 5 I aim to implement a novel scheme to validate WC for the automated classification of icEEG IEDs by comparing the classification of WC to that multiple EEG reviewers from a sample of IEDs detected during the simultaneous fMRI acquisition. Then I apply WC across the entire set of icEEG IEDs detected during simultaneous fMRI acquisition to determine whether WC can produce more biologically meaningful IED-related BOLD maps compared to those obtained using the visual/conventional approach (Chapter 6).

CHAPTER 3: SUMMARY OF SIMULTANEOUS ICEEG-FMRI DATA

In this thesis I will be working on icEEG-fMRI data that was acquired and analysed by Dr Umair Chaudhary, henceforth referred to as EEG reviewer 'H1'. This chapter describes the acquisition and pre-processing of the icEEG and a summary of the icEEG IED marking carried out by 'H1'.

3.1 IcEEG-fMRI acquisition

To date, nineteen patients (11 males: 21-50 years) have undergone simultaneous icEEG-fMRI (see table 3-1) at the National Hospital for Neurology and Neurosurgery. The patients gave informed written consent for participation in this study, which was approved by the joint research ethics committee of the National Hospital for Neurology and Neurosurgery and UCL Institute of Neurology, Queen Square, London, UK. At the time of participation in this study all patients were undergoing invasive icEEG recordings for clinical purposes to establish surgical candidacy. The need for icEEG recordings had been established in a multidisciplinary meeting, to delineate the ictal onset zone and/or to perform direct electro-cortical stimulation for functional mapping. Prior to the invasive EEG recordings, the patients had undergone standard pre-surgical evaluation including long-term video-scalp EEG monitoring, structural MRI and other investigations such as positron emission tomography (PET), magnetoencephalography (MEG) or ictal single photon emission computed tomography (ictal SPECT) when available.

Each patient had between 31-91 implanted electrode contacts, from grids, depths or a mixture of grids and depth electrodes. The electrodes were connected to an MR compatible amplifier system (Brain Products, Gilching, Germany). In accordance with our protocol (Carmichael et al., 2012) MR acquisition was carried out on a 1.5T Siemens Avanto scanner (Erlangen, Germany) with a standard birdcage transmit/receive head coil. Depending on patient comfort inside the scanner and time constraints either one or two 10-minute resting-state echo planar imaging (EPI) sequences (see Table 3-1) and a T1-weighted structural scan was acquired for each patient. The icEEG during simultaneous MR acquisition was acquired at a sampling rate of 5kHz.

3.2 IcEEG pre-processing and analysis by H1

The icEEG was corrected offline for MR scanning artefacts (Allen et al., 2000) and down sampled to 250Hz. For each EEG recording, the EEG was band-pass filtered (2-70Hz).

The recordings were visually inspected by EEG reviewer 'H1' (UJC) for clinical purposes using BrainVision Analyser (Brain Products, Germany). Any epileptiform or potential epileptiform activity was detected by H1 based on the characteristics of the waveform and classified based on the spatial distribution of the epileptiform event (see Section 2.2.1). Pathological IED patterns commonly found in invasive EEG recordings include

individual IEDs (spikes and sharp waves), repetitive IEDs (polyspikes) and paroxysmal fast activity (PFA). Reviewer H1 used two types of event markers: point marker for individual IEDs and onset and offset markers for repetitive IEDs and PFA. Regarding individual IEDs, the approach taken by H1 was to mark IEDs close to the negative/positive peak of the spiky component. These IEDs were marked for the purpose of fMRI modelling therefore, some of these markers were not exactly marked on the peak of the spiky component, as the degree of precision required for fMRI analysis is low. A different label was assigned for each class identified and the channels in which the IED occured in was noted. Across all subjects, the mean number of IED events detected by H1 was 1088 (SD: 871; range: 194 - 3567) and the mean number classes were 5 (SD: 2; range 3 - 10) (see Table 3-1). In Chapter 4 and 5, patients that showed a low number of polyspikes and a high number of individual IEDs were analysed (Patient JR, IH, BS, MB and GC). In Chapter 6, patients that had a good postsurgical outcome were analysed (Patient JR, IH, BS, MB, HD, SH, CB and JN) (see Table 3-1).

Table 3- 1| Electro-clinical information, icEEG-fMRI acquisition details and postsurgical outcome for all patients. M: Male, F: Female, FLE: Frontal lobe epilepsy, TLE: Temporal lobe epilepsy, TOLE: Temporo-occipital lobe epilepsy, PLE: Parietal lobe epilepsy, FPLE: Fronto-parietal lobe epilepsy, NA: Did not undergo surgery

Patient	Age	Sex	Age @ Seizure onset	Type of Epilepsy	No. of resting state fMRI sessions (mins per session separated by ;)	No. of spikes detected by H1	No. of spike classes obtained by H1	Postsurgical outcome (months)
LT	46	F	18	FLE	2(10; 10)	1989	6	ILAE 5 (54)
BS	44	M	8	FLE	2(10; 10)	1033	6	ILAE 1 (59)
JR	36	M	12	FLE	1(10)	590	5	ILAE 1 (58)
MR	50	F	5	FLE	2(10; 10)	1190	3	NA
HD	36	F	7	FLE	1(10)	1035	3	ILAE 1 (55)
IH	37	M	9	FLE	1(10)	892	3	ILAE 1 (44)
SH	37	M	16	FLE	2(10; 10)	1140	5	ILAE 1 (43)
CB	32	F	3	FLE	2(10; 10)	755	4	ILAE 1 (43)
KB	26	F	6	FPLE	1(10)	517	3	NA
CR	31	F	6	TLE	2(10; 10)	463	4	ILAE 5 (54)
MB	34	M	7	TLE	2(10; 10)	1216	6	ILAE 1 (74)
NA*	28	M	10	TLE	---	---	---	---
GC	24	M	18	TOLE	2(10; 10)	1407	6	ILAE 4 (41)
JM	32	F	2	TOLE	2(10; 10)	2570	3	NA
JN	33	M	7	PLE	2(10; 10)	3567	10	ILAE 1 (35)
MP	48	M	14	TLE	2(10; 10)	494	5	ILAE 2 (32)
PL	21	M	8	FPLE	2(10; 10)	194	3	NA
JW	30	F	14	TLE	2(10; 10)	330	5	NA
DD	29	M	20	TOLE	2(10; 10)	207	3	NA

* Unable to correct for MR artefact for this patient therefore, not considered further for the purpose of this thesis

CHAPTER 4: DATA PREPARATION FOR APPLICATION OF WAVE_CLUS TO ICEEG IED CLASSIFICATION

A number of pre-processing steps are necessary to adapt an IED dataset to produce an input to the Wave_clus algorithm. These include: 1- Consistent and precise time marking for each event, in contrast with the approximate marking obtained from the human observer; and 2- Determination of the informative IED classification epoch time window to feed to the WC classification algorithm. In this Chapter, I present the results of a pilot study that was carried out to optimise these pre-processing steps. I present a new automated algorithm[10] to adjust H1's IED markers to ensure their alignment to the peak of the spiky component and I define an optimal IED classification epoch time window by analysing the time-frequency characteristics of IEDs.

[10] This algorithm can be found in github: https://github.com/nirajsharma1/tyclus

4.1 Motivation

As part of standard practice for assessing patients with epilepsy, clinical neurophysiologists are able to detect interictal epileptiform discharges (IED or 'epileptic spikes') during interictal EEG recordings. Although there is no gold standard as to what constitutes an epileptic spike, they tend to comprise a high amplitude deflection event lasting approximately 40-100ms (De Curtis & Avanzani 2001). Some patients evaluated for resective surgical treatment for epilepsy are investigated with intracranial EEG (icEEG) usually when there is strong evidence of an epileptogenic focus but not sufficient information to define a surgically resectable area using non-invasive methods. These patients may be implanted with multiple electrodes targeting deep areas of the brain or placed on the cortex to record epileptic activity (Fernandez & Loddenkemper 2013). In these patients, evidence suggests that a good postsurgical outcome is associated with the removal of the region generating the most frequent epileptic spikes (Asano et al. 2003; Marsh et al. 2010). However, detection of epileptic spikes on icEEG has shown a low level of agreement (< 50%) for both the intra-rater (Brown et al. 2007) and the inter-rater comparisons between clinical neurophysiologists (Dumpelmann and Elger, 1999; Barkmeier et al. 2012; Gaspard et al. 2014). To reduce this subjectivity, computational algorithms designed for the automated detection of IEDs on icEEG have been implemented (Dumplemann and Elger, 1999; Bourien et al. 2005; Valenti et al. 2006; Brown et al. 2007; Barkmeier et al. 2012; Gaspard et al. 2014). However, to our knowledge, the work on IED classification has been limited (Bourien et al. 2005; Yadav et al. 2011; Janca et al. 2013) to algorithms that cluster IEDs visible over multiple channels based on whether they occur in a similar temporal interval but do not take into account the shape of the waveform (Hufnagel et al., 2000, Bourien et al., 2005).

Classification of IEDs into various IED 'populations' generally relies on clinicians distinguishing between different IED types by assessing the EEG waveform which often takes into account the epileptic spike's field distribution (Gotman, 1999; James et al. 1999), which may also help highlight the boundaries of the region responsible for generating them (the so-called irritative zone). A previous study by our group (Pedreira et al. 2014) demonstrated the successful use of an automated neuronal spike classification algorithm, *Wave_clus* (WC) (Quian Quiroga et al. 2004), to classify IEDs, based only on the waveform, on scalp EEG for the purpose of modelling the concurrently acquired functional MRI. Since this algorithm does not make assumptions of the

geometry or spatial distribution of the electrodes, it could also be used to automatically classify IEDs detected on icEEG.

However, the use of Wave_clus on IED waveforms is not a streamlined process. A number of pre-processing steps are necessary to adapt the IED dataset to produce an optimised input to the Wave_clus algorithm in order to obtain the best possible results. Once the IEDs are detected and the channels of interest are selected the temporal marking of each IED is precisely adjusted to the peak of the spiky component (Pedreira et al., 2014). Then the IEDs are segmented using an IED classification epoch time window around the peak of the spiky component and concatenated across the channels of interest to form meta-IEDs. The meta-IEDs constitute the WC input resulting in automated IED classification (Pedreira et al., 2014).

It is important that the IED marking is adjusted to the peak of the spiky component as precise as possible. This is important as Wave_clus performs a time-frequency decomposition of the waveform therefore, the resulting coefficients are time bounded (Quian Quiroga et al., 2004, Pedreira et al., 2014). For example, two IEDs with equal or very similar waveforms but misaligned in the analysis window could lead to different wavelet decomposition and potentially, to different clusters. The IED classification epoch time window must be determined as accurate as possible in order to have the maximum information of the IEDs with the smallest possible time span to minimise the impact of noise. This step is important, as it is this time window that is used to form the meta-IEDs that constitute the WC input.

In the study carried out by Pedreira et al. (2014), for each IED detected, they automatically aligned the original IED marker to the peak of the spiky component, for each channel that showed an IED waveform, independently using a 40ms time window. Regarding the IED classification epoch time window, they determined this using a trial and error method with a training dataset.

In this pilot study our aim is to:

1) Develop an algorithm that can automatically align an IED marker to the peak of the spiky component whilst integrating information across the multichannel signal and that can be used across the entire dataset.
2) Define an optimal IED classification epoch time window, by carrying out a numerical and statistical study of the time-frequency characteristics of the IED signal.

4.2 Data and Methods

4.2.1 Patients, icEEG recording and pre-processing

We analysed icEEG signals recorded in 3 right-handed men (24-39 years) (see Table 4-1) who were undergoing simultaneous intracranial EEG-fMRI from a group of 19. These patients were selected based on the on the low number of polyspikes and a high number of individual IEDs during the recording. In each patient there were between 31 and 84 implanted electrode contacts on configurations including grid electrodes, depth electrodes or both. The icEEG was pre-processed using the methodology described in Section 3.2 and the resulting EEG was band-pass filtered (2-70Hz).

4.2.2 IED detection and classification

IEDs were detected and classified by an EEG reviewer ('H1') for clinical purposes using *BrainVision Analyzer* (Brain Products, Germany) on a referential montage. During this procedure H1 placed a marker close to the negative/positive peak of each IED event (across the entire recording). The summary of IED detection and classification by H1 for each patient is provided in Table 4-2.

Table 4- 1| Patient diagnosis and implantation summary R: right, L: left, A: anterior, P: posterior

Patient	JR	IH	BS
Type of Epilepsy	FLE	FLE	FLE
Implantation Summary	L superior (SFG), middle (MFG) and inferior (IFG) frontal gyrus. L precentral gyrus. L central sulcus and part of postcentral sulcus. L superior frontal sulcus. L postcentral regions	L frontal lobe (laterally and inferiorly). L M (MFG) and I (IFG) frontal gyrus. L frontal pole	R A and P insula. R A (R ASMA) and P(R PSMA) supplementary sensorimotor areas. R A, M and P cingulum (P C)
Number of icEEG contacts (+ channel label)	One 8 x 8 contact grid (G). Two 4-contact depths (DA & DP). One 2 x 8 contact grid (GA)	One 8 x 8 contact grid (GA). One 2 x 8 grid (GD). Two 6-contact depths (DA & DP). Two 6-contact strips (GC & GB).	Two 6-contact depths (ASMA & PSMA). Three 8-contact depths (AC, MC & PC).

Table 4- 2| IED detection and classification summary for all patients

Patient	IED Class (Channels they occur in)	Number of IEDs detected	Number of channels	Class label
JR	G4, 5	70	2	B
	G12-15	30	4	C
	G4-6 + G12, 13 + G22-24 + DP2-4	60	11	E
	G12-15 + G21-24 + DP2-4	218	11	D
	G4-8 + G12-15 + G20-24 +G28-30 + DP2-4	212	20	A
IH	DA3-6	423	4	A
	DA4, 5 + GA51	261	3	B
	DA2-6 + GA49-54	208	11	D
BS	PSMA1-3	211	3	B
	ASMA1-3	46	3	C
	ASMA1-3 + PSMA1-3	476	6	A
	PC5, 6	150	2	F
	PC5, 6 + AI5, 6	150	4	E

4.2.3 Automated IED marker adjustment

We wanted to develop an algorithm that can automatically align an IED marker to the peak of the spiky component. This alignment signal would integrate information across the multichannel signal and provide a general solution to be used across the entire dataset. In this regard:

1) We developed an algorithm that incorporated the global field power (GFP)
2) We determined how far H1's marking was from the IED peak. This allowed us to identify an IED adjustment time-window length that can be integrated into the algorithm allowing its use for all IEDs across the entire dataset.

4.2.3.1 Max-GFP adjusted algorithm

The GFP was a measure selected for the purpose of this algorithm as it quantifies the strength of the voltage field potential at each time point by considering the data from all electrode pairs selected (Skrandies, 1990). It is calculated as the sum of the squared potential between all electrode pairs:

$$GFP = \sum_{i=1}(u_i - \bar{u})^2 \quad \text{(Eqn 4-1)}$$

where u_i = is the voltage at electrode *i*, $\bar{u}$ = voltage at the referential electrode. For each IED component we calculated the GFP for channels *i* marked by the clinician as being part of the event.

When calculating the GFP, voltage field potentials that have pronounced peaks result in a high GFP whereas voltage field potentials that have a flat baseline result in a low GFP (Brunet et al., 2011). Therefore, since the peak of the spiky component of an IED has a pronounced peak, the chosen method is based on the assumption that the maximum GFP within a specific time window corresponds to the peak of the spiky component.

The steps of the *max GFP-adjusted* algorithm are:

1) Apply a high pass filter (a second order Butterworth filter) set at 6Hz to suppress the slow wave of the IED.
2) Calculate the GFP.
3) The adjusted IED marker is set to the position of the GFP maximum (*max GFP-adjusted marker*) within a pre-specified time window (the IED adjustment time window).

The IED adjustment time window length is crucial for the above determination of the IED peak and its applicability across the entire dataset. In this regard it is important to determine how far H1's marking was from the IED peak and to determine the time window length based on these markings.

4.2.3.2 Determining the IED adjustment time window length

We applied our *max GFP-adjusted* algorithm with a generous time window length of +/- 20ms on a sample of 180 IEDs representing 6 classes from the data in the 3 patients: 2 classes per patient (one class involving ≤ 4 channels and the other class involving > 4 channels) and 30 IEDs selected per class. These were chosen to be as representative as possible of H1's temporal marking.

To determine the IED adjustment time window length that can be applicable across the entire IED dataset, we:

1) Calculated how far away H1's IED marking was to the peak of the spiky component (referred to as the *max GFP-adjusted* marker shift) for the first 30 correctly max-GFP adjusted IED markers per class (the marker adjustment shift was not accepted if the *max GFP-adjustment* occurred without the presence of an

IED; see Figure 4-1, Figure 4-2 and Figure 4-3 for an example of a *max GFP-adjusted* marker shift in the presence of an IED and Figure 4-4 for an example of a *max GFP-adjusted marker shift* without the presence of an IED).

2) Calculated the mean (SD) and determined the range of the max-GFP adjusted marker shift of all 180 IEDs
3) The IED adjustment time window length was set to 3 x SD

4.2.4 Defining the IED classification epoch time window length

The aim of this processing step is to determine an IED classification epoch time window as accurate as possible in order to have maximum information of the IEDs with the smallest possible time span to minimise the impact of noise. To do this we selected the IED in the channel in which the waveform was most prominent in an IED class (which we will refer to for the purpose of this process as *IED class channel*) of a small representative dataset of IEDs that were *max GFP-adjusted* from the previous section.

The IED classification epoch time window was determined by analysing the temporal and spectral characteristics of the *IED class channel* waveform using two methods:

1) By calculating the average IED waveform
2) By measuring the time-frequency characteristics of the IED waveform

4.2.4.1 Calculation of the average IED

To calculate the average IED waveform, the *max GFP-adjusted* IED class channels were segmented with a generous time window of +/- 250ms from the *max GFP-adjusted* IED marker. The average waveform was then displayed to represent the IED in the time domain with the aim of comparing the temporal characteristics of the IED (i.e. the duration of spiky component and duration of the slow wave) to the results of the spectral characteristics of the waveform.

4.2.4.2 Measuring the time-frequency characteristics of the IED waveform

To measure the time-frequency characteristics of the IED waveform, we calculated a normalised spectrogram using the following steps:

1. The *max GFP-adjusted* IED class channels were segmented using the same time window of +/- 250ms from the *max GFP-adjusted* IED marker. The signal was decomposed from the time domain to the frequency domain using Morlet wavelets (Rosa et al., 2010) to create a power spectrum. The power spectrum of

each IED within an IED class channel was calculated and averaged, creating an average IED spectrogram (see Figure 4-5a).

2. We calculated the average power spectrum of 500ms of 100 background epochs (where there are no IEDs occurring; these background epochs were manually selected) for the IED class channel (see Figure 4-5b).
3. The normalised power spectrogram was obtained by dividing the power of the average IED spectrogram with the power of the average background spectrum (see Figure 4-5d)

The IED epoch classification time window was determined by visually observing the time-frequency energy of the normalised signal (across all the normalised spectrograms) and seeing when the energy of the average signal decreases to baseline level.

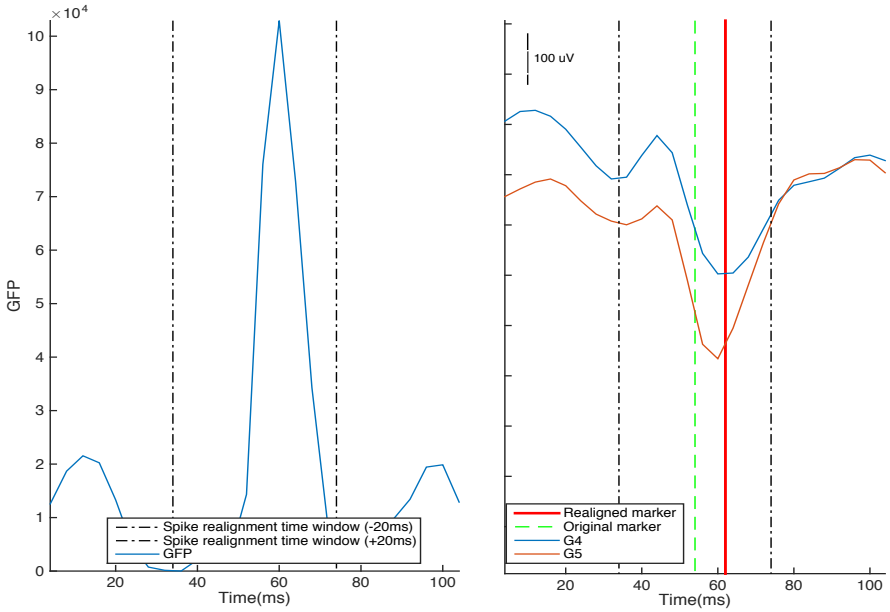

Figure 4- 1| Max GFP-adjusted marker for an IED event in class B, patient JR (a) GFP +/- 20ms around the original IED marker (b) EEG showing IED marker adjustment with regards to the maximum GFP +/- 20ms around the original IED marker. The *max-GFP adjusted* marker shift was 8ms

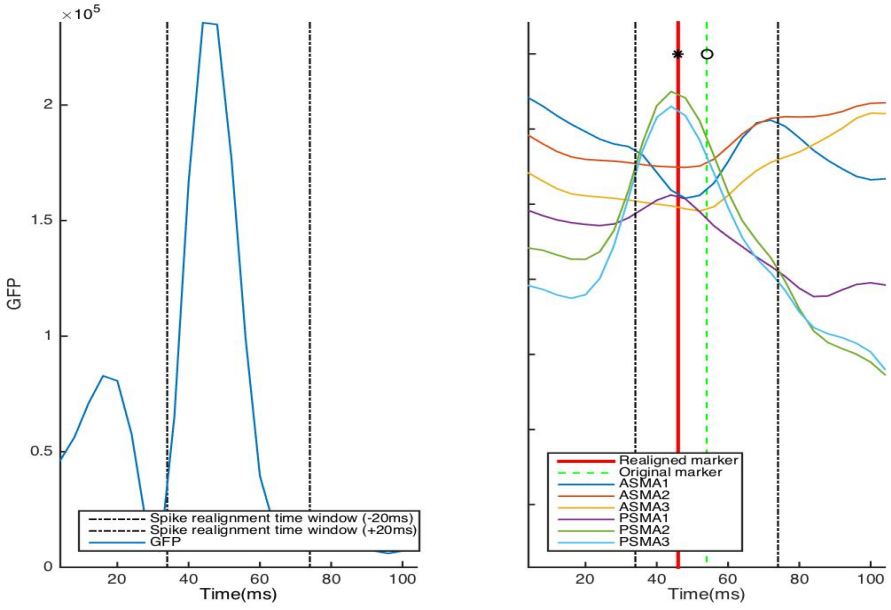

Figure 4- 2| Max GFP-adjusted marker for an IED event in class A, patient BS (a) GFP +/- 20ms around the original IED marker (b) EEG showing an IED marker adjustment with regards to the maximum GFP +/- 20ms around the original marker. The *max-GFP adjusted* marker shift was 8ms.

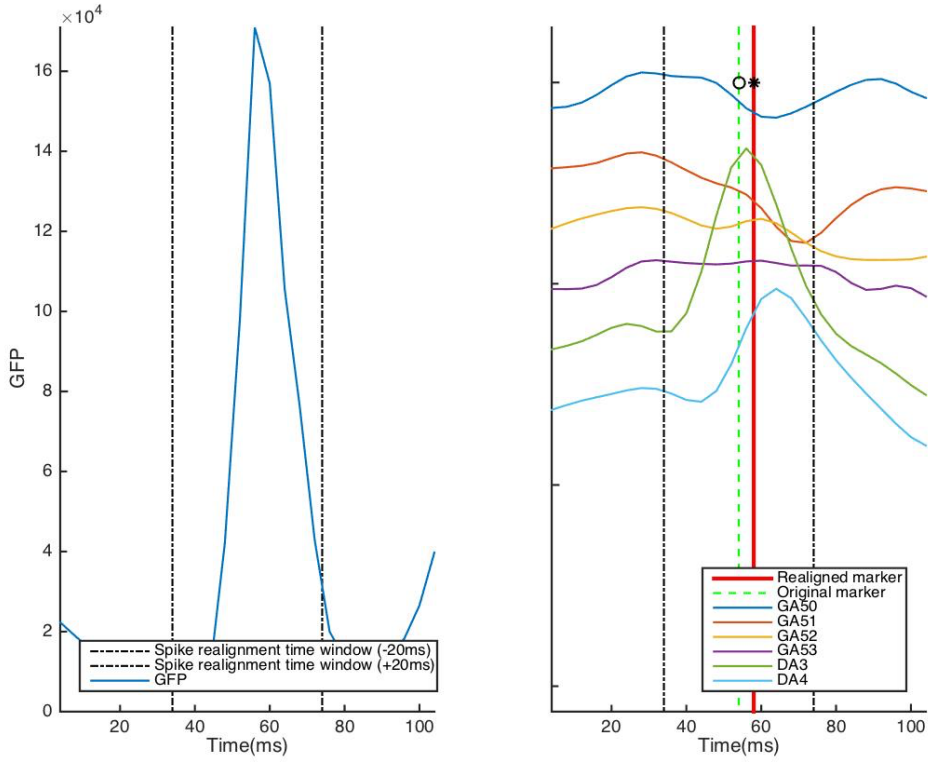

Figure 4- 3| Max GFP-adjusted marker for an IED event in class D, patient IH (a) GFP +/- 20ms around the original IED marker (b) EEG showing an IED marker adjustment with regards to the maximum GFP +/- 20ms around the original marker. The *max-GFP adjusted* marker shift was 4ms.

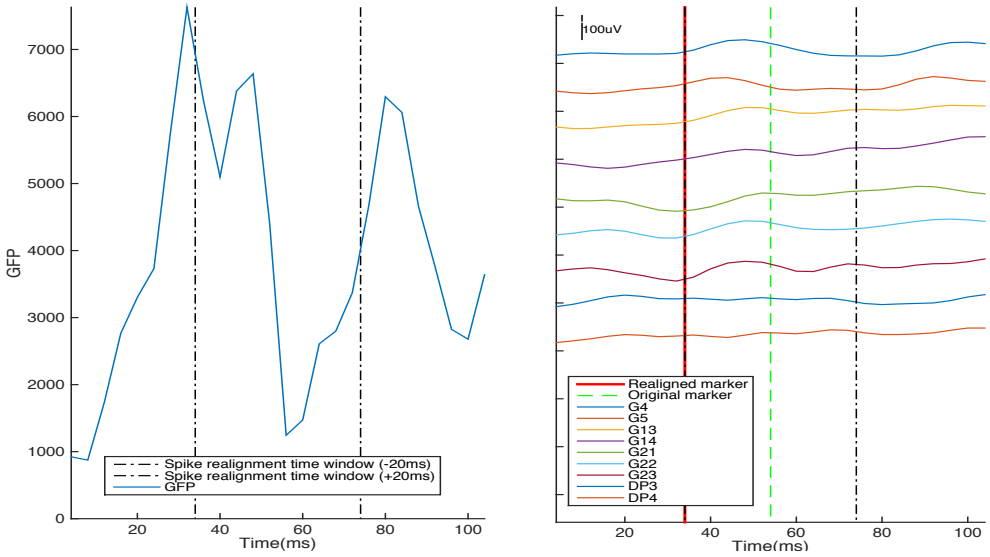

Figure 4- 4| Max GFP-adjusted marker for a non-IED event for an event in class A, patient JR (a) GFP +/- 20ms around the original IED marker (b) EEG showing IED marker adjustment with regards to the maximum GFP +/- 20ms around original IED marker

4.3 Results

4.3.1 IED adjustment time window length

The *max GFP-adjusted marker shift* values were obtained from H1's IED detection markings in class B and class A for patient JR, class A and class D for patient IH and class B and class A for patient BS (see Table 4-2). The mean (SD) of the max GFP-adjusted shift across all 180IEDs was 4.5(3.9) and the range was 0-12ms. Therefore, the IED adjustment time window length to be applied across the entire dataset is +/-12ms.

4.3.2 IED classification epoch time window

To determine the optimal IED classification epoch time window, the average IED and the time-frequency characteristics were measured in *max-GFP adjusted* IEDs that occurred in channel G4 and G5 for patient JR (class B), channel DA4 and DA5 for patient IH (class B) and channel PSMA 3 for patient BS (class A).

The time frequency energy of the normalised signal, for the spiky component of the IED in channel G4 and G5 for patient JR was around 21.7Hz (see figure 4-5d, f) and between 13-21.7Hz for channel DA4 and DA5 for patient IH (see Figure 4-6b, d) and channel PSMA3 for patient BS (see Figure 4-6b). The spiky component had a high intensity signal of around 100ms (50ms pre peak and 50ms post peak) for all 3 patients. There was a high intensity signal at a lower frequency for the IED in channel G4 and G5 for patient JR (13Hz; 100ms pre and 150ms post) (see Figure 4-5f) and channel DA5 for patient IH (4.7Hz; 100ms pre and 150ms post) (see Figure 4-6d) characteristic of the slow wave as seen in the average IED (see Figure 4-5c, e for patient JR and Figure 4-6c for patient IH). Channel PSMA3 for patient BS also had a high intensity signal at a lower frequency (see Figure 4-7b) that was due to the width of the IED (see Figure 4-7a). Therefore, the normalised spectrograms indicate that the duration of the spiky component of the IED is generally 100ms (50ms pre peak of the spiky component and 50ms post peak) and the slow wave extends to 150ms after the spiky component.

Based on the above results we defined an optimal IED classification epoch time window as 100ms pre peak and 200ms post peak of the spiky component to give flexibility for unseen data.

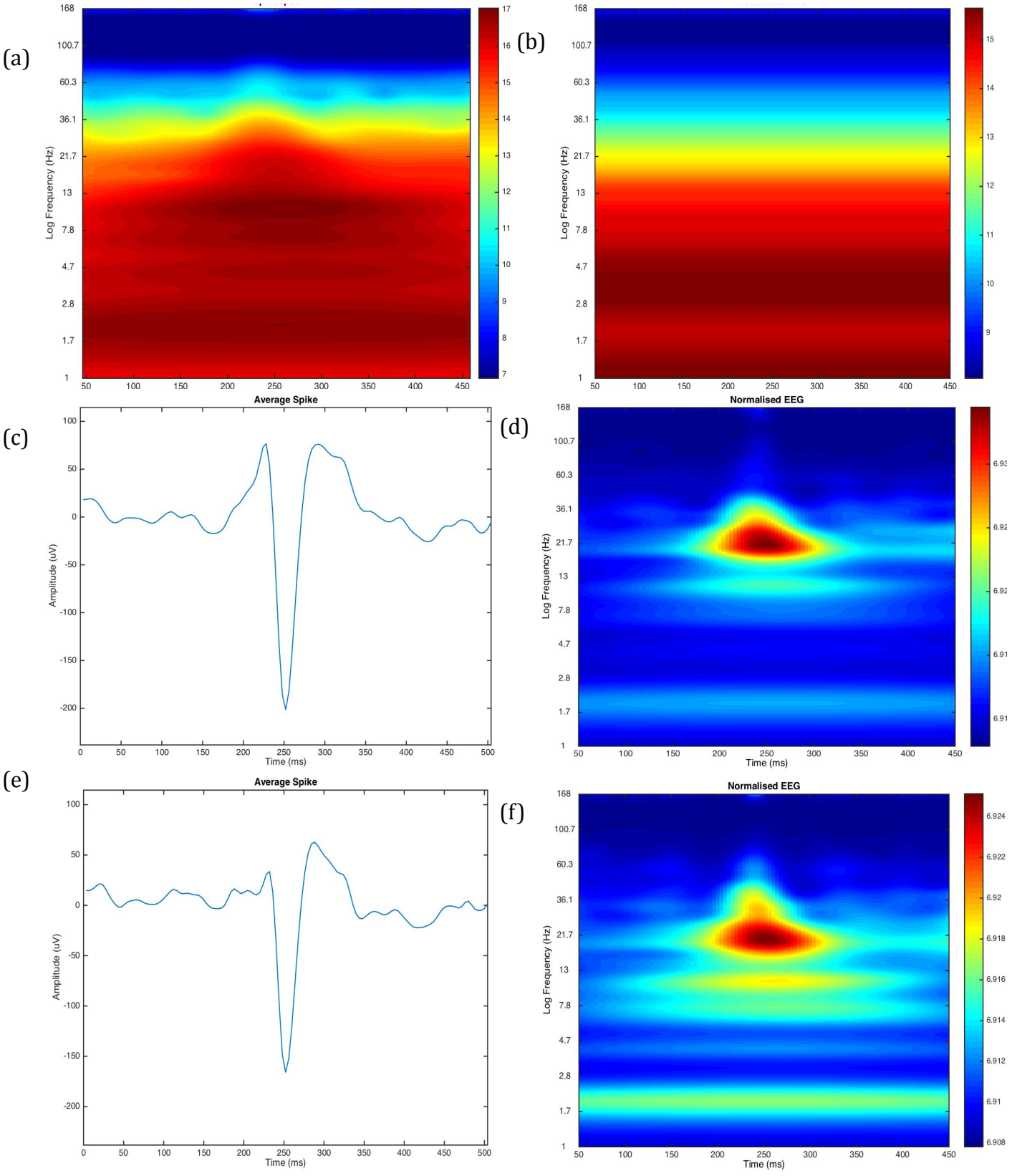

Figure 4- 5| Power spectrum and average IED summary for patient JR class B channel G4 and G5 (a) Average spectrogram (400ms) for all IEDs occurring in channel G4 (b) Average background spectrogram (400ms) for non-IED activity in channel G4 (c) Average IED from channel G4 (d) Normalised spectrogram for IEDs occurring in channel G4 (e) Average IED from channel G5 (f) Normalised spectrogram for spikes occurring in channel G5

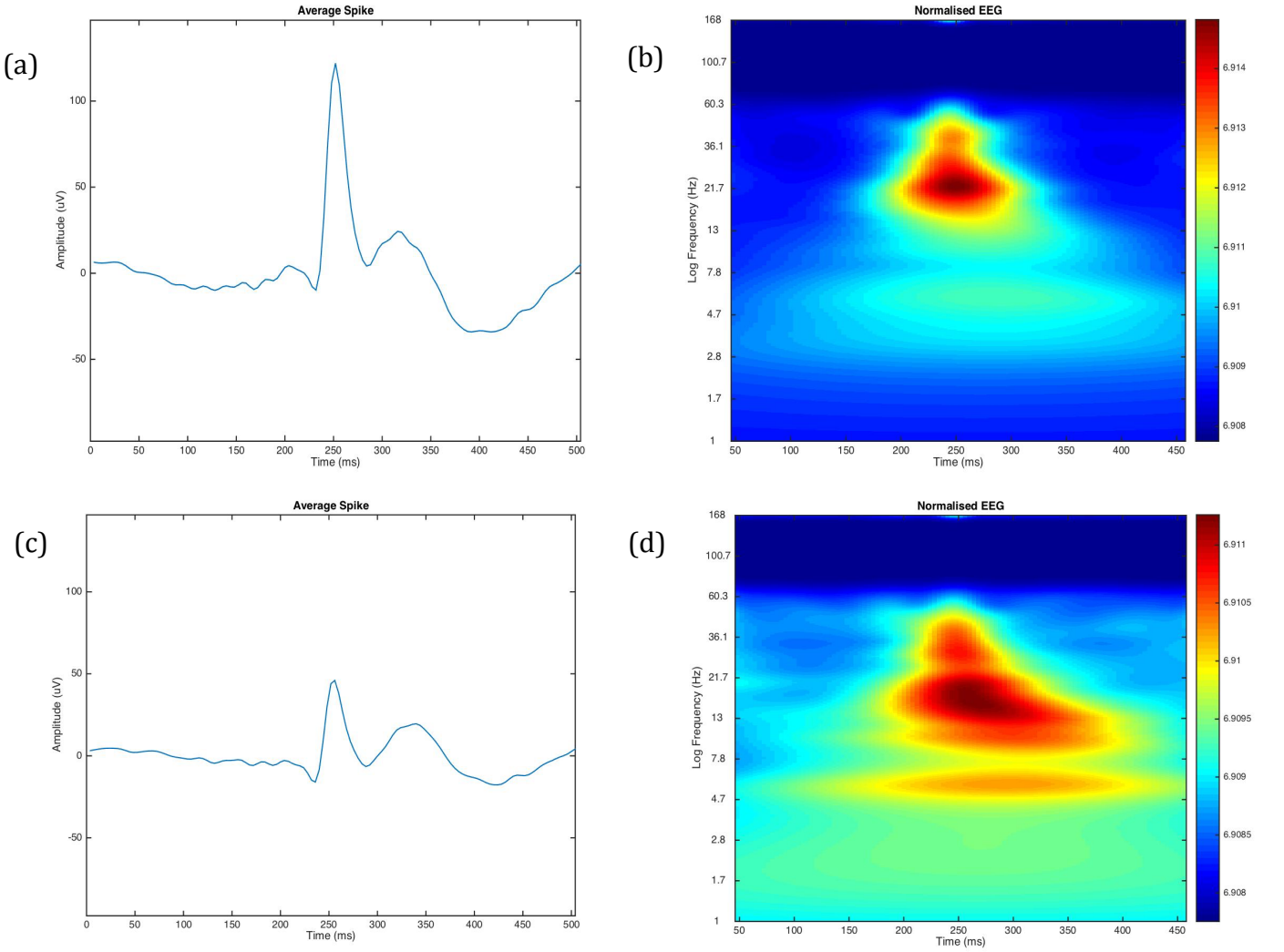

Figure 4- 6| Power spectrum and average IED summary for patient IH class B channel DA4 and DA5 (a) Average IED from channel DA4 (b) Normalised spectrogram for IEDs occurring in channel DA4 (c) Average IED from channel DA5 (d) Normalised spectrogram for IEDs occurring in channel DA5

(a)

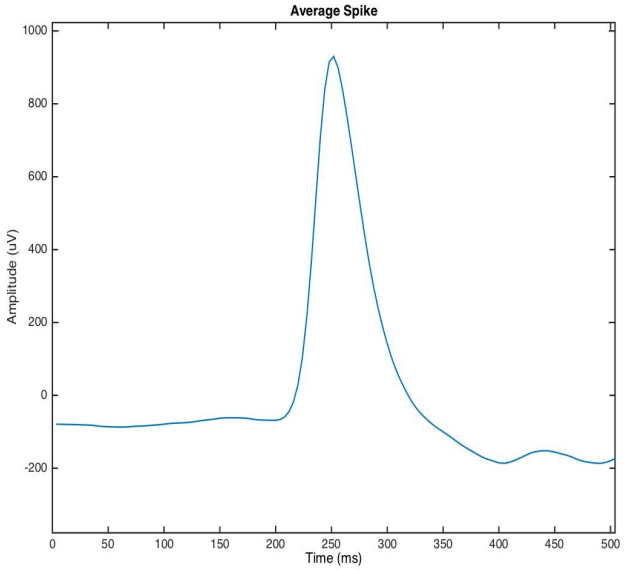

(b)

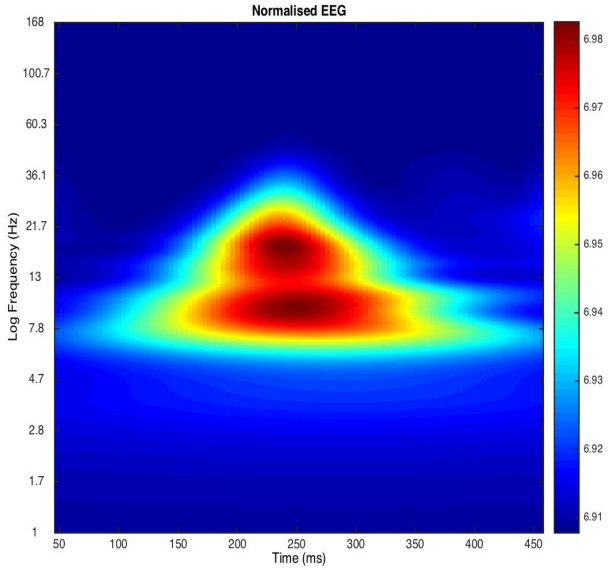

Figure 4- 7| Power spectrum and average IED summary for patient BS class A channel PSMA3 (a) Average IED from channel PSMA3 (b) Normalised spectrogram for IEDs occurring in channel PSMA 3

4.4 Discussion

Our aim was to 1) develop an automated algorithm that can align an IED marker to the peak of the spiky component, whilst integrating information across the multichannel signal that can be applied to the entire IED dataset and 2) to define an optimal IED classification epoch time window.

We developed an algorithm that incorporated the GFP of all the channels selected and determined how far H1's IED peak marking was in order to define a time window that can be applicable to the entire dataset. In this regard our results indicate that a time window of +/- 12ms can be used across the entire dataset. In relation to the IED classification epoch time window, we chose an optimal approach based on analysing the time frequency characteristics of a representative sub-sample of the data. Our results show that the most optimal time window is 100ms pre peak and 200ms post peak of the spiky component.

In the study carried out by Pedreira et al. (2014), for each IED detected, they automatically aligned the original IED marker to the peak of the spiky component, for each channel that showed an IED waveform, independently (Pedreira et al., 2014). However, this can be very time consuming and can result in the loss of temporal information between channels. In this study, we used the GFP to align H1's marking to the peak of the spiky component. The GFP is a measure that integrates information across multiple channels (Skrandies, 1990). Therefore, in comparison to Pedreira et al. (2014), where each channel showing an IED was independently aligned to the peak, our algorithm is able to maintain the temporal relationship between channels (see Figure 4-3 for an example) and be less time consuming. Furthermore, by defining a time-window that can be used across the entire dataset, the process of adjusting the original marker to the peak of the spiky component is fully automated.

Regarding the IED classification epoch time window, Pedreira et al. (2014) determined this by using a trial and error method with a training dataset. By measuring the time-frequency characteristics of a sub-sample of IEDs, we were able to provide a more scientifically accurate methodology for the definition of the IED classification epoch time window.

The results obtained in this study were carried out on a representative subset of our data to make it possible to determine the IED marker adjustment time window and the IED

classification epoch time window by checking each IED. Furthermore, this data subset was also selected to partly reduce the effects of H1's classification (bias) on the automated classification due to these markings being used in the rest of the thesis. Future work can involve increasing the sample size of the dataset and further optimising the max GFP-adjusted algorithm by including the temporal derivative in the algorithm.

4.5 Conclusion

We have developed an optimal pre-processing pipeline for IED classification using Wave_clus. This involved developing an algorithm that automatically adjusts H1's IED marking to the peak of the spiky component, and defining an optimal IED classification epoch time window based on empirical evidence. The quality of the results warrant the use of the *max GFP-adjusted* algorithm and the optimal IED classification time window in pre-processing steps for WC classification to the rest of our dataset as demonstrated in the following two chapters.

CHAPTER 5: VALIDATING WAVE_CLUS BY COMPARISON WITH MULTIPLE EEG REVIEWERS§§§

This chapter is based on validating Wave_clus as an automated icEEG IED classifier using a novel validation scheme. This study was carried out on a select number of individual IEDs detected by EEG reviewer 'H1', which were then automatically classified using WC. To validate WC I compared the automated IED classification to that of multiple EEG reviewers. First, I determined whether WC-human agreement variability falls within inter-reviewer agreement variability by calculating the variation of information for each classifier pair and quantifying the overlap between all WC-reviewer and all reviewer-reviewer pairs. Second, I compared WC and EEG reviewers' IED identification and individual IED class labels visually and quantitatively.

§§§ This chapter was adapted from Sharma, N.K., Pedreira, C., Centeno, M., Chaudhary, U.J., Wehner, T., França, L.G., Yadee, T., Murta, T., Leite, M., Vos, S.B. and Ourselin, S., 2017. A novel scheme for the validation of an automated classification method for epileptic spikes by comparison with multiple observers. *Clinical Neurophysiology*, *128*(7), pp.1246-1254.

5.1 Motivation

Validating an automated algorithm requires a gold standard to which one can compare its performance. Due to the lack of a gold standard as to what constitutes an IED, the majority of automated IED detection algorithms use the combined opinions (e.g. consensus or majority) of a group of expert EEG reviewers (Brown et al., 2007, Barkmeier et al., 2012, Halford et al., 2013, Gaspard et al., 2014, Janca et al., 2015) as to what maybe called a silver standard. This allows for the calculation of the sensitivity and other performance metrics such as the precision of the algorithm (Brown et al., 2007, Barkmeier et al., 2012, Gaspard et al., 2014, Janca et al., 2015). Pedreira et al. (2014) demonstrated the successful use of an automated neuronal spike classification algorithm (WC) (Quian Quiroga et al., 2004), to classify IEDs on scalp EEG for the purpose of modelling the concurrently acquired functional MRI. In Chapter 4, we optimised the pre-processing steps for WC IED classification to our icEEG IED dataset. However, to our knowledge no formal comparison of automated vs multiple human observer classification of IEDs on icEEG has been published to date.

Our aim was to compare human expert IED classification as it is performed in normal ('optimal') conditions against the automated classification method to be used with WC. Our approach targets the following questions:

- Does WC-human epileptic spike classification agreement variability fall within inter-human classification agreement variability?
- Looking at the classification labels (or clustering groups) of individual spikes; are WC results similar to those of human observers?

To validate this framework we used data from 5 patients reviewed by 3 human observers for the comparison with WC. We hypothesise that WC can produce similar IED classification results to that of human EEG reviewers whilst also providing additional information.

5.2 Data and Methods

5.2.1. Patients, icEEG recording and pre-processing

We analysed icEEG signals recorded in 5 right-handed men (24-39 years) who were undergoing simultaneous intracranial EEG-fMRI (see Table 5-1). The five patients were selected based on the small number of polyspikes observed during the recording. The icEEG recording obtained during the simultaneous icEEG-fMRI study was used since we ultimately want to apply WC in the analysis of icEEG fMRI data however, no fMRI data was analysed for the purpose of this study.

In each patient there were between 31 and 84 implanted electrode contacts on configurations including grid electrodes, depth electrodes or both. The icEEG was pre-processed using the method described in Section 3.2 and was band-pass filtered (2-70Hz). The same referential montage was used for all 4 EEG reviewers.

Table 5- 1| Patient implantation summary and the channels of interest selected for all patients. R: right, L: left, A: anterior, P: posterior

Patient	JR	IH	BS	MB	GC
Type of Epilepsy	FLE	FLE	FLE	TLE	TOLE
Implantation Summary	L superior (SFG), middle (MFG) and inferior (IFG) frontal gyrus. L precentral gyrus. L central sulcus and part of postcentral sulcus. L superior frontal sulcus. L postcentral regions	L frontal lobe (laterally and inferiorly). L M (MFG) and I (IFG) frontal gyrus. L frontal pole	R A and P insula. R A (R ASMA) and P(R PSMA) supplementary sensorimotor areas. R A, M and P cingulum (P C)	R and L amygdalae (R A). R and L hippocampi.	Lateral temporal. Temporo-occipital junction.
Number of icEEG contacts (+ channel label)	One 8 x 8 contact grid (G). Two 4-contact depths (DA & DP). One 2 x 8 contact grid (GA)	One 8 x 8 contact grid (GA). One 2 x 8 grid (GD). Two 6-contact depths (DA & DP). Two 6-contact strips (GC & GB).	Two 6-contact depths (ASMA & PSMA). Three 8-contact depths (AC, MC & PC).	Five 6-contact depths (LA, LAH, LPH, RA & RH)	One 4 x 8 grid (GA). One 4 x 5 grid (GP). Three 6-contact strips (SAT, SMBT & SPBT).
Channels of Interest	G4 G5 G13 G20 G21 G22 G23 G29 DP2 DP3	GA50 GA51 GA52 GA53 DA4 DA5	ASMA1 ASMA2 ASMA3 PSMA1 PSMA2 PSMA3 PC4 PC5 AI5 AI6	LAH1 LAH2 LPH1 RA1 RA2 RA3 RH1	GA1 GA2 GA9 GA10 GA11 GA17 GA18 DH1 DH2 SAT3 SAT4 SPBT4 SPBT5 SPBT6

5.2.2 IED detection

The 5 icEEG recordings were inspected by EEG reviewer 'H1' for clinical purposes using *BrainVision Analyser* (Brain Products, Germany). During this procedure H1 placed a marker close to the negative/positive peak of each IED event (across the entire recording) that had a single sharp component. We then randomly selected 100 IEDs, using a random number generator, from each recording for this study (see Figure 5-1; step 1).

5.2.3 IED classification by human observers (H2, H3 and H4)

Reviewers H2 (10 years of experience in icEEG interpretation), H3 (4 years of experience in icEEG interpretation) and H4 (2 years of experience in icEEG interpretation) independently classified the IED events selected by H1 through visual inspection of the waveforms in a 300ms time window using BrainVision Analyzer. H2-4 performed the classification by visualizing the EEG activity in all recorded channels, in order to replicate their standard modus operandi. For each patient they were asked to classify the events into IED classes or as non-IEDs. H2-4 were free to define and use as many IED classes as they felt appropriate for each recording. Of the three EEG reviewers, two (H2 and H3) were trained at the same institution. Implantation diagrams, showing the position of the electrodes in relation to the brain, were provided (see Figure 5-2 for an example).

5.2.4 Automated IED classification (WC)

The automated classification method Wave_clus is a modification of the one described in Pedreira et al. (2014) and summarised in a flow chart (see Figure 5-1, step 2). First, between 8 and 14 channels of interest were selected for each patient based on channels in which the IEDs were noted in the clinical EEG report as being most prominent and frequent. Second, we modified the IEDs' temporal marking (by H1) by automatically adjusting them to the peak of the spiky component across the channels of interest. The IEDs were segmented in 300ms epochs around the peak of the spiky component (100ms pre-peak to 200ms post-peak) and concatenated across the channels of interest to form meta-IEDs (Pedreira et al., 2014) (see Figure 5-1; step 2)[12]. WC was then used to perform automated classification on the meta-IEDs similarly to our previous work (Pedreira et al., 2014). Based on the morphology and distribution of the IEDs, the algorithm automatically determined the number of classes per case and the events assigned to

[12] The code for these steps have been uploaded on to github: https://github.com/nirajsharma1/tyclus

them. Then, the user performed a visual verification of the final classes obtained; including some events which were labelled as 'non-IED'.

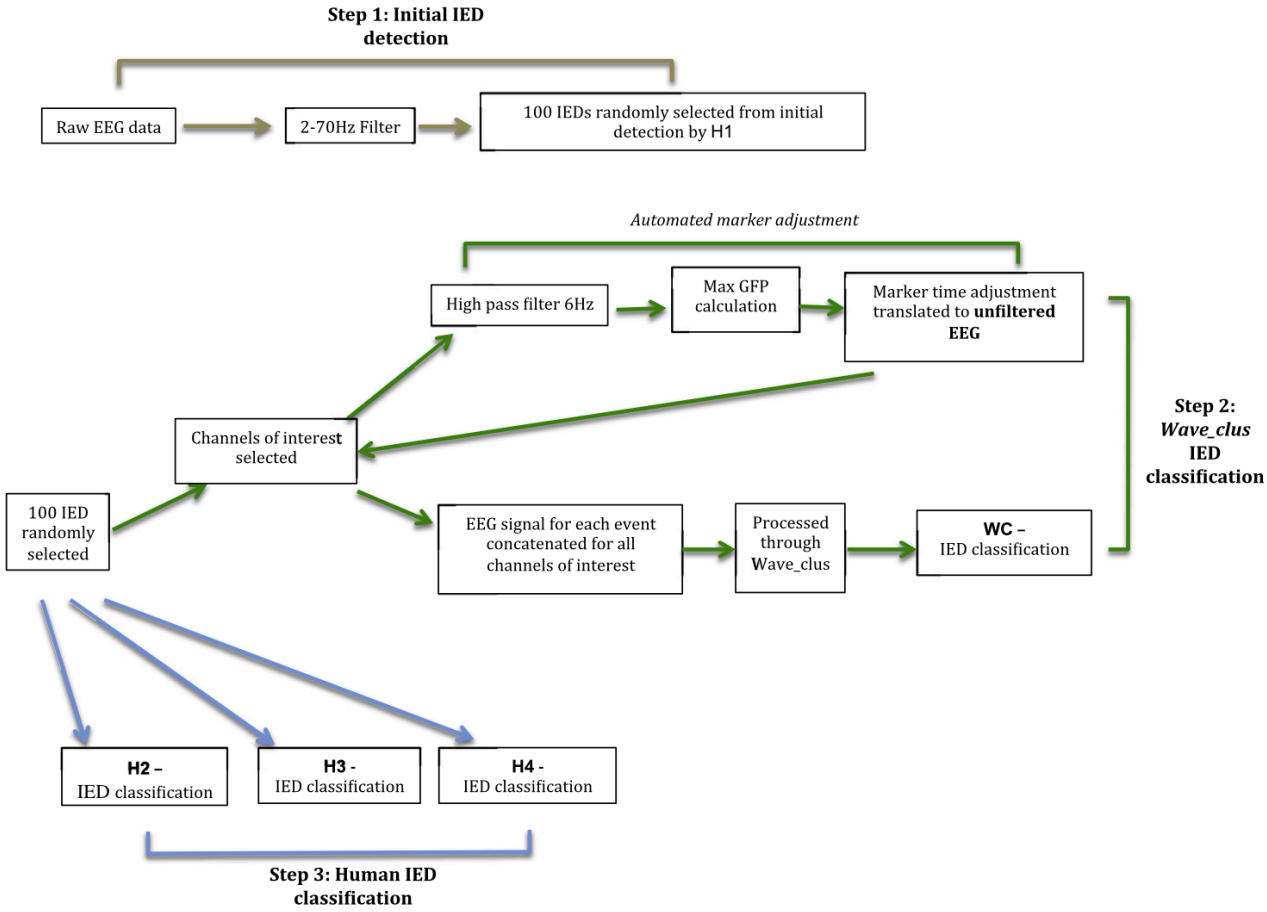

Figure 5- 1| EEG reviewer and WC classification: Step 1: Initial IED detection of 100 IEDs carried out by H1. Step 2: The 100 IEDs detected by H1 are classified by Wave_clus. This involves selecting channels of interest and adjusting the marker to the peak of the spiky component of the IED according to the GFP. Step 3: The same set of 100 IEDs detected by H1 are independently classified by 3 EEG reviewers H2, H3 and H4. These three steps are carried out for all patients

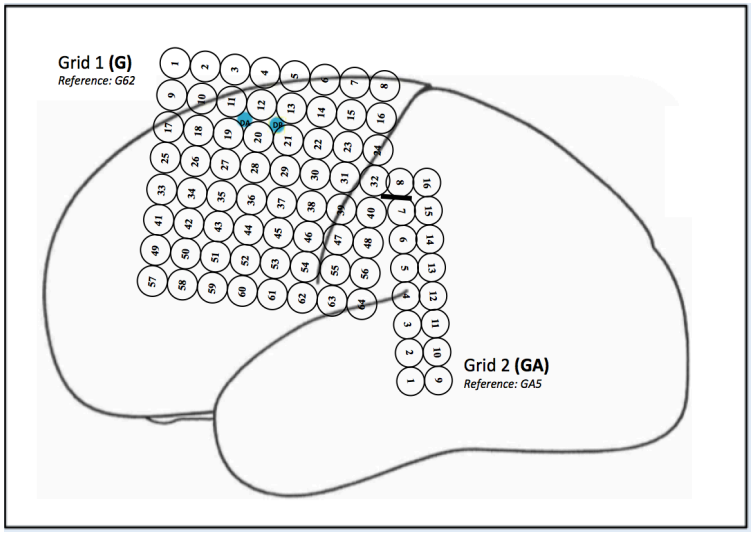

Figure 5- 2| Schematic of implanted electrode map for patient JR. Grid G: 8x8 lateral frontal grid; Grid GA: 2x8 grid covering the postcentral regions located over the; 4 contact depth electrode DA and DP targeting the lesion deeper in the superior frontal gyrus

5.2.5 Automated IED classification validation

We wanted to answer the question: can the results of the automated classification be distinguished from those obtained from humans? More specifically, we compared the two types of IED classification in two ways: first, we determined whether WC-human reviewer agreement variability falls within inter-human reviewer agreement variability; second, we compared *Wave_Clus* and human reviewers' classifications in terms of comparing IED identification and classification between *Wave_Clus* and all H reviewers.

5.2.5.1. Does WC-Human IED classification variability fall within inter-human variability?

5.2.5.1.1 Variation of information (VI)

We compared Wave_clus-human classification agreement variability to inter-human classification variability at a summary level. To this effect we calculated the variation of information (VI) between classifications in a pair-wise fashion. The variation of information is a general method to assess the relationship (distance) between two classifications (partitions) of elements (IEDs in this case) (Meila, 2007). One can quantify the variation of information using the following equation:

$$VI(\mathrm{X};\mathrm{Y}) = -\sum_{i,j} r_{ij}\left[\log 2\left(\frac{r_{ij}}{p_i}\right) + \log 2\left(\frac{r_{ij}}{q_j}\right)\right] \qquad \text{(Eqn 5-1)}$$

where p_i = number of IEDs in class i for X, q_j = number of IEDs in class j for Y, r_{ij} = number of IEDs classified as i by X and j by Y. Therefore, for each classifier pair *VI* quantifies how similar the classification results were. Two classifications with perfect agreement have a VI value of 0. In order to determine a threshold of similarity between two classifications, we generated randomised surrogate classifications for 50 artificial observers (see Appendix A – A.M); two classifications were considered similar if their VI value was below the mean of VI minus 2 SD from the randomised surrogate sample.

To compensate for the small sample size, non-parametric bootstrapping (Singh and Xie, 2008) was used on the 100 IEDs for each classification pair. As a result, 1000 *VI* values were calculated for each pair.

To compare the performance between WC and H classifications, the *VI* values for all possible WC-H pairs (WC-H2, WC-H3, WC-H4) were merged to represent *Wave_Clus* classification agreement as a whole (WC_all), and all possible human expert classification agreement H-H pairs (H2-H3, H2-H4, H3-H4) were merged to give an overall human classification agreement (H_all). If *Wave_Clus* is to be applied practically then it is probably preferable that it performs in a way that is indistinguishable from humans, and therefore, WC_all and H_all distribution should overlap. We calculated the Bhattacharyya coefficient (Kailath 1967, Comaniciu et al., 2000) to measure the percentage of the distribution overlap between WC_all and H_all.

5.2.5.2 Does Wave_Clus produce similar IED marking and classifications to H reviewers?

5.2.5.2.1 IEDs vs non-IEDs

First, we considered an event labelled as an IED by reviewer H1 to be a "true" IED if at least two of the reviewers, H2-4, labelled it as an IED. If two reviewers of H2-4 labelled an event as a non-IED, we considered it a non-IED for the purpose of this study (Barkmeier et al., 2012; Gaspard et al., 2014, Janca et al., 2015). Second, we calculated the sensitivity and the specificity for each classifier (H classifiers and *Wave_Clus*). Then we compared *Wave_Clus* sensitivity and specificity with the ones obtained from the 3 reviewers H2, H3 and H4. We used the pair-wise Cohen's Kappa statistic to assess the inter-rater agreement for all possible H classifier pairs, with a kappa value > 0.4 noted as a high inter-rater agreement (Zijlmans et al., 2008).

5.2.5.2.2 Visual comparison of IED classes and classification overlap

In order to compare the similarity between WC and H IED classes, the average of the IEDs (over 200ms) in each WC class was calculated and plotted (see Figure 5-3). The average WC class was compared visually to the classes of each EEG reviewer. In addition to this, the agreement $A_{i,j,}$ between WC class *i* and H class *j* was calculated as a percentage (the classification overlap):

$$A_{ij}(WC;H) = \left(\frac{r_{ij}}{|WC_i|}\right)\times 100 \quad \text{(Eqn 5-2)}$$

where $|WC_i|$ is the number of IEDs in WC class i , r_{ij} = the proportion of IEDs labelled as WC_i and H_j. The H class with the greatest agreement with each WC class was noted.

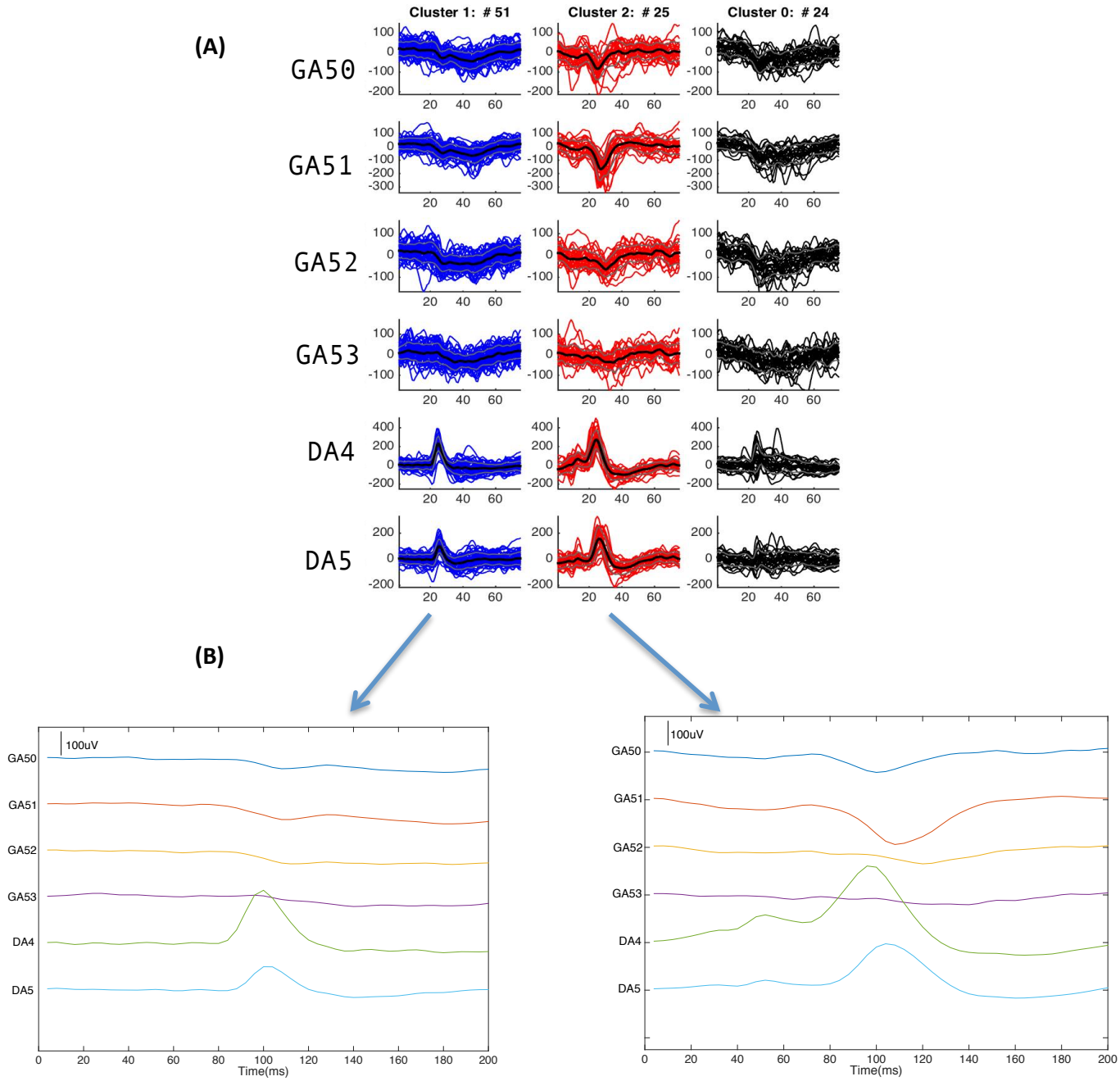

Figure 5- 3| *Wave_clus* clustering results for patient IH. (A) Output of *Wave_clus* classification. (B) Average waveform of the IED classes over 200ms

5.3 Results

5.3.1 IED classification by human observers (H2, H3 and H4) and WC

The agreement between different classifiers (either H or WC) was not perfect and no two classifications were identical in any given patient. Furthermore, the number of IED classes varied across patients (range: 1-8). Across the group, *Wave_clus* identified 15 classes, 23 classes were identified by H2, 20 classes were identified by H3 and 24 classes were identified by H4 (see Table 5-2).

Table 5- 2| Number of classes assigned by WC, H2, H3 and H4

Patient / EEG Classifier	JR (# IED classes + # non-IED)	IH (# IED classes + # non-IED)	BS (# IED classes + # non-IED)	MB (# IED classes + # non-IED)	GC (# IED classes + # non-IED)
WC	3 + 1	2 + 1	2	5 + 1	3
H2	8 + 1	1 + 1	3	6 + 1	5
H3	6 + 1	1 + 1	3	6 + 1	4
H4	6 + 1	4 + 1	3	5 + 1	6

5.3.2 Automated IED classification validation

We present here the results of the analysis for the 3 H observers and WC classifications, following the procedure described in the methods section to address the questions: *Does WC-Human IED classification variability fall within inter-human variability?* And *Does Wave_clus obtain similar IED marking and classifications to H reviewers?*

5.3.2.1 Does WC-Human IED classification variability fall within inter-human variability?

The mean (SD) for the randomly generated VI values was 408.60(49.29). Looking at the classification agreement at the individual classifier pair-wise level, the overlap values ranged between [239-288] for patient JR, [121-222] for patient IH, [80-135] for patient BS, [169-211] for patient MB and [77-167] for patient GC (see Table 5-3). The *VI* distribution for each classification pair was significantly different from the randomly generated distribution for both H-H pairs and WC-H pairs (p<0.05; see Table 5-3).

Figure 5-4 shows the *VI* results for each patient for WC_all and H_all. The *VI* distribution overlap between WC_all and H_all were: 93.4% for patient JR, 66.3% for patient IH, 58% for patient BS, 96.4% for patient MB, 81.1% for patient GC (see Table 5-3 and Figure 5-4). Therefore, WC classification falls within inter-human variation.

Table 5- 3| Variation of information for all classified pairs and the VI distribution overlap between WC_all and H_all for all patients

Patient / Classification pair	JR	IH	BS	MB	GC
WC-H2	288.56**	220.21**	112.1**	211.44**	109.28**
WC-H3	239.82**	162.54**	117.49**	169.51**	77.58**
WC-H4	276.13**	206.6**	135.97**	179.87**	146.08**
H2-H3	252.06**	121.74**	83.61**	172.49**	128.2**
H2-H4	262.3**	222.14**	84.2**	188.9**	167.29**
H3-H4	256.17**	134.91**	80.28**	169.75**	129.63**
Overlap (%) (WC_all/H_all)	93.4	66.3	58	96.4	81.1

** Significance at $p<0.05$

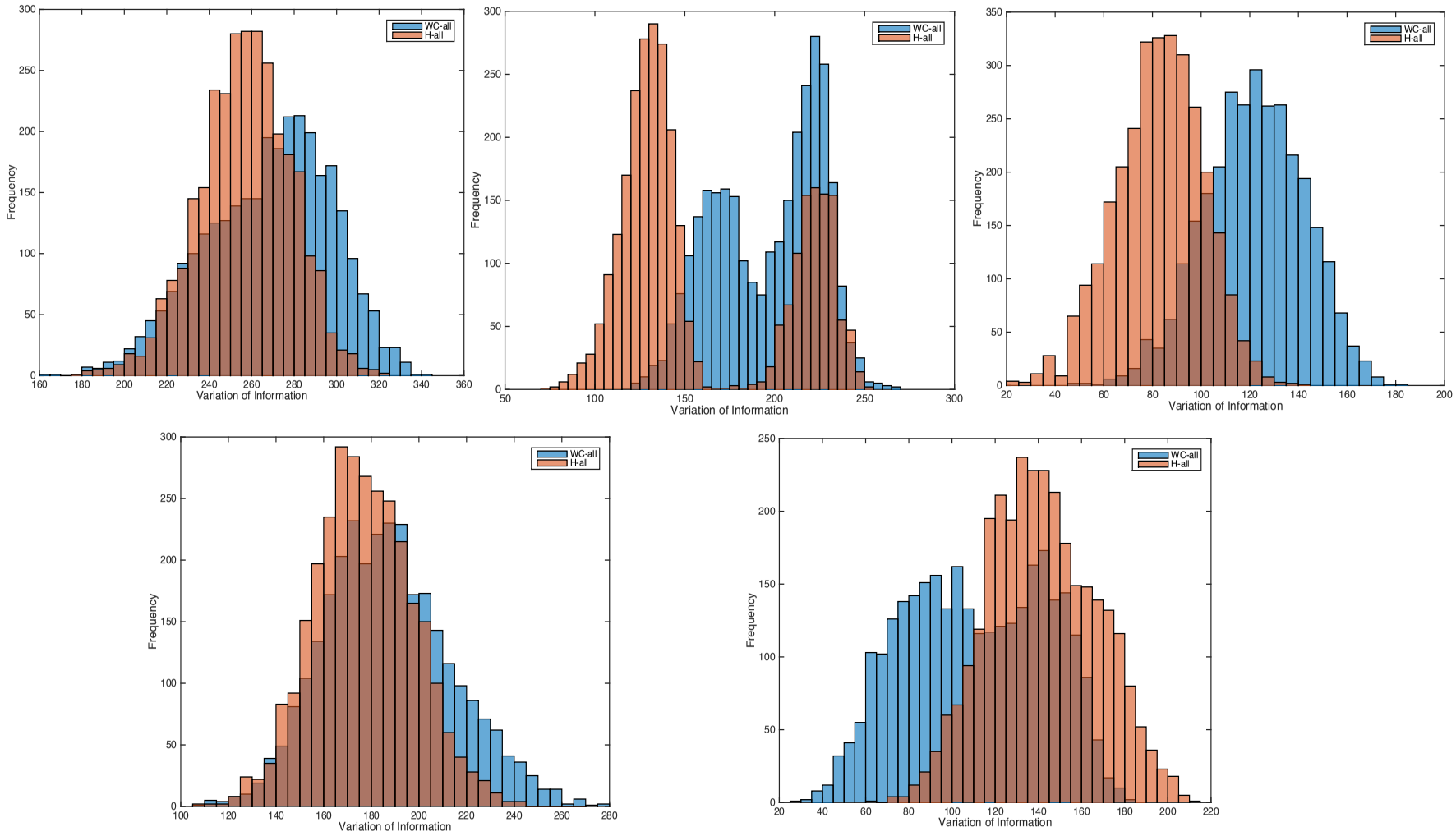

Figure 5- 4| VI distribution for WC_all (blue) and H_all (orange). 1st row (left to right): Patient JR, IH & BS; 2nd row (left to right): Patient MB and GC. The values for the null distribution are: mean = 408.60 and SD = 49.29.

5.3.2.2 Does Wave_clus obtain similar IED marking and classifications to H reviewers?

5.3.2.2.1 Sensitivity and specificity: IED vs Non-IEDs

Across the group, IED detection sensitivity was in the range [0.76-1] for WC, [0.62-1] for H2, [0.91-1] for H3, [0.95-1] for H4 (see Figure 5-5). At the level of individual patients, sensitivity was in the range [0.92-0.95] for patient JR, [0.8-1] for patient IH, [0.62-0.99] for patient BS and 1 for patient MB and GC (see Figure 5-5).

Across the group, IED detection specificity was in the range [0.29-0.87] for WC, [0.8-1] for H2, [0.38-1] for H3 and [0.38-0.93] for H4 (see Figure 5-6). At the level of individual patients, specificity across classifiers was in the range [0.38-0.9] for patient JR, [0.8-1] for patient IH and [0.29-1] for patient BS. There were no specificity values for patient BS and GC due to none of the events being identified as a non-IED. Of note, for patient JR, the specificity of WC was 0.38 vs 0.9 for H2, which is the largest discrepancy (see Figure 5-6).

In summary, WC sensitivity is high and similar to that of the Human reviewers while its specificity is similar to that of Human reviewers for 2/3 patients.

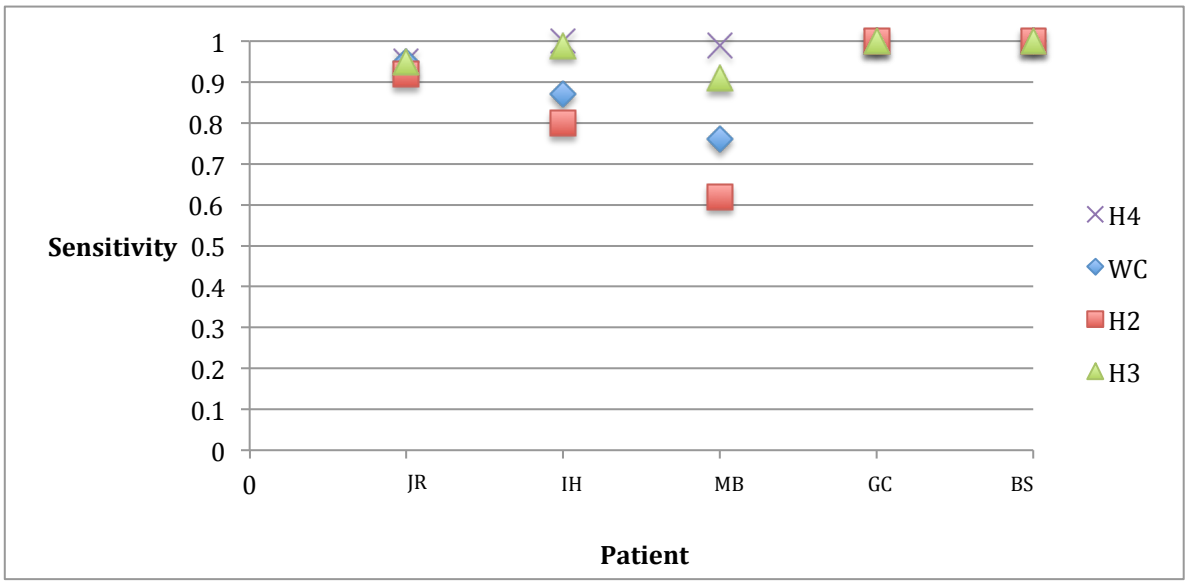

Figure 5- 5| Sensitivity of IED marking of WC and H2, H3 and H4 for all 5 patients

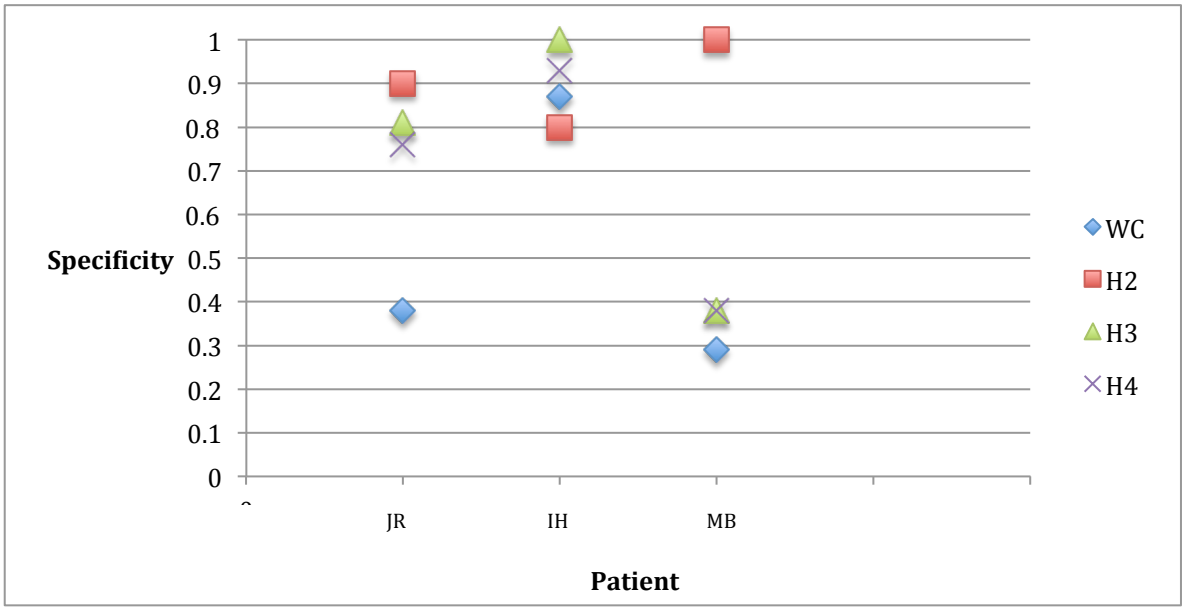

Figure 5- 6| | Specificity of IED marking of WC and H2, H3 and H4 for patient JR, IH and MB

5.3.2.2.2 Visual comparison of IED classes and classification overlap: Case reports

In all patients, visual inspection of the class representative IEDs allowed us to find meaningful correspondences between the majority of WC and H classes. This was reflected in the classification overlap values (see Appendix A Tables A2-6). The results for two patients (patient IH and BS) are summarised below. Patient IH was chosen to illustrate WC's capacity to identify an IED class not previously identified by H2 and H3. The results for patient BS were chosen as an illustration of good classification agreement between WC and all 3 H reviewers. The case reports for the other three patients can be found in Appendix A (A.CR).

Case reports

Patient IH

WC identified three classes, H2 and H3 identified two and H4 identified five; all four classifiers identified a non-IED class (see Table 5-2). The numbers of events assigned to the non-IED class were 24 for WC, 29 for H2, 16 for H3 and 14 for H4 (see Table 5-4).

WC Class A

Fifty-one IEDs were assigned to class WC_A and involved channels DA4 and DA5 which is identical to H2_A, H3_A and H4_A (see Table 5-4).

The visual similarity between these classes was further reflected in the classification overlap where WC_A agreed the most with H2_A (71%), H3_A (94%) and H4_A (78%) (see Appendix A Table A3).

WC Class B

Twenty-five IEDs were assigned to class WC_B and involved channels DA4 and DA5 with the field extending to channel GA51 (see Table 5-4).

This class involved similar channels for H4_B and _C for reviewer H4 but did not correspond to any of the classes for reviewers H2 and H3.

The visual similarity between WC_B and H4_B and H4_C was further reflected in the classification overlap where WC_B agrees equally with H4_B (48%) and H4_C (48%) (see Appendix A Table A3).

The visual comparison and classification overlap indicated that WC classes did not correspond to H4_D.

Patient BS

WC identified two classes, and H2, H3 and H4 identified three classes. None of the classifiers had a non-IED class (see Table 5-2).

WC Class A

Thirty-nine IEDs were assigned to class WC_A and involved the channels PSMA2 PSMA3. The channels involved in this class were identical to those in classes H2_A, H3_B and H4_A (see Table 5-4).

This visual similarity was further reflected in the classification overlap where WC_A agreed the most with H2_A (79%), H3_B (64%) and H4_A (64%) (see Appendix A Table A4).

WC Class B

Sixty-one IEDs were assigned to class WC_B and involved the channels ASMA1 ASMA2 PSMA2 PSMA3. The channels involved in this class were identical to H2_B, H3_A and H4_B (see Table 5-4).

This visual similarity was further reflected in the classification overlap where WC_B agreed the most with H2_B (90%), H3_A (95%) and H4_B (90%) (see Appendix A Table A4).

The visual comparison and classification overlap indicated that WC classes did not correspond to classes H2_C, H3_C and H4_C.

Table 5- 4| Summary of classes and the channels for each class assigned by WC, H2, H3 and H4 for patient IH and BS

EEG Classifier / Patient	WC			H2			H3			H4		
IH	A	DA4 DA5	51	A	DA4 DA5	71	A	DA4 DA5	84	A	DA4 DA5	45
	B	GA51 DA4 DA5	25	NS		29	NS		16	B	DA4-5 GA51-52	18
	NS		24							C	DA4-5 GA43 GA51	21
										D	GA51-52	1
										NS		14
BS	A	PSMA2 PSMA3	39	A	PSMA2 PSMA3	37	A	ASMA1 ASMA2 PSMA2 PSMA3	71	A	PSMA2 PSMA3	31
	B	ASMA1 ASMA2 PSMA2 PSMA3	61	B	ASMA1 ASMA2 PSMA2 PSMA3	62	B	PSMA2 PSMA3	27	B	ASMA1 ASMA2 PSMA2 PSMA3	68
				C	PC1-5	1	C	PC1-5	1	C	PC1-5	1

5.4 Discussion

The focus of this work was to provide a validation framework to determine whether automated classification of epileptic spikes on icEEG can produce results comparable to those obtained by expert human observers, and apply it to a modified version of the spike classification algorithm *Wave_clus.* Our approach to validation is based on answering the question: can the new (automated) classifier provide a similar outcome to humans? We answered this question in two ways: first, by determining whether *Wave_clus* classification falls within the range of human EEG reviewer variability using information theory metrics. In this regard we found comparable overlap between *Wave_Clus*-human and inter-human classification comparisons, indicating that *Wave_clus* classifications cannot be distinguished from human results. Second, we compared the human and automated IED classifications at the level of the individual events; we found that the sensitivity of *Wave_clus* was similar to that of the humans, and that there was generally good classification overlap.

There is significant interest in the quantification of epileptic spikes recorded in icEEG using automated algorithms (Dümpelmann and Elger, 1999; Bourien et al., 2005; Valenti et al., 2006; Brown et al., 2007; Barkmeier et al., 2012; Gaspard et al., 2014). However, only a few algorithms exploit the relationship between the activity across channels (Hufnagel et al., 2000; Bourien et al., 2005), which is an important step in the human ability to distinguish between different IED types (Gotman 1999; James et al., 1999). Some algorithms cluster IEDs visible over multiple channels based on whether they occur in a similar temporal interval (Hufnagel et al., 2000; Bourien et al., 2005) but do not take the details of the waveform into account. Our spike classification algorithm is able to cluster multiple features by considering the details of the waveform across multiple channels. We also note the lack of comparison of the results of automated IED classification with human expert observers (Hufnagel et al., 2000; Bourien et al., 2005; Janca et al., 2013). In this study we validated the performance of *Wave_clus* as an automated IED classifier by comparing it to the performance of expert EEG reviewers.

5.4.1 Validating automated icEEG waveform classification algorithms

Validating an automated algorithm often requires a gold standard to which one can compare its performance. Due to the lack of a gold standard as to what constitutes an IED, the combined opinions (e.g. consensus or majority) of a group of expert EEG reviewers can be used as what may be called a silver standard (Barkmeier et al., 2012;

Halford et al., 2013; Gaspard et al., 2014), allowing calculation of sensitivity and specificity. The greater complexity of the epileptiform activity recorded intra-cranially compared to scalp EEG means that validation methods used for the latter are generally inadequate, either due to their reliance on scalp topography or on the IED field's at the lobar level (Wilson et al., 1999; van Hese et al., 2008; Scherg et al., 2012). As we have shown, the greater complexity means that the number of classes assigned by each reviewer can vary greatly (see Table 5-2 and Appendix A Table A-1).

As a result, we quantified agreement using a more general, information theoretical metric (Meila, 2007) to determine overall spike classification similarity between automated and human spike classification. The theoretical advantage of this approach is its generalisability; in particular it allows the comparison of classification results for any number of classes. The indistinguishable performance of WC spike classification to H spike classification is demonstrated in the *VI* distribution overlap between WC_all and H_all that ranges between 58% and 96% (mean 78%) across the 5 datasets (see Table 5-3 and Figure 5-4). To help better understand these results, let us examine the results for patient BS, with the lowest *VI* distribution overlap (58%), indicating the greatest difference between WC and H classification results. We found that the overwhelming majority of events were assigned in two classes by WC and the three H reviewers, that were visually very similar (see Table 5-4 and Appendix A Table A4 for the classification overlap statistics). Nonetheless in this patient dataset, the human raters tend to agree amongst themselves slightly more than with WC, as reflected in the lower *VI* values for the former. We argue that this observation is not very striking from browsing the results of the event classification overlap table (e.g. Appendix A Table A4), while it is evident in Figure 5-4. It is important to note that while the statistics of *VI* distribution overlap are unknown (a much greater sample would be required), there will be a lower value in any given dataset, and we argue that 58% overlap, while suggestive of a degree of WC classification bias in this particular patient, represents a good level of agreement. Second, in the absence of ground truth there will always be uncertainty about the true level of performance, and therefore it may be argued that the WC result is in fact superior in some way; in effect that humans make the same mistakes. In this regard, we note that, when applied to IED recorded on scalp EEG during fMRI, WC classification resulted in fMRI maps that had in some cases, a higher of localisation concordance with the well-characterised generators (Pedreira et al., 2014).

5.4.2 WC performance in IED marking and classification

Similarly to our previous study (Pedreira et al., 2014), we focused on the clustering of IEDs that have already been detected and therefore, did not include the automatic detection step. Instead, we allowed our expert reviewers to 'declassify' the IED previously labelled by H1: this seemed necessary given the anticipated results and our knowledge of the way EEG raters work, and had the benefit of allowing us to quantify sensitivity and specificity. Previous studies investigating the sensitivity of automated IED detection algorithms on icEEG have demonstrated mixed results with some algorithms having a low (between 14-25%) (Dümpelmann and Elger, 1999; Barkmeier et al., 2012) and some having a high (between 63-75%) (Brown et al., 2007; Gaspard et al., 2014) sensitivity. We found the sensitivity of WC to be high (>76%) and similar to that of our group of EEG reviewers (see Figure 5-5). Furthermore, our results show that WC classifies IEDs similar to H raters (see Table 5-4 and Appendix A Table A-1), and it can identify additional classes that were not initially identified by H raters. For example WC was able to find one additional class (WC class B: GA51 DA4 DA5) for patient IH that was not identified by H2 or H3 (see Figure 5-3 and Table 5-4), which may indicate different generators. Furthermore, WC is also able to distinguish different IED types based on the amplitude (patient JR class A, class B – see Appendix A Table A-1). An important finding in this investigation was that while there was a low specificity for WC and a high specificity for H2 (see Figure 5-6), the classification of IEDs was very similar for patient MB. Both WC and H2 separated IEDs occurring in channel RA1 and RA2 with regards to polarity; WC class B (RA1 RA2 -ve) agreed the most with H2 class A (RA1 RA2 -ve) – 89%, and WC class E (RA1 RA2 +ve) agreed the most with H2 class B (RA1 RA2 +ve) – 100% (see Appendix A Table A-1 and Table A-5).

Although the present work has focussed on the validation of intracranial EEG, our approach could be generalised to other automated EEG algorithms since the validation analysis does not make any assumption about the particular nature or distribution of the electrodes or the exact nature of the signal.

5.4.3 Methodological considerations and future work

Our icEEG data was acquired during fMRI scanning and therefore, requires an offline correction for the MR gradient artefact (Carmichael et al., 2012, Boucousis et al., 2012). Carmichael et al. (2012) has shown that the EEG quality, once corrected for the MR gradient artefact, is comparable to icEEG recorded outside the scanner. We also note that quantitative analysis of the same data has been done meaningfully to study the

relationship between haemodynamic changes and electrophysiological features (Murta et al., 2016, Murta et al., 2017).

Concerning the selection of the channels of interest, by relying on the notes of experienced clinician and technicians, this allowed us to ignore channels that did not contain information relevant for the classification, thereby circumventing the possibility that the distribution of the epileptiform events being unduly affected by non-epileptiform events. This approach also has the benefits of being independent of our judgment (as investigators), thereby possibly reducing bias, and having some clinical grounding (and therefore greater relevance). The issue of the method for the selection of the channels of interest may be addressed in the context of a study on automated IED detection.

Regarding the sample size used for our validation analysis, our preliminary finding as part of an imaging study is that the number and characteristics of the classes found by WC was similar when applied to the entire recordings. This provides additional evidence of the validity of our findings. We also note the lack of comparable study to provide us with a suitable standard. As an alternative comparison, for IED detection algorithm validation, we find sample sizes ranging from 279 to 6534 IEDs (Dümpelmann and Elger 1999; Barkmeier et al., 2012; Gaspard et al., 2014; Janca et al., 2015) however, detection is a much less complex and arduous task than IED classification (Gotman, 1999; James et al., 1999). Furthermore, fatigue and error of the EEG reviewer can be a source of error in IED marking (Barkmeier et al., 2012) which may also result in erroneous IED classification. By keeping our IED sample size to 100 per recording (for a total sample size of 500), we minimised human rater fatigue and related error. Our human observers noted that while they found the task demanding, they felt that their performance level was sustainable throughout.

Training bias has been reported as a possible explanation regarding disagreement between EEG reviewers (Barkmeier et al., 2012). In our study reviewer H2 and H3 were trained at the same institution however, the mean inter-rater agreement across all EEG reviewer pairs was not significantly different (see Appendix A Table A-7), indicating that there was little institutional bias.

We note that automated icEEG IED detection algorithms have paid little attention to IED event classification (Dümpelmann and Elger, 1999; Brown et al., 2007; Barkmeier et al., 2012; Gaspard et al., 2014). The high sensitivity of *Wave_clus* in IED marking (see Figure

5-5) as demonstrated in this study suggests that it could be combined usefully with existing automated detection algorithms. As a result *Wave_clus* can further improve the sensitivity of IED marking by eliminating false positive automated IED detections and make the process of quantifying IEDs as accurate as possible.

The results obtained in this study are encouraging enough to apply WC across the whole EEG time course to the entire dataset of IEDs. As a result this should provide a more reliable and unbiased IED classification, which can be used to quantify the IEDs based on their frequency and morphology to determine their relationship to the seizure-onset zone. Since the EEG analysed was recorded during simultaneous fMRI acquisition this provides us with a unique opportunity to localise haemodynamic changes associated with epileptic spikes at a fundamental level (further explored in the next chapter).

5.5 Conclusion

We describe and apply a comprehensive framework for the evaluation of automated classifications of IEDs for clinical use in icEEG, based on a set of statistical tests chosen for their generalisability. We demonstrated the framework's utility to show that an automated waveform EEG classification algorithm (*Wave_clus*) is practically indistinguishable to that of human EEG reviewers and can occasionally identify additional IED classes. These results also suggest that *Wave_clus* used in combination with automated spike detection algorithms, has the potential to provide a more reliable identification of the irritative zone.

CHAPTER 6: BOLD MAPPING OF ICEEG IEDS RECORDED DURING SIMULTANEOUS FMRI ACQUISITION USING WAVE_CLUS‡‡‡‡

In this Chapter I determine whether the WC classification produces more biologically meaningful BOLD patterns with the epileptogenic zone compared to the BOLD patterns obtained using the conventional/ visual classification. To do this, I apply Wave_clus to the entire icEEG time course of eight patients that have undergone simultaneous icEEG-fMRI and have had a good postsurgical outcome (i.e. with a confirmed EZ). For each patient, two fMRI analyses were performed: one based on the conventional visual IED classification and the other based on WC classification. For each IED class in the EZ, I compared the concordance level between their associated BOLD maps and the location of the EZ, for the automated and visual classification.

‡‡‡‡ This chapter is adapted from: Sharma, N.K., Pedreira, C., Chaudhary, U.J., Centeno, M., Carmichael, D.W., Yadee, T., Murta, T., Diehl, B., Lemieux, L., 2017. BOLD mapping of human epileptic spikes recorded during simultaneous intracranial EEG-fMRI: the impact of automated spike classification. *Neuroimage. In submission*

6.1 Motivation

Simultaneous EEG-fMRI has been shown to be a useful tool in mapping the regions associated with the generation of interictal epileptiform discharges (IEDs). For example, blood-oxygen level dependent (BOLD) mapping of IEDs detected on scalp EEG can provide added value to the localisation of the EZ (Zijlmans et al., 2007, Moeller et al., 2009, Thornton et al., 2010, Thornton et al., 2011, Pittau et al., 2012, An et al., 2013, Coan et al., 2016, Centeno et al., 2017). In one study, patients were reconsidered for surgery after identifying the BOLD correlates of IEDs (Zijlmans et al., 2007) and others have suggested its potential use in predicting postsurgical outcome (Thornton et al., 2010, An et al., 2013, Coan et al., 2016, Centeno et al., 2017). In these studies, IED-related BOLD changes have been found to be located in proximity, but also often remote from the EZ suggesting that their generators can involve a widespread network. This may partly reflect the area of synchronous neural activity required for their detection on scalp EEG (Tao et al., 2005). However, the sensitivity of detecting IEDs during an fMRI scan can be a limitation for scalp EEG-fMRI studies (Aghakhani et al., 2006, Salek-Haddadi et al., 2006). In contrast, the sensitivity of intracranial EEG (icEEG) to IEDs is much greater, due to the lack of attenuation and spatial integration from the scalp and the skull (Carreño and Lüders, 2001), which has led to the implementation of simultaneous icEEG and fMRI acquisitions (icEEG-fMRI) in an effort to better understand the haemodynamic changes associated with epileptic activity (Carmichael et al., 2012, Boucousis et al., 2012).

To date, there have only been three studies investigating the whole-brain haemodynamic correlates of IEDs detected on icEEG (Vulliemoz et al., 2011, Cunningham et al., 2012, Aghakhani et al., 2015). In these studies, the IEDs were detected and classified by EEG reviewers in the usual visual manner and a general linear model (GLM) was used to map the BOLD correlates of each IED class. From a theoretical viewpoint, in order to create the optimal model of the IED-related BOLD changes, it is important that once the IEDs have been detected, that they be classified so that each regressor represents the activity of a specific neuronal population to the exclusion of other generators (Liston et al., 2006). In the conventional approach the classification of IEDs generally requires the reviewer distinguishing different IEDs based on their field distribution: essentially the EEG channels in which they occur (Gotman, 1999, James et al., 1999). However as noted above, the high sensitivity of icEEG can result in much more abundant IED than in scalp recordings, and often more varied in their morphology and distribution than on scalp EEG (Spencer et al., 2015). Indeed, the detection and classification of IEDs on icEEG by clinical neurophysiologists can be time consuming and is unreliable (Dümpelmann and

Elger, 1999, Barkmeier et al., 2012, Gaspard et al., 2014, Sharma et al., 2017). Furthermore, the incorrect and inconsistent markings of IEDs have been shown to result in an excess of false positive and false negative BOLD clusters (Flanagan et al., 2009).

Automated algorithms for the analysis of IEDs on icEEG have been designed with the principal aim of reducing the subjectivity of EEG marking (Dümpelmann and Elger, 1999, Bourien et al., 2005, Valenti et al., 2006, Brown et al., 2007, Barkmeier et al., 2012, Gaspard et al., 2014). Such methods are able to detect IEDs but do not exploit the relationship between the activity across channels. Given that IED field distribution is an important consideration in the way IEDs are typically classified visually, we favour automated schemes that incorporate the waveforms across several channels (Hufnagel et al., 2000, Bourien et al., 2005, Pedreira et al., 2014, Sharma et al., 2017). To our knowledge, the only such classification scheme evaluated by comparison with multiple observers was Sharma et al. (2017) (the study described in Chapter 5). This study validated an automated neuronal spike classification algorithm, *Wave_clus* (WC) (Quian Quiroga et al., 2004) for the automated classification of icEEG IEDs (Sharma et al., 2017).

In the present work, our aim was to use this automated IED classification algorithm (WC) (Sharma et al., 2017) to determine whether the models of the IED-related BOLD changes obtained based on the resulting IED classification are comparable to those obtained using the traditional, visual approach. To investigate this, we analysed icEEG-fMRI data collected from patients who subsequently underwent resective surgery that resulted in a good postsurgical outcome, thereby providing some confirmation of the epileptogenic zone (EZ). We compared the level of spatial concordance between the IED-related BOLD maps and confirmed EZ, for the IEDs classified automatically vs classified visually. We hypothesised that an automated approach to IED classification can result in more biologically meaningful IED-related BOLD maps.

6.2 Methods

6.2.1 Patients

Eight patients (6 males; age range: 32-42 years) who underwent simultaneous intracranial EEG-fMRI at the National Hospital for Neurology and Neurosurgery (UCLH NHS Foundation Trust, Queen Square, London, UK) were included in this study. These patients were part of a group of 19 who underwent icEEG-fMRI; we retrospectively selected all those who subsequently underwent resective surgery with a good postsurgical outcome (ILAE 1) (at least 3 years post-resection).

6.2.2 Simultaneous icEEG-fMRI acquisition

Between 31 and 91 electrode contacts were implanted in each patient, with grid electrodes, depth electrodes or a combination of both. The electrodes were connected to an MR- compatible EEG amplifier system (BrainAmp MR+; Brain Products, Gilching, Germany). In accordance with our icEEG-fMRI protocol (Carmichael et al., 2012), echo planar images (EPI) were acquired using a 1.5T Siemens Avanto scanner (Erlangen, Germany) with a standard birdcage transmit/receive head-coil. Depending upon patient comfort inside the scanner and time constraints either one (for patients JR, IH, HD and MB) or two (patients BS, SH, CB and JN) 10-minute resting-state EPI time series; a T1-weighted structural scan was also acquired. The icEEG signals were recorded at a sampling rate of 5 kHz. In the case of patient HD the scanning-related artefacts on icEEG for one of the EPI could not be corrected satisfactorily due to a technical problem at acquisition. Patient MB had a subclinical seizure during one of two EPI series (see Chaudhary et al., 2016 for a report on the analysis of this data). Therefore, 2/12 sessions were not included in this study.

6.2.3 icEEG pre-processing and analysis

Offline correction for MR scanning artefacts was applied to the EEG (Allen et al., 2000) and the resulting signals were down sampled to 250 Hz, and band-pass filtered (2-70Hz).

The processed recordings were visually inspected by EEG reviewer 'H1' (UJC) for clinical purposes using BrainVision Analyser (Brain Products, Germany), marking any epileptiform or potential epileptiform activity, as described in the following section.

6.2.3.1 Visual IED marking and classification

Pathological EEG patterns commonly found in invasive recordings include individual IEDs (spikes and sharp waves), repetitive IEDs (polyspikes) and paroxysmal fast activity (PFA) (Widdess Walsh et al., 2007). Individual and repetitive IEDs can occur as single isolated epileptiform discharges (SED) or continuous epileptiform discharges (CED) (Palmini et al., 1995, Turkdogan et al., 2005). Reviewer H1 used two types of event markers: point marker for individual IEDs and onset and offset markers for repetitive IEDs and PFA.

This study concerns the effect of choice of IED classification strategy as applied to the SEDs and CEDs (< 1 IED/sec) for BOLD mapping using the GLM approach: firstly, classified visually by H1 based on their morphology and field and secondly, using a version of *Wave_clus* adapted for this purpose (Sharma et al., 2017). The H1 classification was used if a CED event type occurred >1 IED/sec for both BOLD modelling schemes; in other words the automated process (see below) was not applied to those CEDs. The remainder of the events marked by H1 (namely the SEDs and CEDs (< 1 IED/sec)) were automatically classified using *Wave_clus* as described in the following section.

6.2.3.2 Wave_clus IED classification

Following our previous work (Sharma et al., 2017) the *Wave_clus* waveform classification algorithm (Pedreira et al., 2014) was used to automatically classify the IEDs identified as described above. In summary, *Wave_clus* is an automated neuronal spike classification algorithm that identifies and exploits small but consistent differences across multiple waveforms using wavelet decomposition and a superparamagnetic clustering algorithm (Quian Quiroga et al., 2004). For the purpose of automatically classifying icEEG IEDs, this process was carried out over the event waveforms captured on between 8 to 14 icEEG channels (the channels of interest) in which the IEDs were noted in the clinical EEG report as being most frequent and prominent (see Sharma et al., 2017 for a more detailed description). The result of this process was a set of IED classes (and corresponding labels) with every IED assigned to one of the classes. Polyspikes with the same field as a given *Wave_clus* class were subsequently added to this class.

6.2.3.3 Electro-clinical labelling of IED classes

In order to facilitate the interpretation and presentation of the findings across the visual and automated classifications, the IED classes were also labelled based on two criteria: 1) extent of their field distribution and 2) spatial relationship to the EZ.

6.2.3.3.1 Extent of field distribution

For field distribution, IEDs were labelled according to their spatiotemporal localization and distribution across the implanted electrodes as either:

- Focal: if they involved 1-4 contiguous electrode contacts,
- Regional: if they involved 5-10 contiguous electrode contacts,
- Widespread: if they involved more than 10 contiguous electrode contacts, or:
- Non-contiguous: if they had a focal or regional field but also extended to non-contiguous electrode contacts

6.2.3.3.2 Relationship to the EZ

IED classes were also labelled according to their spatial relationship to the EZ. All IED classes recorded in, and limited to, the brain area overlapping the EZ were labelled as IZ1 ('primary irritative zone'). IED classes in brain areas outside the EZ were labelled as IZ2 ('secondary irritative zone') (Bettus et al., 2011). In this study our attention is focused on the IZ1 IEDs as the most clinically relevant (Cunningham et al., 2011, Vulliemoz et al., 2011, An et al., 2013).

6.2.4 fMRI data analysis

For each patient, we created two GLMs to map the IED-related BOLD changes using Statistical Parametric Mapping (SPM8) (www.fil.ion.ucl.ac.uk): one based on the visually classified IEDs (GLM1) and the other based on the automated IED classification (GLM2). This is in line with our previous study on the application of *Wave_Clus* to scalp EEG-fMRI (Pedreira et al., 2014).

The first two volumes of the fMRI time series data were discarded to account for the T1-saturation effect; slice timing correction, scan realignment to the mean and spatially smoothed using an isotropic Gaussian kernel of 8mm Full Width Half Maximum (FWHM) were employed (Friston et al., 1995). For patients who underwent two EPI series, these were included in a single GLM as separate sessions.

Each class was modelled as a separate effect. Individual IED markers were represented as a zero-duration stick function and polyspikes and paroxysmal fast activity were represented as variable duration blocks and convolved with the canonical hemodynamic response function, and its temporal and dispersion derivatives (canonical HRF+TD+DD). Twenty-four inter-scan realignment parameters - 6 realignment parameters from image pre-processing and a Volterra expansion of these (Friston et al., 1996) were included in

the GLM as confounds to account for motion-related effects. We then applied a robust weighted least squares toolbox (Diedrichsen and Shadmehr, 2005) to reduce the influence of potential physiological and other sources of noise and artefacts.

For each IZ1 IED class, the presence of significant BOLD changes was assessed over the whole brain using a F contrast across the canonical HRF+TD+DD regressors, at a statistical threshold of $p < 0.001$ (uncorrected for multiple comparisons) and a cluster size threshold of 5 contiguous voxels (Grouiller et al., 2011, Centeno et al., 2017). The resulting SPMs were co-registered with pre- and post-surgical T1-weighted MRI scans using the rigid-body registration tool in SPM.

6.2.4.1 Comparison of IED-related BOLD clusters with EZ

For each IZ1 IED class, we evaluated the level of spatial concordance with the EZ, irrespective of the sign of BOLD change considering that both increases and decreases have been found in the epileptogenic zone (Thornton et al., 2011, Chaudhary et al., 2012; Pittau et al., 2013). Similar to our previous work (Coan et al., 2016) the level of concordance of each IED-related BOLD map with the EZ was assessed as either:

- *Concordant (C):* when one or more BOLD clusters overlapped with the area of surgical resection or were within up to 2 cm of the resection margin.
- *Discordant* (*D*): all clusters were remote (different lobe or opposite hemisphere) from the EZ.

For each patient we calculated the proportion of *C* maps for GLM1 and GLM2: (number of *C* maps)/(number of maps); the Wilcoxon signed-rank test was used at the group level.

6.3 Results

Six of the eight patients were diagnosed with frontal lobe epilepsy, one had temporal lobe epilepsy and one had parietal lobe epilepsy (see Table 6-1). The mean number of months they were seizure free post resective surgery was 51 months (*SD*: 12; range: 35 - 74) (see Table 6-2). Across all subjects, the mean number of IED events that were detected by H1 was 1206 (*SD*: 989; range: 460 - 3567) and the mean number of events classified by WC was 1105 (*SD*: 915; range: 277-3246) (see Appendix B Table B-1). In the following we summarise the IED classes obtained by the EEG reviewer and the automated algorithm.

6.3.1 IED detection and visual and automated classification

6.3.1.1 Visual classification

Thirty-two classes were IZ1 IEDs, with at least two in every patient: patient JR, *N* = 5 (Focal: 2, Regional: 2, Widespread: 1); patient IH, *N* = 3 (Focal: 2, Regional: 1); patient HD, *N* = 2 (Focal and regional); patient MB, *N* = 4 (Focal: 3, Regional: 1), patient SH, *N* = 2 (Focal: 1, Regional: 1), patient BS, *N* = 3 (Focal: 2, Regional: 1); patient CB, *N* = 4 (Focal: 1, Regional: 2, Non-contiguous: 1), patient JN, *N* = 9 (Focal: 9) (see Table 6-3). The mean number of IZ1 IEDs was 1039 (*SD*: 1024; range: 223 - 3505) (see Table 6-2) (see Appendix B Table B-1 for details on IZ2 classes).

6.3.1.2 Wave_clus classification

Twenty-two classes were labelled as IZ1 IEDs with at least two in every patient: patient JR, *N* = 4 (Focal: 2, Regional: 1, Non-contiguous: 1); patient IH, *N* = 3 (Focal: 2, Regional = 1); patient HD, *N* = 1 (Focal); patient MB, *N* = 2 (Focal), patient SH, *N* = 2 (Focal and Regional); patient BS, *N* = 2 (Focal); patient CB, *N* = 3 (Focal: 2, Non-contiguous: 1); patient JN, *N* = 5 (Focal: 1, Regional: 3, Widespread: 1) (see Table 6-3). The mean number of IZ1 IEDs was 946 (*SD*: 931; range: 277 - 3190) (see Appendix B Table B-1 for details on IZ2 classes).

Two out of three CED IZ1 IED classes (patient HD: 1 Focal IED class; *N* = 770 and patient JN: 1 Focal IED class; *N* = 2481) were not classified using *Wave_clus* as they occurred >1 per sec (see Appendix B Table B-1 for details on the observed EEG patterns).

Table 6- 1| Non-invasive electro-clinical information on all patients

Patient	Age/Sex	Age at Seizure Onset	Type of Epilepsy	Scalp EEG	MRI findings	Other non-invasive investigations
JR	36/M	12	FLE	Spikes: L fronto-central Seizure: Regional central	FCD L posterior SFG + MFG	PET: normal Ictal SPECT: L frontal lobe
IH	37/M	9	FLE	Spikes: Regional L temporal-frontal Seizure: Regional L fronto-central	FCD L posterior MFG	PET: normal
HD	41/F	7	FLE	Spikes: Regional L inferior frontal/orbital frontal Seizure: Regional L frontal	FCD L IFG	PET: L frontal hypometabolism
MB	34/M	7	TLE	Spikes: Regional L and R temporal regional Seizure: Regional L temporal	L HS	None
SH	37/M	16	FLE	Spikes: Regional R frontal, bi frontal and L fronto-temporal Seizure: Regional frontocentral	NL	PET: R frontal hypometabolism
BS	44/M	8	FLE	Spikes: Regional R centro-parietal Seizure: Central fast activity	*L HS	PET: R parietal and posterior frontal hypometabolism Ictal SPECT: bi frontocentral and R insula hyperperfusion MEG: R temporo-occipital and frontocentral spikes
CB	32/F	3	FLE	Spikes: None Seizure: Regional L frontocentral	FCD L superior frontal sulci	PET: L SFG hypometabolism Ictal SPECT: L frontal and insular hyperperfusion MEG: No spikes recorded
JN	33/M	7	PLE	Spikes: Regional right anterior parietal Seizure: Regional R postcentral	FCD R frontoparietal	None

Abbreviations| M, Male; F, Female; FLE, Frontal lobe Epilepsy; PLE, Parietal lobe epilepsy; R, Right; L, Left; FCD, Focal cortical dysplasia; HS, Hippocampal sclerosis; NL, Non-lesional; SFG, Superior frontal gyrus; IFG, Inferior frontal gyrus; MFG, Middle frontal gyrus; * incidental finding

Table 6- 2| EZ localisation, postsurgical outcome and icEEG-fMRI details for all patients.

Patient	Implantation summary	Number of icEEG contacts (+ channel label)	EZ	Postsurgical outcome (months)	No. of fMRI sessions (mins per session separated by ;)	Total no. of IZ1 IEDs detected during fMRI scan by H1	Channels of Interest for WC classification
JR	L superior (SFG), middle (MFG) and inferior (IFG) frontal gyrus. L precentral gyrus. L central sulcus and part of postcentral sulcus. L superior frontal sulcus. L postcentral regions.	One 8x8 contact grid (G). Two 4-contact depths (DA & DP). One 2x8 contact grid (GA).	L Posterior SFG, MFG, SMA	ILAE 1 (58)	1(10)	590	**G4 G5 G13 G20 G21 G22 G23 G29 DP2 DP3**
IH	L frontal lobe (laterally and inferiorly). L middle (MFG) and inferior (IFG) frontal gyrus. L frontal pole.	One 8x8 contact grid (GA). One 2x8 grid (GD). Two 6-contact depths (DA & DP). Two 6-contact strips (GC & GB).	L IFG, MFG and lateral orbitofrontal	ILAE 1 (44)	1(10)	892	**GA50 GA51 GA52 GA53 DA4 DA5**
HD	L inferior (IFG) and middle (MFG) frontal gyrus. L frontal pole	One 8x8 contact grid (G1). One 2x8 contact grid (G2). Two 6-contact depths (DA & DP). One 6-contact strip (S1).	L anterior IFG and MFG	ILAE 1 (55)	1(10)	1035	**DA3 DA4 G1_26 G1_34 G1_35 G1_36 G1_42 G1_43 G1_44 G1_50 G2_5 G2_6 G2_13 G2_14**
MB	R and L amygdalae (R A). R and L hippocampi.	Five 6-contact depths (LA, LAH, LPH, RA and RH)	L anterior temporal lobe	ILAE 1 (74)	1(10)	572	**LA2 LA3 LH1 LH2 LP1 LP2 RA1 RA2 RA3 RH1**
SH	R A and P mesial frontal lobe. R orbitofrontal lobe. R A (R ASMA) and P (R PSMA) supplementary sensorimotor areas. R frontal pole.	Three 16-contact depths (AM, PM and PMFG). Four 12-contact depths (FP, ASMA, PSMA, IFG). One 10-contact depth (FOF).	R anterior orbitofrontal	ILAE 1 (43)	2(10; 10)	223	**AM2 AM3 AM4 Fp1 Fp2 Fp3 Fp4 PMFG3 PMFG4 IFG9**
BS	R A and P insula. R A (R ASMA) and P (R ASMA) supplementary sensorimotor areas. R A, M and P cingulum (PC).	Two 6-contact depths (ASMA & PSMA). Three 8-contact depths (AC, MC and PC).	R SMA and SFG	ILAE 1 (59)	2(10; 10)	733	**ASMA1 ASMA2 ASMA3 PSMA1 PSMA2 PSMA3 PC4 PC5 AI5 AI6**
CB	L superior (SFG) and middle (MFG) frontal gyrus. L frontal pole.	One 8x8 contact grid (GA). One 2x8 contact grid (GB). One 4x8 contact grid (GC). One 8-contact strip (SF).	L posterior SFG (lateral and medial)	ILAE 1 (43)	2(10; 10)	755	**SF5 SF6 SF7 SF8 GB4 GB5 GB6 GB7**
JN	R fontoparietal lobe (laterally and inferiorly).	One 8x8 contact grid (G). Two six-contact depths (D1 and D2).	R frontoparietal	ILAE 1 (35)	2(10; 10)	3505	**D1_3 D1_4 G22 G23 G29 G30 G31 G37 G38 G39 G40 G45 G46 G47**

Abbreviations| R: right, L: left, A: anterior, P: posterior, SMA: supplementary motor area, C: cingulum, IFG: inferior frontal gyrus, MFG: middle frontal gyrus, SFG: superior frontal gyrus

Table 6- 3| IED classification and fMRI data analysis results

	GLM1 (Visual)				GLM2 (Automated)			
Patient	**Spike class (number)**	**Field distribution**	**Concordance**	**% Concordance**	**Spike class (number)**	**Field distribution**	**Concordance**	**% Concordance**
JR	G4,5 (70)	Focal	Y	100	G23 (127)	Focal	Y	100
	G12-15 (30)	Focal	Y		G4_5_13_21_29_ DP (131)	Regional	Y	
	G4-6 + G12,13 +G22-24 + G28-30 (60)	Regional	Y		G4_5_29 (78)	NC	Y*	
	G12-15 + G21-24 + DP2-4 (218)	Regional	Y*		G13_20_21_DP (152)	Focal	Y	
	G4-8 +G12-15 + G20-24 + G28-30 + DP2-4 (212)	Widespread	Y*					
IH	DA3-6 (423)	Focal	Y	66	D4_5 (498)	Focal	Y	66
	DA4,5 + GA51 (261)	Focal	N		D4_5_GA50_51_52 (106)	Regional	N	
	DA2-6 + GA49-54 (208)	Regional	Y		D4_5_GA51(156)	Focal	Y	
HD	DA3,4 (770)	Focal	N	50	DA3_4 (770)	Focal	N	0
	DA3,4 + G1 18,27,35,43 (265)	Regional	Y*		DA3_4_G1_35_G1_4 2 (75)	Focal	N	
MB	LAH1,2 + LPH1,2 + LA3,4 (60)	Regional	Y	50	LA2_LAH1_2 (360)	Focal	Y	100
	LAH1-2 (359)	Focal	Y		LAH1_2_LPH1(112)	Focal	Y*	
	LA3-4 (57)	Focal	N					
	LPH1-2 (96)	Focal	N					
SH	FP2-4 (142)	Focal	Y	50	FP4 (333)	Focal	Y	100
	FP2-4 + AM2-4 (81)	Regional	N		AM2-4 + FP1-4 (591)	Regional	Y	
BS	PSMA1-3 (211)	Focal	Y	100	ASMA1-2 + PSMA2-3 (364)	Focal	Y	100
	ASMA1-3 (46)	Focal	Y		PSMA2-3 (250)	Focal	Y	
	ASMA1-3 + PSMA1-3 (476)	Regional	Y					
CB	SF5-7 (168)	Focal	N	75	SF5-7 + GB4-7 (68)	NC	Y	100
	GB4-6 + 14-16 (90)	Regional	Y		SF6_7 (177)	Focal	Y	
	GC5-16 (474)	Regional	Y		SF8 (32)	Focal	Y	
	SF5-7 + GB5-8 + GC5,10,11,12,15,16 (23)	NC	Y					
JN	D1 _3_4 (43)	Focal	Y	78	D2_3_4 (2481)	Focal	Y*	83
	D2_3_4 (2481)	Focal	Y*		G38-39-40-46-47 (256)	Regional	Y*	
	G23 (83)	Focal	Y		D1_3_4 G37-38-39 (184)	Regional	Y	
	G31 (72)	Focal	Y		D1_3_4 (75)	Focal	Y*	
	G36 (209)	Focal	Y		G45-46(128)	Focal	N	
	G38 (226)	Focal	Y*		D1_3_4 G22_23_29_30_3 1_37_38 (66)	Widespread	Y	
	G44 (140)	Focal	N					
	G45 (127)	Focal	Y					
	G47 (124)	Focal	N					

Note: * = BOLD cluster in area of resection is the global maximum (GM)

6.3.2 Concordance of IZ1 IED-related BOLD changes: visual (GLM1) vs *Wave_clus* (GLM2) classification

There was no significant difference in the proportion of *C* maps (Wilcoxon signed rank test: Z = -0.96, p = 0.3) between GLM1 and GLM2 across the group; For GLM1, 75% (24/32) of the BOLD maps were *C*; 83% (20/24) of GLM2 BOLD maps were *C* (see Table 6-3). Four patients showed greater concordance for GLM2 compared to GLM1 (patient MB, SH, CB and JN), three patients had equal concordance for GLM1 and GLM2 (patient JR, IH and BS), and one patient showed lower concordance (patient HD) (see Table 6-3).

In relation to IED field, for GLM1 there was a degree of concordance in 14/21 of Focal, 8/9 of Regional, 1/1 of Widespread, and 1/1 of Non-contiguous IED classes. For GLM2, there was a degree of concordance in 13/16 of Focal, 4/5 of Regional, 1/1 Widespread and 2/2 of Non-contiguous classes (see Table 6-3).

6.3.2.2 Case reports

To better illustrate the range of results obtained for our study we present four case reports: two in which GLM2 showed greater BOLD concordance (patients SH and MB), one in which concordance was the same for GLM1 and GLM2 (patient BS) and one in which the maps obtained from the automated classification were less concordant (patient HD).

6.3.2.2.1 Patient SH: improved concordance

This patient was diagnosed with frontal lobe epilepsy and the EZ was located in the right anterior orbitofrontal region (see Table 6-2).

IED Classification

Reviewer H1 detected 1140 IED (see supplementary table 1).

Visual classification: Reviewer H1 classified the IEDs into five classes. Two classes were labelled IZ1 (classes #1 and #2); class #1 consisted of focal spikes in contacts FP2-4 (N=142), class #2 consisted of regional spikes in contacts FP2-4 and AM2-4 (N = 81) (see Figure 6-1 and Table 6-3). Three classes were labelled IZ2 (classes #3-5) (see Appendix B Table B-1).

Automated classification: The automated algorithm classified the IEDs into three classes (see Appendix B Table B-1 and Figure B-1). Two classes were labelled IZ1 (classes #1 and #2); class #1 consisted of focal spikes in contact FP4 (*N* = 333), class #2 consisted of regional spikes in contacts AM2-4 and FP1-4 (N = 591) (see Figure 6-1 and Table 6-3). Class #3 was labelled IZ2 (see Appendix B Table B-1 and Figure B-1).

BOLD Results

GLM1: the degree of concordance for the two IZ1 classes was: *C* for class #1 and *D* for class #2 (see Figure 6-1 and Table 6-3). For IED class #1 and #2, the global maximum was located in the right mesial occipital lobe (see Appendix B Table B-2).

GLM2: the degree of concordance for the two IZ1 classes was: *C* for class #1 and class #2 (see Figure 6-1 and Table 6-3). For IED class #1, the global maximum was located in the right occipital lobe and for IED class #2; the global maximum was located in the left superior parietal lobe (see Appendix B Table B-3).

6.3.2.2.2 Patient MB: Improved concordance

This patient was diagnosed with temporal lobe epilepsy and the EZ was located in the left anterior temporal lobe (see Table 6-2).

IED Classification:

Reviewer H1 detected 1216 IEDs (see Appendix B Table B-1).

Visual classification: Reviewer H1 classified the IEDs into six classes (see Appendix B Table B-1). Four classes were IZ1 (class #1-4); class #1 consisted of regional spikes observed in contacts LAH1-2 + LPH1-2 + LA3-4 (*N* = 60), class #2 consisted of focal spikes observed in contacts LAH1-2 (*N*=359), class #3 consisted of focal spikes in contacts LA3-4 (*N* = 57), class #4 consisted of focal spikes in contacts LPH1-2 (*N* = 96) (see Figure 6-2 and Table 6-3). There were two spike classes in IZ2 (class #5 and #6) (see Appendix B Table B-1).

Automated classification: The automated algorithm classified the IEDs into four classes (see Appendix B Table B-1 and Figure B-2). Two classes were in IZ1 (class #2 and #3); class #2 consisted of focal spikes in contacts LA2 + LAH1-2 (*N*=360), class #3 consisted of focal spikes in contacts LAH1-2 + LPH1 (*N* = 112) (see Figure 6-3 and Table 6-3). Two classes were in IZ2 (class #1 and #4) (see Appendix B Table B-1 and Figure B-2).

BOLD Results:

GLM1: the degree of concordance for the three IZ1 classes was: *C* for class #1 and class #2 and *D* for class #3 and class #4 (see Figure 6-2 and Table 6-3). For classes #1 and #2 the global maximum was located in the left lateral occipital lobe, in the right superior frontal gyrus for class #3 and in the left orbital frontal cortex for class #4 (see Appendix B Table B-2).

GLM2: the degree of concordance for the two IZ1 classes was: *C* for class #2 and class #3 (see Figure 6-3 and Table 6-3). For class #2 the global maximum was located in the anterior cingulate cortex (see Appendix B Table B-3) and for class #3 the global maximum was located in the EZ (see Table 3).

6.3.2.2.3 Patient BS: no change in concordance

This patient was diagnosed with frontal lobe epilepsy and the EZ was located in the right supplementary motor area and right superior frontal gyrus (see Table 6-2).

IED classification:

Reviewer H1 detected 1033 IEDs (see Appendix B Table B-1).

Visual classification: Reviewer H1 classified the IEDs into five classes (see Appendix B Table B-1). Three classes were IZ1 (classes #1-3); class #1 consisted of focal spikes at contacts PSMA1-3 (*N* = 211), class #2 consisted of focal spikes at contacts ASMA1-3 (*N* = 46), class #3 consisted of regional spikes at ASMA1-3 + PSMA1-3 (*N* = 476) (see Figure 6-4 and Table 6-3). There were two IZ2 spike classes (classes #4 and #5) (Appendix B Table B-1).

Automated classification: The automated algorithm classified the IEDs into three classes (see Appendix B Table B-1 and Figure B-3). Two classes were in IZ1 (classes #1 and #2); class #1 consisted of focal spikes at ASMA1-2 + PSMA2-3 (*N*=364), class #2 consisted of focal spikes at PSMA2-3 (*N* = 250) (see Figure 6-4 and Table 6-3). Class #3 was labelled as IZ2 (see Appendix B Table B-1 and Figure B-3).

BOLD results:

GLM1: the degree of concordance for the three IZ1 classes was *C* (see Figure 6-4 and Table 6-3). For class #1 the global maximum was located in the left orbital frontal cortex, for class #2 the global maximum was located in the right inferior frontal gyrus and for

class #3 the global maximum was located in the right fronto-temporal lobe (see see Appendix B Table B-2).

GLM2: the degree of concordance for the two IZ1 IED classes was *C* (see Figure 6-4 and Table 6-3). For class #1 the global maximum was located in the left frontal pole and for class #2 the global maximum was located in the right posterior temporal lobe (see see Appendix B Table B-3).

6.3.2.2.4 Patient HD: decreased concordance

This patient was diagnosed with frontal lobe epilepsy and the EZ was in the left anterior inferior and middle frontal gyri (see Table 6-2).

IED classification:

Reviewer H1 detected 1230 IEDs (see Appendix B Table B-1).

Visual classification: Reviewer H1 classified the IEDs into 3 classes (see Appendix B Table B-1). Two classes were IZ1 classes (classes #1 and #2); class #1 consisted of focal IEDs in contacts DA3-4 (*N* = 770) with a CED pattern of >1 per sec, class #2 consisted of regional IEDs in contacts DA3-4 + G1 18, 27, 35, 43 (*N* = 265) (see Figure 6-5 and Table 6-3), and one IZ2 class (class #3) (see Appendix B Table B-1).

Automated classification: Visual class #1 with the CED pattern was not automatically classified using WC (see Appendix B Table B-1). WC classified the remaining 313 IED into three classes: one class was an IZ1 class (class #1), consisting of focal IEDs at contacts DA3-4 + G1 35, 42 (*N* = 75) (see Figure 6-5 and Table 6-3). The other two were IZ2 classes (#2 and #3) (see Appendix B Table B-1 and Figure B-4).

BOLD results:

GLM1: the degree of concordance for the two IZ1 classes was: *D* for class #1 and *C* for class #2 (see Figure 6-5 and Table 6-3). For class #1 the global maximum located in the right lateral occipital lobe (see Appendix B Table B-2) and in the EZ for class #2 (see Table 6-3).

GLM2: the degree of concordance for the two IZ1 classes was *D* (see Figure 6-5 and Table 6-3). For class #1 the global maximum was located in the posterior cingulate cortex and for class #2 the global maximum was located in the left posterior temporal lobe (see Appendix B Table B-3).

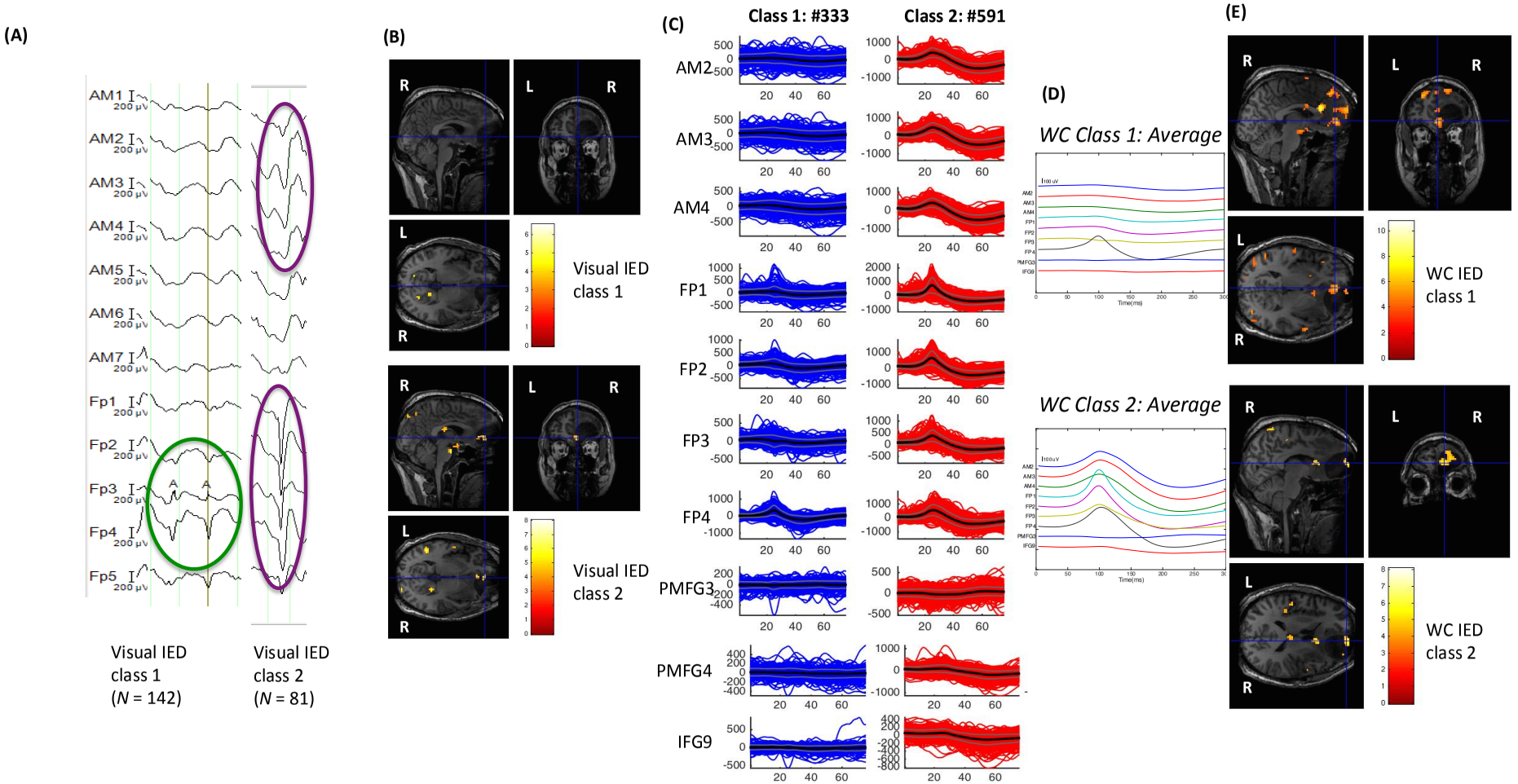

Figure 6- 1| Patient SH: IED-related BOLD for IZ1 classes from GLM1 and GLM2 (A) IZ1 IED classes by the EEG reviewer. (B) IED-related BOLD maps of the IZ1 IEDs for GLM1 coregistered to the T1-weighted postoperative MRI. Top; IED-related BOLD map for visual IED class 1 (discordant). Bottom: IED-related BOLD map for visual IED class 2 (concordant). (C) The two IZ1 IED classes obtained using Wave_clus and (D) the average of these clusters (E) IED-related BOLD maps of the IZ1 IEDs for GLM2 coregistered to the postoperative T1-weighted MRI. Top: IED-related BOLD map for the WC IED class 1 (concordant). Bottom: IED-related BOLD map for the WC IED class 2 (concordant). Note: the SPM cross hairs point to the centroid of the cluster in the EZ if concordant and only the EZ if discordant

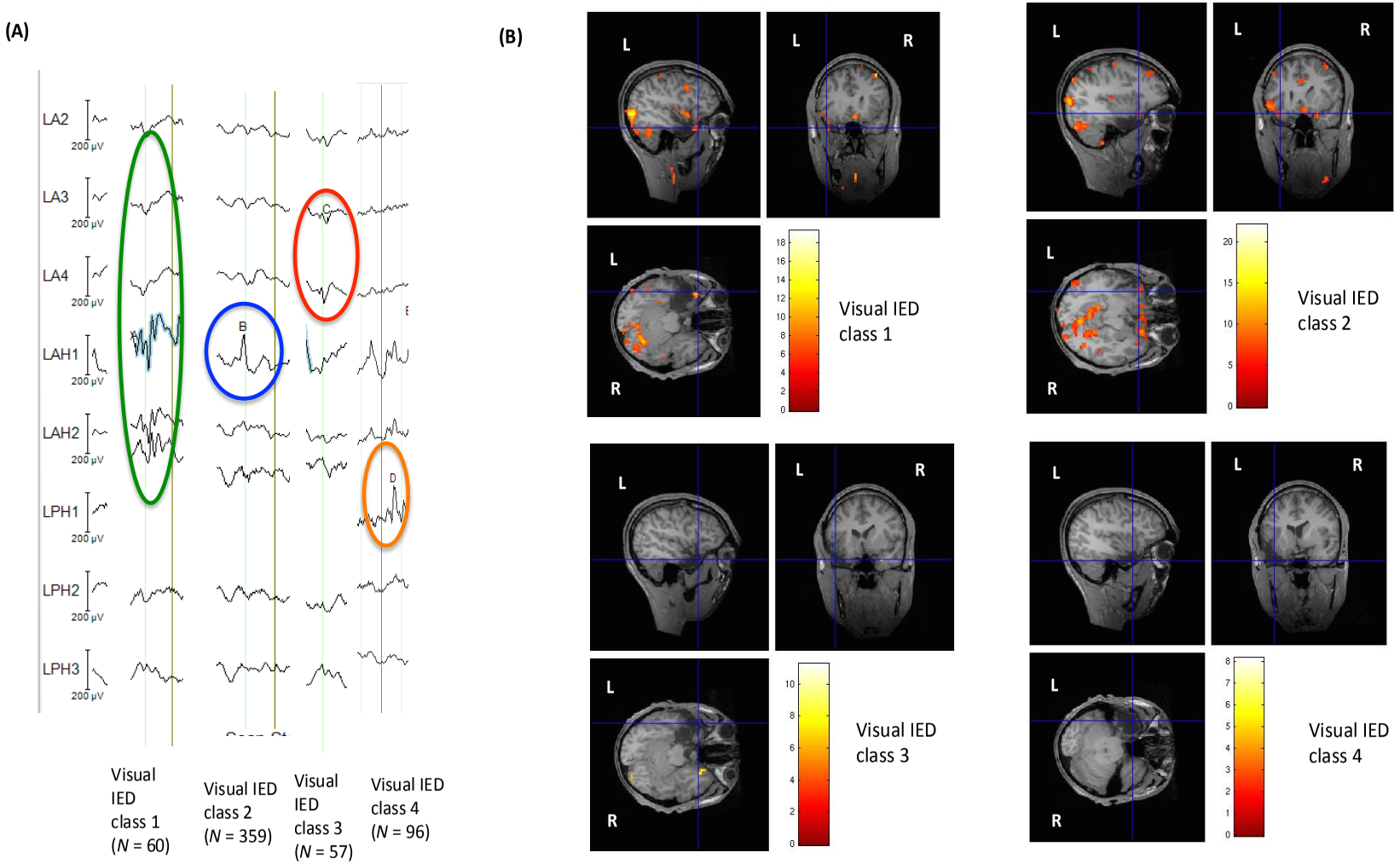

Figure 6- 2| Patient MB: IED-related BOLD for IZ1 classes from GLM1 (A) IZ1 IED classes by the EEG reviewer (B) IED-related BOLD maps of the IZ1 IED classes for GLM1 coregistered to postoperative T1-weighted MRI. Top left: IED-related BOLD maps for visual IED class 1 (concordant). Top right; IED-related BOLD maps for visual IED class 2 (concordant). Bottom left; IED-related BOLD maps for visual IED class 3 (discordant). Bottom right; IED-related BOLD for visual IED class 4 (discordant). Note: the SPM cross hairs point to the centroid of the cluster in the EZ if concordant and only the EZ if discordant

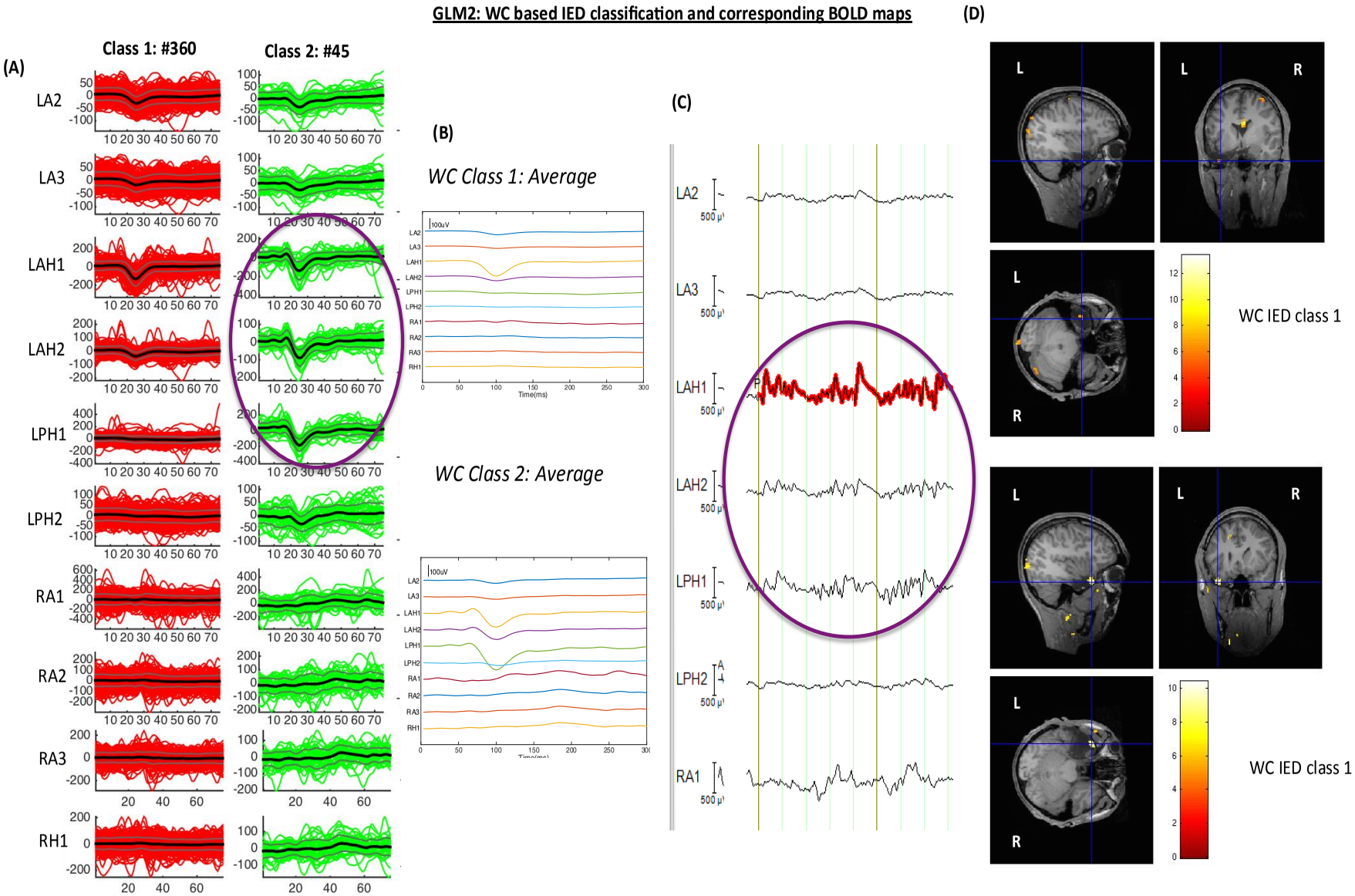

Figure 6- 3| Patient MB: IED-related BOLD for IZ1 classes from GLM2 (A) IZ1 IED classes obtained using Wave_clus and (B) their average over 300ms. (C) Example of polyspikes in EEG recording manually classified after the automated step; this was classified into Wave_clus class 2. (D) IED-related BOLD maps for GLM2 coregistered to postoperative T1-weighted MRI. Top: IED-related BOLD map for Wave_clus class 1 (concordant). Bottom: IED-related BOLD map for Wave_clus class 2 coregistered to postoperative T1-weighted MRI (concordant - GM). Note: the SPM cross hairs point to the centroid of the cluster in the EZ

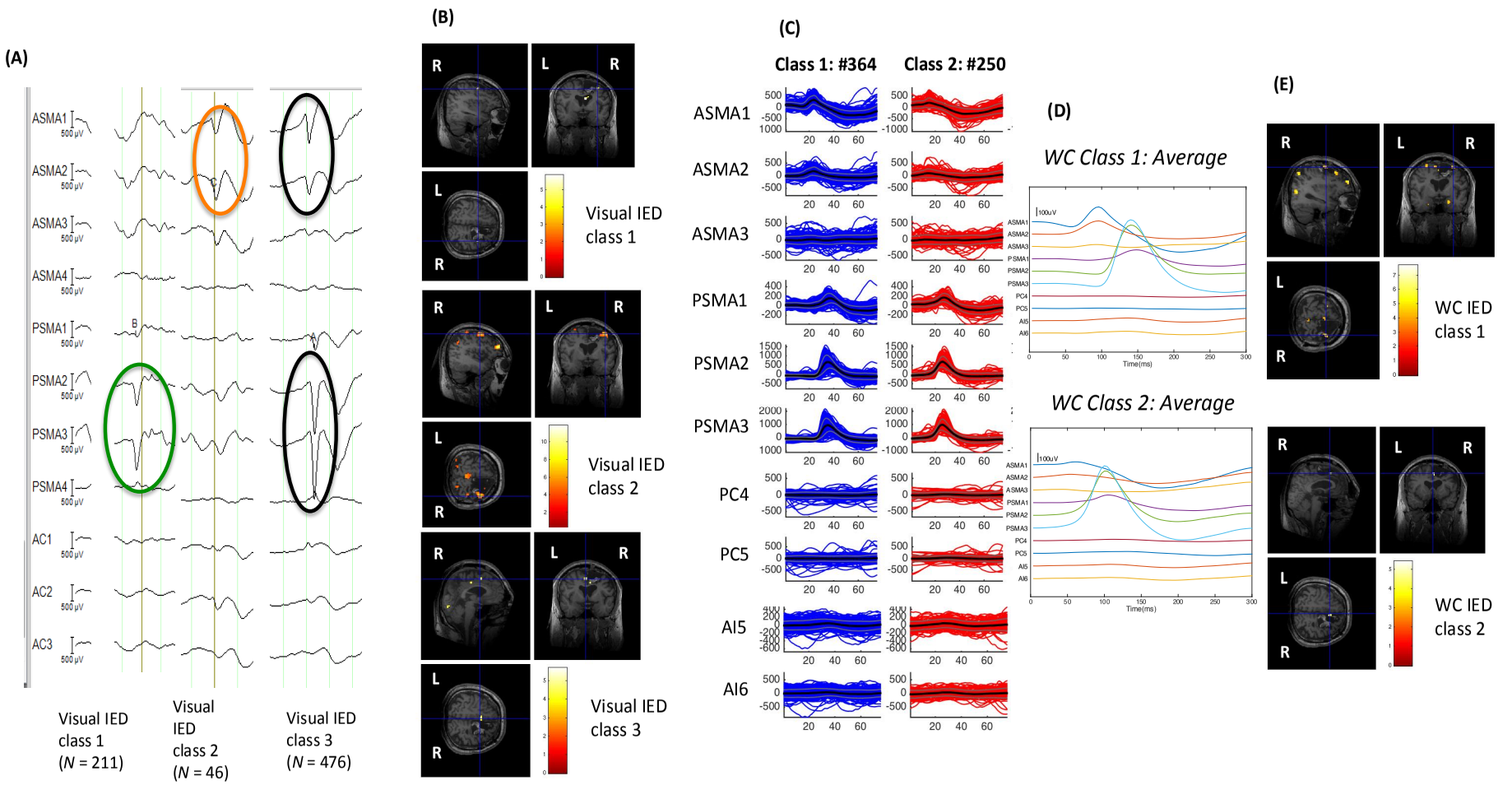

Figure 6- 4| Patient BS: IED-related BOLD maps for IZ1 classes from GLM1 and GLM2. (A) IZ1 IED classes by the EEG reviewer (B) IED-related BOLD maps for IZ1 IEDs for GLM1 coregistered to postoperative T1-weighted MRI. Top: IED-related BOLD map for visual IED class 1 (concordant). Middle: IED-related BOLD map for visual IED class 2 (concordant). Bottom: IED-related BOLD map for visual IED class 3 (concordant) (C) IZ1 IED classes obtained by Wave_clus and (D) their average over 300ms. (E) IED-related BOLD maps for IZ1 IEDs for GLM2 coregistered to postoperative T1-weighted MRI. Top: IED-related BOLD maps for Wave_clus IED class 1 (concordant). Bottom: IED-related BOLD map for Wave_clus IED class 2 (concordant). Note: the SPM cross hairs point to the centroid of the cluster in the EZ if concordant and only the EZ if discordant

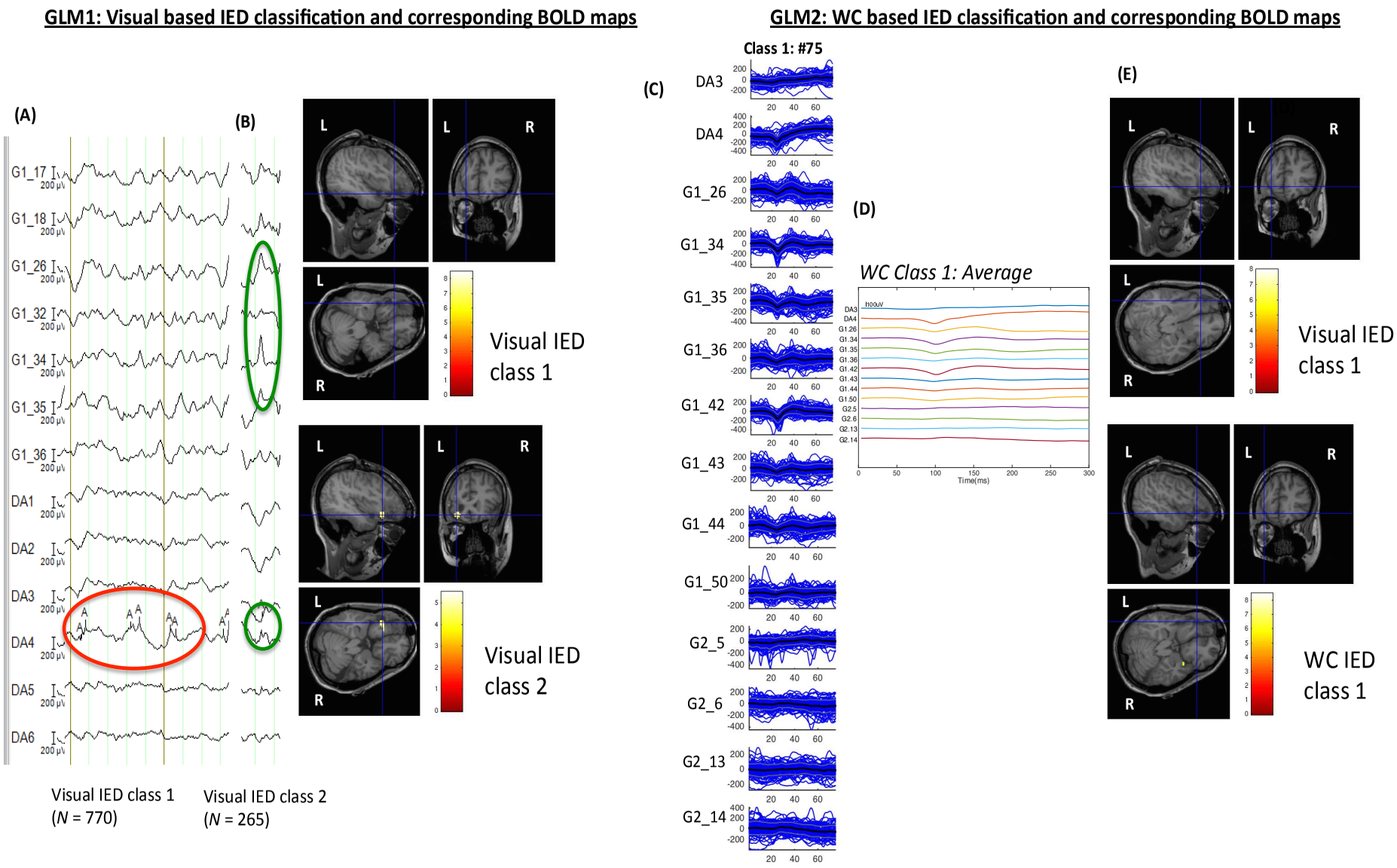

Figure 6- 5| Patient HD: IED-related BOLD maps for IZ1 classes from GLM1 and GLM2. (A) IZ1 classes by the EEG reviewer (visual IED class 1 had a CED pattern of >1 per second and therefore was not processed through Wave_clus). (B) IED-related BOLD maps for IZ1 IEDs for GLM1 coregistered to postoperative T1-weighted MRI. Top: IED-related BOLD map for visual IED class 1 (discordant). Bottom: IED-related BOLD map for visual IED class 2 (concordant - GM). (C) IZ1 IED class obtained by Wave_clus and (D) the average of this class over 300ms. (E) IED-related BOLD maps for IZ1 IEDs for GLM2 coregistered to postoperative T1-weighted MRI. Top: IED-related BOLD maps for visual IED class 1 (discordant). Bottom: IED-related BOLD map for WC IED class 1 (discordant). Note: the SPM cross hairs point to the centroid of the cluster in the EZ if concordant and only the EZ if discordant

6.4 Discussion

Our aim was to determine whether classifying intracranially recorded IEDs with simultaneous fMRI using an automated spike classification algorithm could provide more biologically meaningful IED-related BOLD maps compared to those obtained following visual expert analysis in a group of patients with well characterised EZ.

To do this, IED-related BOLD maps obtained based on the automated algorithm were compared to the visual (classic / standard) classification (along the lines of our previous work on scalp EEG-fMRI; Pedreira et al., 2014) in terms of the presence or absence of BOLD changes in the EZ. To facilitate interpretation of the findings, we limited this analysis to the IEDs observed within the EZ (IZ1 IEDs) since we can be more confident of the location of their generators than the propagation IEDs.

One of the main challenges associated with the use of icEEG data for fMRI mapping is the difficulty of forming a parsimonious model of potential BOLD changes that reflects the complex spatio-temporal dynamics of IEDs. We found that the IED-related BOLD maps were concordant to the area of resection for 83% of the IZ1 classes for the automated algorithm compared to 75% for the visual classes (see Table 6-4). At the single-subject level, we found an improved level of concordance in four patients using the automated algorithm, the same level of concordance between the automated and visual classification in three patients and a worse degree of concordance in one. These results suggest that the automated classification of IEDs using WC on icEEG recordings can be used to create a more biologically meaningful model of the associated haemodynamic changes in some patients. Therefore automated IED classification can help circumvent the problem of highly subjective and time-consuming visual classification of IEDs.

6.4.1 Clinical and biological significance

To date, there have only been three studies focusing on the whole-brain mapping of IED-related BOLD changes using simultaneous icEEG-fMRI (Vulliemoz et al., 2011, Cunningham et al., 2012, Aghakhani et al., 2015). For these studies, the IEDs were detected and classified by EEG reviewers (Vulliemoz et al., 2011, Cunningham et al., 2012, Aghakhani et al., 2015). However, our previous study confirmed that the classification of icEEG IEDs can be inconsistent between EEG reviewers and that the automated classifications obtained using *Wave_clus* fall within inter-observed variability (Sharma et al., 2017). Furthermore, we also previously demonstrated that the same algorithm, when applied to scalp EEG, showed an improved fMRI localisation compared

to visual classification as 72% of the BOLD changes associated with WC classification were concordant to the presumed irritative zone (compared to the 50% of the visual classes) (Pedreira et al., 2014). Therefore, although WC classifications are statistically indistinguishable from the human ones (Sharma et al., 2017), the results from Pedreira et al. (2014) indicate that WC may yet reveal a specific capability of classifying IEDs that is different from humans. Therefore, in the absence of a ground truth in terms of IED classification, and similar to Pedreira et al. (2014), we sought to compare IED classification through independent data, namely the associated BOLD changes and in particular their relationship with the EZ.

Previous icEEG-fMRI studies involved in mapping IED-related BOLD across the whole brain assessed concordance based on location of a significant BOLD cluster to the most active spiking electrode contact (Vulliemoz et al., 2011, Aghakhani et al., 2015). The largest study carried out by Aghakhani et al. (2015) speculated that discordant (BOLD changes outside the lobe of the most active electrode) IED-related BOLD changes was due to the EZ being located elsewhere as this finding was found in patients with a poor postsurgical outcome (Aghakhani et al., 2015). This is consistent with previous scalp EEG-fMRI studies that indicate the absence of statistically significant BOLD changes in the area of resection can be predictive of a poor postsurgical outcome (Thornton et al., 2010, An et al., 2013, Coan et al., 2016). Therefore, we assessed the presence of IZ1 IED-related BOLD changes using the best available gold standard defined as the area of resection in good postsurgical outcome patients (Grouiller et al., 2011).

In this study, any significant BOLD cluster was labelled concordant if it overlapped or was close to the area of surgical resection (Coan et al., 2016). Some previous scalp EEG-fMRI studies have focused on the use of the location of the statistically most significant BOLD cluster as the putative marker of the EZ (Moeller et al., 2009, Thornton et al., 2010, Pittau et al., 2012, An et al., 2013). This is mainly based on two considerations: the cluster containing the statistical maximum is unique for any given map, which is a convenient simplification, and it represents the most likely location of the generator by some, albeit indirect, measure of the statistically strongest haemodynamic change. However, the sensitivity of the GM in localising the EZ is still inconclusive as some studies have shown that it localises the EZ (defined as the area of resection in good postsurgical outcome patients) in less than half of the patients (Grouiller et al., 2011, An et al., 2013, Centeno et al., 2017). As mentioned previously, we defined concordance similar to Coan et al. (2016), as the presence of any significant BOLD cluster within or

close to the EZ, and who showed that the presence of a significant BOLD cluster within or in close proximity to the EZ is strongly associated with good outcome (and absence of any cluster in the EZ, with a poor outcome). Indeed, in the present study only a small percentage of IED datasets showed the GM to be within or in the immediate proximity of the EZ for BOLD maps obtained using the visual and automated approach (16% and 17% respectively) (see Table 6-3) raising further question on the notion of the global maximum as a marker of EZ.

In this study, four patients showed an improved level of concordance following automated IED classification (patient MB, SH, CB and JN). As mentioned previously, our main focus was comparing concordance levels for the classes obtained by WC and visual classification and not comparing the spatial distribution of the EEG classes themselves. However, the advantage of using our automated approach can be seen for patient SH for example (see Figure 6-1). In this patient, the EEG reviewer and WC identified two IZ1 IED classes involving similar electrodes with same distribution: one with a focal distribution involving the FP electrodes and the second with a regional distribution involving FP and AM electrodes (see Table 6-3 and Figure 6-1). Close examination of the two classifications shows that WC identified more IEDs for both classes (FP-focal: N = 333, FP-AM regional: N = 591) compared to the visual classification (FP-focal: N = 142, FP-regional: N = 81). Given the BOLD result is concordant for the FP-focal class for WC classification (compared to a discordant result for the visual classification) (see Figure 6-1), this may suggest that the IEDs were more accurately classified using WC.

6.4.2 Methodological considerations and future work

Our automated classification pipeline was designed for the automated classification of individual IEDs as reflected in its use of a fixed-length time window centred around the peak of the IED to incorporate the maximum information of the IEDs with smallest possible time span to minimise the impact of noise (Sharma et al., 2017). Therefore it is not suitable in its current form to be applied to the EEG patterns with a fast repetitive nature such as polyspikes, PFA and very continuous CEDs; commonly observed EEG patterns in FCD patients (Palmini et al., 1995, Turkdogan et al., 2005, Widdess-Walsh et al., 2007). Therefore, to ensure that our BOLD models were as statistically efficient as possible, we included a manual step in our classification using *Wave_clus*. For example, regarding CEDs the EEG reviewer made a note of the frequency of the CEDs and if they occurred >1 per second, they were not automatically classified but modelled in the GLM; this was carried out in two patients (patient HD and patient JN) (see Figure 6-5 for an

example for patient HD). The automated classification of IEDs for patient HD resulted in more discordant maps than the visual classification (see Table 6-3 and Figure 6-5). We note that uniquely for this patient the channels of interest, which were selected entirely based on information gained from the clinical report, included those in which CEDs (see Figure 6-5 and Table 6-2). Therefore, the continuous nature of this EEG pattern, which the algorithm is not designed to handle, may have resulted in sub-optimal classification. Regarding polyspikes and PFA, these were classified after the automated classification of single events (see Figure 6-4 for an example) across the same channels of interest. Although these steps are not automated, we believe that we have been able to minimise subjectivity as much as possible by reducing the number of events to be classified.

The loss of MR signal in the vicinity of the electrodes in our data dataset due to the susceptibility artefact (Carmichael et al., 2012) is likely to result in reduced statistical power to detect local BOLD changes, which may partly explain why the GM was found to be distant to the EZ in some cases.

However, one of the main potential advantages of icEEG-fMRI compared to scalp EEG-fMRI is the opportunity to map the haemodynamic response associated with very focal discharges, as observed on depth EEG for example. In this study we defined focal discharges as IEDs occurring between 2-4 contiguous electrode contacts. The IED-related BOLD maps acquired using WC show that 81% of the WC IZ1 focal IEDs (13/16) show significant BOLD changes in the EZ as well as distant from the EZ (see Appendix B Table B-3 and Figure 6-1 for an example). These findings clearly show that even for IEDs that are classified as being focal, distant regions are involved in their generation. Therefore, our results further reinforce the notion that even for very focal discharges, the epileptic network can be widespread, involving regions responsible for generating the IED and seizures, and regions remote from this area.

The practical benefits of our approach include time saving and dispensation of the need for reproducibility studies (Flanagan et al., 2009) and therefore, the uncertainty associated with changes in human EEG rater marking. Similar to previous studies using WC (Pedreira et al., 2014, Sharma et al., 2017) this study focused on the classification of IEDs detected by an EEG reviewer. In this regard it would be useful to also automate the detection of IEDs and then classify the markings using WC.

The application of our technique to a group of patients with varied surgical outcome would allow us to determine whether similar BOLD patterns (as described in previous

scalp EEG-fMRI studies) are observed in the area of resection in good and poor postsurgical outcome patients.

6.5 Conclusion

We have demonstrated that the application of an automated IED classification algorithm can provide more biologically meaningful IED-related BOLD maps compared to the visual/conventional approach. This approach has the advantages of increased time efficiency and reducing the impact of human EEG raters, for the modelling of IED-related BOLD changes. We have shown that the BOLD changes associated with IEDs observed on icEEG, even if very localised, in patients with focal epilepsy can be widespread. This tool can therefore provide a less biased new insight into the regions responsible for generating IEDs.

CHAPTER 7: CONCLUSION AND FUTURE WORK

7.1 General Conclusions

The aim of this thesis was to provide a solution for a more consistent and less biased marking of icEEG IEDs using an automated neuronal spike classification algorithm, Wave_clus, for the purpose of producing more biologically meaningful IED-related BOLD maps. A study by Pedreira et al. (2014), demonstrated the successful use of Wave_clus (WC) (Quian Quiroga et al., 2004), to classify IEDs on scalp EEG for the purpose of modelling the concurrently acquired fMRI. Since Wave_clus, does not make assumptions of the geometry or spatial distribution of the electrodes, it can potentially be used in the classification of icEEG IEDs. However, the use of Wave_clus on IED waveforms is not a streamlined process and a number of pre-processing steps are required to adapt an IED dataset to WC. Once the IEDs are detected and the channels of interest are selected the temporal marking of each IED is precisely adjusted to the peak of the spiky component (Pedreira et al., 2014). Then the IEDs are segmented using an IED classification epoch time window around the peak of the spiky component and concatenated across the channels of interest to form meta-IEDs. The meta-IEDs constitute the WC input resulting in automated IED classification (Pedreira et al., 2014).

In the pilot study (Chapter 4), I optimised the pre-processing pipeline necessary to adapt an IED dataset to WC. I developed a new algorithm (*max GF-adjusted* algorithm) that adjusted the original IED marker to the peak of the spiky component, by incorporating the GFP and a universal IED marker adjustment time window (+/-12ms). As a result this algorithm is able to fully automate the alignment of the original IED marker to the peak of the spiky component, whilst maintaining the temporal relationship across channels. I also defined an optimal IED classification epoch time window (-100ms pre peak and 200ms post peak of the spiky component) by analysing the time-frequency characteristics of a sub sample of the IEDs. The results in this study were encouraging enough to incorporate the *max GFP-adjusted* algorithm and the optimal IED classification epoch time window in the pre-processing pipeline prior to WC classification for the next two studies.

In the following chapter (Chapter 5) I validated the application of Wave_clus as an automated IED classification algorithm on icEEG IEDs. I did this by comparing human expert IED classification of three EEG reviewers, as it is performed in normal ('optimal') conditions, against the classification of WC on 100 IEDs from five patients. To our knowledge, no formal comparison of automated vs human observer classification of IEDs

on icEEG has been published to date. Therefore, I designed a novel validation scheme that targeted the following questions: 1) does WC-human IED classification agreement variability fall within inter-human IED classification variability 2) looking at the classification labels (or clustering groups) of individual IEDs and determining whether WC results are similar to those of the human reviewers. I used the variation of information metric (Meila, 2007) to determine whether WC-human IED classification agreement variability falls within inter-human variability. In this regard I found comparable overlap between WC-human and inter-human classification comparisons indicating that WC classifications cannot be distinguished from human results. Secondly by comparing the classification labels of IEDs, I found that the sensitivity of WC was similar to that of humans and there was generally a good classification overlap. Therefore, this study indicates that WC performance is indistinguishable to that of EEG reviewers' suggesting it could be a valuable clinical tool for the assessment of IEDs. Although the sample size of our study (100 IEDs per patient) was lower compared to studies that validate IED detection algorithms (sample sizes ranging from 279-6534 IEDs per patient) (Dumpelmann and Elger, 1999, Barkmeier et al., 2012, Gaspard et al., 2014, Janca et al., 2015), it is important to note that IED detection is a much less complex and arduous task than IED classification. As a result I kept the IED sample size to 100 per recording (for a total sample size of 500), to minimise human rater fatigue and related error (Barkmeier et al., 2012). It is also important to note that the number and characteristics of the classes found by WC in this study was similar to when applied to the entire recordings in the next study. The results in this study were encouraging enough to apply WC across the whole EEG time course to the entire dataset of IEDs.

In Chapter 6 I applied WC across the entire EEG time course to the entire dataset of IEDs in patients that had a good postsurgical outcome (ILAE 1). This was carried out to determine whether Wave_clus can produce more biological meaningful BOLD patterns with the EZ compared to the BOLD patterns obtained based on the conventional, visual classification. For each IED class in the area of resection (the EZ), I compared the concordance level between their associated BOLD maps and EZ, for the automated and visual classifications. I found that BOLD maps showed the same degree of concordance for three patients for the automated and visual approach and in four patients, there was a higher degree of concordance for the automated approach. In this regard, I found automated IED classification, using WC, to be both feasible and to produce more biologically meaningful IED-related BOLD maps compared to the visual/conventional

approach. This demonstrates the benefits of using automated IED classification to map the IED-related BOLD changes for an icEEG-fMRI dataset.

Therefore, in this thesis I have validated WC as an automated icEEG IED classification algorithm and demonstrated that it can produce more biologically meaningful IED-related BOLD maps.

7.2 Future Work

Although in this thesis, I have shown that WC is an efficient tool to automatically classify IEDs, it is important to note that human intervention is required in this process in the form of IED detection. Future studies should be carried out to determine the reproducibility of WC classification for the IEDs detected by different EEG reviewers.

Most automated icEEG IED detection algorithms are designed to temporally detect IEDs (Dümpelmann and Elger, 1999, Brown et al., 2007, Barkmeier et al., 2012, Gaspard et al., 2014) and studies have used these algorithms to quantify the relationship of IEDs to the invasively defined SOZ (Hufnagel et al., 2000, Asano et al., 2003, Marsh et al. 2010, Gaspard et al., 2014). Some studies have shown that channels with high frequency of IEDs overlap most with the SOZ (Asano et al., 2003, Marsh et al., 2010) whereas other algorithms have shown that high amplitude IEDs overlap with the SOZ (Hufnagel et al., 2000, Gaspard et al., 2014). However, these algorithms do not incorporate spatial classification. Wave_clus can be used to complement these algorithms and provide further information on the relationship of IEDs and the invasively defined SOZ.

To date we have recruited 19 patients that have undergone simultaneous IcEEG-fMRI with eight patients having a good postsurgical outcome (analysed in Chapter 6) and 5 showing a poor postsurgical outcome (see Table 3-1). Classifying icEEG IEDs using the Wave_clus approach can be used to compare the BOLD patterns associated with good postsurgical and poor postsurgical outcome patients to determine whether icEEG-fMRI can predict postsurgical outcome.

Some previous studies analysing whether scalp EEG-fMRI studies can predict postsurgical outcome have focused on the GM BOLD cluster as the marker that best represents the EZ (Thornton et al., 2010, An et al., 2013, Centeno et al., 2017). However, in two of these studies the sensitivity of the GM being present in the EZ in good postsurgical outcome patients was <50% (An et al., 2013, Centeno et al., 2017) indicating that the GM may not be the most accurate marker of the EZ. In the study carried out by

Centeno et al. (2017), the use of concordance with a cluster using electrical source imaging (ESI) was shown to be more sensitive in localising the EZ than the GM BOLD cluster (Centeno et al., 2017). When both the ESI cluster and a BOLD cluster were concordant to the EZ, this correctly predicted postsurgical outcome in all patients (Centeno et al., 2017). However, it is important to note that the GM BOLD cluster was closest to the ESI cluster in only a small percentage of these cases indicating that clusters with a lower statistical value may also be clinically relevant (Centeno et al., 2017). Future work comparing the ESI cluster to the clusters obtained using icEEG-fMRI in our patients can be carried out to complement this new approach in combining ESI with EEG-fMRI.

References

Aghakhani, Y., Kobayashi, E., Bagshaw, A.P., Hawco, C., Benar, C.G., Dubeau, F. and Gotman, J., 2006. Cortical and thalamic fMRI responses in partial epilepsy with focal and bilateral synchronous spikes. *Clinical Neurophysiology*, *117*(1), pp.177-191.

Aghakhani, Y., Beers, C.A., Pittman, D.J., Gaxiola-Valdez, I., Goodyear, B.G. and Federico, P., 2015. Co-localization between the BOLD response and epileptiform discharges recorded by simultaneous intracranial EEG-fMRI at 3 T. *NeuroImage: Clinical*, *7*, pp.755-763.

Allen, P.J., Polizzi, G., Krakow, K., Fish, D.R. and Lemieux, L., 1998. Identification of EEG events in the MR scanner: the problem of pulse artifact and a method for its subtraction. *Neuroimage*, *8*(3), pp.229-239.

Allen, P.J., Josephs, O. and Turner, R., 2000. A method for removing imaging artifact from continuous EEG recorded during functional MRI. *Neuroimage*, *12*(2), pp.230-239.

An, D., Fahoum, F., Hall, J., Olivier, A., Gotman, J. and Dubeau, F., 2013. Electroencephalography/functional magnetic resonance imaging responses help predict surgical outcome in focal epilepsy. *Epilepsia*, *54*(12), pp.2184-2194.

Asano, E., Muzik, O., Shah, A., Juhász, C., Chugani, D.C., Sood, S., Janisse, J., Ergun, E.L., Ahn-Ewing, J., Shen, C. and Gotman, J., 2003. Quantitative interictal subdural EEG analyses in children with neocortical epilepsy. *Epilepsia*, *44*(3), pp.425-434.

Barkmeier, D.T., Shah, A.K., Flanagan, D., Atkinson, M.D., Agarwal, R., Fuerst, D.R., Jafari-Khouzani, K. and Loeb, J.A., 2012. High inter-reviewer variability of spike detection on intracranial EEG addressed by an automated multi-channel algorithm. *Clinical Neurophysiology*, *123*(6), pp.1088-1095.

Bartolomei, F., Trébuchon, A., Bonini, F., Lambert, I., Gavaret, M., Woodman, M., Giusiano, B., Wendling, F. and Bénar, C., 2016. What is the concordance between the seizure onset zone and the irritative zone? A SEEG quantified study. *Clinical Neurophysiology*, *127*(2), pp.1157-1162.

Bautista, R.E.D., Spencer, D.D. and Spencer, S.S., 1998. EEG findings in frontal lobe epilepsies. *Neurology*, *50*(6), pp.1765-1771.

Boesebeck, F., Schulz, R., May, T. and Ebner, A., 2002. Lateralizing semiology predicts the seizure outcome after epilepsy surgery in the posterior cortex. *Brain*, *125*(10), pp.2320-2331.

Boucousis, S.M., Beers, C.A., Cunningham, C.J., Gaxiola-Valdez, I., Pittman, D.J., Goodyear, B.G. and Federico, P., 2012. Feasibility of an intracranial EEG–fMRI protocol at 3T: Risk assessment and image quality. *Neuroimage*, *63*(3), pp.1237-1248.

Bourien, J., Bartolomei, F., Bellanger, J.J., Gavaret, M., Chauvel, P. and Wendling, F., 2005. A method to identify reproducible subsets of co-activated structures during interictal spikes. Application to intracerebral EEG in temporal lobe epilepsy. *Clinical Neurophysiology*, *116*(2), pp.443-455.

Brown, M.W., Porter, B.E., Dlugos, D.J., Keating, J., Gardner, A.B., Storm, P.B. and Marsh, E.D., 2007. Comparison of novel computer detectors and human performance for spike detection in intracranial EEG. *Clinical neurophysiology*, *118*(8), pp.1744-1752.

Brunet, D., Murray, M.M. and Michel, C.M., 2011. Spatiotemporal analysis of multichannel EEG: CARTOOL. *Computational intelligence and neuroscience*, *2011*, p.2.

Berg, A.T., Berkovic, S.F., Brodie, M.J., Buchhalter, J., Cross, J.H., van Emde Boas, W., Engel, J., French, J., Glauser, T.A., Mathern, G.W. and Moshé, S.L., 2010. Revised terminology and concepts for organization of seizures and epilepsies: report of the ILAE Commission on Classification and Terminology, 2005–2009. *Epilepsia*, *51*(4), pp.676-685.

Bettus, G., Ranjeva, J.P., Wendling, F., Bénar, C.G., Confort-Gouny, S., Régis, J., Chauvel, P., Cozzone, P.J., Lemieux, L., Bartolomei, F. and Guye, M., 2011. Interictal functional connectivity of human epileptic networks assessed by intracerebral EEG and BOLD signal fluctuations. *PloS one*, *6*(5), p.e20071.

Buxton, R.B., 2012. Dynamic models of BOLD contrast. *Neuroimage*, *62*(2), pp.953-961.

Carmichael, D.W., Thornton, J.S., Rodionov, R., Thornton, R., McEvoy, A.W., Ordidge, R.J., Allen, P.J. and Lemieux, L., 2010. Feasibility of simultaneous intracranial EEG-fMRI in humans: a safety study. *Neuroimage*, *49*(1), pp.379-390.

Carmichael, D.W., Vulliemoz, S., Rodionov, R., Thornton, J.S., McEvoy, A.W. and Lemieux, L., 2012. Simultaneous intracranial EEG–fMRI in humans: protocol considerations and data quality. *Neuroimage*, *63*(1), pp.301-309.

Carreño, M., Lüders, H O., 2001. General prinicples of pre surgical evaluation. In: Lüders, H., Comair, Y *Epilepsy surgery*. Philadelphia: Lippincott Williams & Wilkins. pp185-199.

Centeno, M., Tierney, T.M., Perani, S., Shamshiri, E.A., StPier, K., Wilkinson, C., Konn, D., Vulliemoz, S., Grouiller, F., Lemieux, L., Pressler, R.M., Clark, C.A., Cross, J.H. and Carmichael, D.W., Combined EEG-fMRI and ESI improves localisation of paediatric focal epilepsy. *Annals of Neurology*. In press

Chaudhary, U.J., Carmichael, D.W., Rodionov, R., Thornton, R.C., Bartlett, P., Vulliemoz, S., Micallef, C., McEvoy, A.W., Diehl, B., Walker, M.C. and Duncan, J.S., 2012. Mapping preictal and ictal haemodynamic networks using video-electroencephalography and functional imaging. *Brain*, *135*(12), pp.3645-3663.

Chaudhary, U.J., Duncan, J.S. and Lemieux, L., 2013. Mapping hemodynamic correlates of seizures using fMRI: a review. *Human brain mapping*, *34*(2), pp.447-466.

Chung, M.Y., Walczak, T.S., Lewis, D.V., Dawson, D.V. and Radtke, R., 1991. Temporal lobectomy and independent bitemporal interictal activity: what degree of lateralization is sufficient?. *Epilepsia*, *32*(2), pp.195-201.

Coan, A.C., Chaudhary, U.J., Grouiller, F., Campos, B.M., Perani, S., De Ciantis, A., Vulliemoz, S., Diehl, B., Beltramini, G.C., Carmichael, D.W. and Thornton, R.C., 2015. EEG-fMRI in the presurgical evaluation of temporal lobe epilepsy. *J Neurol Neurosurg Psychiatry*, pp.jnnp-2015.

Comaniciu, D., Ramesh, V. and Meer, P., 2000. Real-time tracking of non-rigid objects using mean shift. In *Computer Vision and Pattern Recognition, 2000. Proceedings. IEEE Conference on* (Vol. 2, pp. 142-149). IEEE.

Chaudhary, U.J., Rodionov, R., Carmichael, D.W., Thornton, R.C., Duncan, J.S. and Lemieux, L., 2012. Improving the sensitivity of EEG-fMRI studies of epileptic activity by modelling eye blinks, swallowing and other video-EEG detected physiological confounds. *Neuroimage*, *61*(4), pp.1383-1393.

Chaudhary, U.J., Centeno, M., Thornton, R.C., Rodionov, R., Vulliemoz, S., McEvoy, A.W., Diehl, B., Walker, M.C., Duncan, J.S., Carmichael, D.W. and Lemieux, L., 2016. Mapping human preictal and ictal haemodynamic networks using simultaneous intracranial EEG-fMRI. *NeuroImage: Clinical*, *11*, pp.486-493.

Cunningham, C.B., Goodyear, B.G., Badawy, R., Zaamout, F., Pittman, D.J., Beers, C.A. and Federico, P., 2012. Intracranial EEG-fMRI analysis of focal epileptiform discharges in humans. *Epilepsia*, *53*(9), pp.1636-1648.

De Curtis, M. and Avanzini, G., 2001. Interictal spikes in focal epileptogenesis. *Progress in neurobiology*, *63*(5), pp.541-567.

Diedrichsen, J. and Shadmehr, R., 2005. Detecting and adjusting for artifacts in fMRI time series data. *Neuroimage*, *27*(3), pp.624-634.

Dümpelmann, M. and Elger, C.E., 1999. Visual and automatic investigation of epileptiform spikes in intracranial EEG recordings. *Epilepsia*, *40*(3), pp.275-285.

Duncan, J.S., 2010. Epilepsy in 2010: Refinement of optimal medical and surgical treatments. *Nature Reviews Neurology*, *7*(2), pp.72-74.

Fahoum, F., Lopes, R., Pittau, F., Dubeau, F. and Gotman, J., 2012. Widespread epileptic networks in focal epilepsies: EEG-fMRI study. *Epilepsia*, *53*(9), pp.1618-1627.

Ferrier, C.H., Alarcon, G., Engelsman, J., Binnie, C.D., Koutroumanidis, M., Polkey, C.E., Janota, I. and Dean, A., 2001. Relevance of residual histologic and electrocorticographic abnormalities for surgical outcome in frontal lobe epilepsy. *Epilepsia*, *42*(3), pp.363-371.

Fernández, I.S. and Loddenkemper, T., 2013. Electrocorticography for seizure foci mapping in epilepsy surgery. *Journal of Clinical Neurophysiology*, *30*(6), pp.554-570.

Fisher, R.S., Boas, W.V.E., Blume, W., Elger, C., Genton, P., Lee, P. and Engel, J., 2005. Epileptic seizures and epilepsy: definitions proposed by the International League Against Epilepsy (ILAE) and the International Bureau for Epilepsy (IBE). *Epilepsia*, *46*(4), pp.470-472.

Flanagan, D., Agarwal, R. and Gotman, J., 2002. Computer-aided spatial classification of epileptic spikes. *Journal of clinical neurophysiology*, *19*(2), pp.125-135.

Flanagan, D., Abbott, D.F. and Jackson, G.D., 2009. How wrong can we be? The effect of inaccurate mark-up of EEG/fMRI studies in epilepsy. *Clinical Neurophysiology*, *120*(9), pp.1637-1647.

Fox, P.T. and Raichle, M.E., 1986. Focal physiological uncoupling of cerebral blood flow and oxidative metabolism during somatosensory stimulation in human subjects. *Proceedings of the National Academy of Sciences*, *83*(4), pp.1140-1144.

Friston, K.J., Holmes, A.P., Worsley, K.J., Poline, J.P., Frith, C.D. and Frackowiak, R.S., 1994. Statistical parametric maps in functional imaging: a general linear approach. *Human brain mapping*, *2*(4), pp.189-210.

Friston, K., Ashburner, J., Frith, C.D., Poline, J.B., Heather, J.D. and Frackowiak, R.S., 1995. Spatial registration and normalization of images. *Human brain mapping*, *3*(3), pp.165-189.

Friston, K.J., Williams, S., Howard, R., Frackowiak, R.S. and Turner, R., 1996. Movement-related effects in fMRI time-series. *Magnetic resonance in medicine*, *35*(3), pp.346-355.

Friston, K.J., Josephs, O., Rees, G. and Turner, R., 1998. Nonlinear event-related responses in fMRI. *Magnetic resonance in medicine*, *39*(1), pp.41-52.

Gaspard, N., Alkawadri, R., Farooque, P., Goncharova, I.I. and Zaveri, H.P., 2014. Automatic detection of prominent interictal spikes in intracranial EEG: Validation of an algorithm and relationsip to the seizure onset zone. *Clinical Neurophysiology*, *125*(6), pp.1095-1103.

Glover, G.H., 1999. Deconvolution of impulse response in event-related BOLD fMRI. *Neuroimage*, *9*(4), pp.416-429.

Glover, G.H., Li, T.Q. and Ress, D., 2000. Image-based method for retrospective correction of physiological motion effects in fMRI: RETROICOR. *Magnetic resonance in medicine*, *44*(1), pp.162-167.

Gold, C., Henze, D.A., Koch, C. and Buzsaki, G., 2006. On the origin of the extracellular action potential waveform: a modeling study. *Journal of neurophysiology*, *95*(5), pp.3113-3128.

Goncharova, I.I., Spencer, S.S., Duckrow, R.B., Hirsch, L.J., Spencer, D.D. and Zaveri, H.P., 2013. Intracranially recorded interictal spikes: relation to seizure onset area and effect of medication and time of day. *Clinical Neurophysiology*, *124*(11), pp.2119-2128.

Gotman, J., 1999. Automatic detection of seizures and spikes. *Journal of Clinical Neurophysiology*, *16*(2), pp.130-140.

Graan, L.A.V., Lemieux, L. and Chaudhary, U.J., 2013. Scalp and Intracranial EEG-fMRI in Epilepsy. *J Neurol Neurophysiol*, *4*(156), pp.19-22.

Grech, R., Cassar, T., Muscat, J., Camilleri, K.P., Fabri, S.G., Zervakis, M., Xanthopoulos, P., Sakkalis, V. and Vanrumste, B., 2008. Review on solving the inverse problem in EEG source analysis. *Journal of neuroengineering and rehabilitation*, *5*(1), p.25.

Grouiller, F., Thornton, R.C., Groening, K., Spinelli, L., Duncan, J.S., Schaller, K., Siniatchkin, M., Lemieux, L., Seeck, M., Michel, C.M. and Vulliemoz, S., 2011. With or without spikes: localization of focal epileptic activity by simultaneous electroencephalography and functional magnetic resonance imaging. *Brain*, *134*(10), pp.2867-2886.

Halford, J.J., Schalkoff, R.J., Zhou, J., Benbadis, S.R., Tatum, W.O., Turner, R.P., Sinha, S.R., Fountain, N.B., Arain, A., Pritchard, P.B. and Kutluay, E., 2013. Standardized database development for EEG epileptiform transient detection: EEGnet scoring system and machine learning analysis. *Journal of neuroscience methods*, *212*(2), pp.308-316.

Hardy, S.G., Miller, J.W., Holmes, M.D., Born, D.E., Ojemann, G.A., Dodrill, C.B. and Hallam, D.K., 2003. Factors predicting outcome of surgery for intractable epilepsy with pathologically verified mesial temporal sclerosis. *Epilepsia*, *44*(4), pp.565-568.

Harris, K.D., Henze, D.A., Csicsvari, J., Hirase, H. and Buzsáki, G., 2000. Accuracy of tetrode spike separation as determined by simultaneous intracellular and extracellular measurements. *Journal of neurophysiology*, *84*(1), pp.401-414.

Hirsch, L.J., Spencer, S.S., Williamson, P.D., Spencer, D.D. and Mattson, R.H., 1991. Comparison of bitemporal and unitemporal epilepsy defined by depth electroencephalography. *Annals of neurology*, *30*(3), pp.340-346.

Holmes, M.D., Kutsy, R.L., Ojemann, G.A., Wilensky, A.J. and Ojemann, L.M., 2000. Interictal, unifocal spikes in refractory extratemporal epilepsy predict ictal origin and postsurgical outcome. *Clinical Neurophysiology*, *111*(10), pp.1802-1808.

Hufnagel, A., Dümpelmann, M., Zentner, J., Schijns, O. and Elger, C.E., 2000. Clinical relevance of quantified intracranial interictal spike activity in presurgical evaluation of epilepsy. *Epilepsia*, *41*(4), pp.467-478.

James, C.J., Jones, R.D., Bones, P.J. and Carroll, G.J., 1999. Detection of epileptiform discharges in the EEG by a hybrid system comprising mimetic, self-organized artificial neural network, and fuzzy logic stages. *Clinical Neurophysiology*, *110*(12), pp.2049-2063.

Janca, R., Jezdik, P., Cmejla, R., Krsek, P., Jefferys, J.G., Marusic, P. and Jiruska, P., 2013, May. Automatic detection and spatial clustering of interictal discharges in invasive recordings. In *Medical Measurements and Applications Proceedings (MeMeA), 2013 IEEE International Symposium on* (pp. 219-223). IEEE.

Janszky, J., Janszky, I., Schulz, R., Hoppe, M., Behne, F., Pannek, H.W. and Ebner, A., 2005. Temporal lobe epilepsy with hippocampal sclerosis: predictors for long-term surgical outcome. *Brain*, *128*(2), pp.395-404.

Kailath, T., 1967. The divergence and Bhattacharyya distance measures in signal selection. *IEEE transactions on communication technology*, *15*(1), pp.52-60.

Khoo, H.M., Hao, Y., Ellenrieder, N., Zazubovits, N., Hall, J., Olivier, A., Dubeau, F. and Gotman, J., 2017. The hemodynamic response to interictal epileptic discharges localizes the seizure-onset zone. *Epilepsia*, *58*(5), pp.811-823.

Krendl, R., Lurger, S. and Baumgartner, C., 2008. Absolute spike frequency predicts surgical outcome in TLE with unilateral hippocampal atrophy. *Neurology*, *71*(6), pp.413-418.

Kwan, P. and Sander, J.W., 2004. The natural history of epilepsy: an epidemiological view. *Journal of Neurology, Neurosurgery & Psychiatry*, *75*(10), pp.1376-1381.

Laskowitz, D.T., Sperling, M.R., French, J.A. and O'connor, M.J., 1995. The syndrome of frontal lobe epilepsy Characteristics and surgical management. *Neurology*, *45*(4), pp.780-787.

Laufs, H., Daunizeau, J., Carmichael, D.W. and Kleinschmidt, A., 2008. Recent advances in recording electrophysiological data simultaneously with magnetic resonance imaging. *Neuroimage*, *40*(2), pp.515-528.

Laufs, H., 2012a. A personalized history of EEG–fMRI integration. *Neuroimage*, *62*(2), pp.1056-1067.

Laufs, H., 2012b. Functional imaging of seizures and epilepsy: evolution from zones to networks. *Current opinion in neurology*, *25*(2), pp.194-200.

Liston, A.D., Lund, T.E., Salek-Haddadi, A., Hamandi, K., Friston, K.J. and Lemieux, L., 2006a. Modelling cardiac signal as a confound in EEG-fMRI and its application in focal epilepsy studies. *Neuroimage*, *30*(3), pp.827-834.

Liston, A.D., De Munck, J.C., Hamandi, K., Laufs, H., Ossenblok, P., Duncan, J.S. and Lemieux, L., 2006b. Analysis of EEG–fMRI data in focal epilepsy based on automated spike classification and Signal Space Projection. *Neuroimage*, *31*(3), pp.1015-1024.

Logothetis, N.K., Guggenberger, H., Peled, S. and Pauls, J., 1999. Functional imaging of the monkey brain. *Nature neuroscience*, *2*(6), pp.555-562.

Logothetis, N.K., Pauls, J., Augath, M., Trinath, T. and Oeltermann, A., 2001. Neurophysiological investigation of the basis of the fMRI signal. *Nature*, *412*(6843), pp.150-157.

Lu, Y., Bagshaw, A.P., Grova, C., Kobayashi, E., Dubeau, F. and Gotman, J., 2006. Using voxel-specific hemodynamic response function in EEG-fMRI data analysis. *Neuroimage*, *32*(1), pp.238-247.

Lüders, H.O., Najm, I., Nair, D., Widdess-Walsh, P. and Bingman, W., 2006. The epileptogenic zone: general principles. *Epileptic disorders*, *8*(2), pp.1-9.

Marsh, E.D., Peltzer, B., Brown III, M.W., Wusthoff, C., Storm Jr, P.B., Litt, B. and Porter, B.E., 2010. Interictal EEG spikes identify the region of electrographic seizure onset in some, but not all, pediatric epilepsy patients. *Epilepsia*, *51*(4), pp.592-601.

Meilă, M., 2007. Comparing clusterings—an information based distance. *Journal of multivariate analysis*, *98*(5), pp.873-895.

Moeller, F., Tyvaert, L., Nguyen, D.K., LeVan, P., Bouthillier, A., Kobayashi, E., Tampieri, D., Dubeau, F. and Gotman, J., 2009. EEG-fMRI Adding to standard evaluations of patients with nonlesional frontal lobe epilepsy. *Neurology*, *73*(23), pp.2023-2030.

Murta, T., Leite, M., Carmichael, D.W., Figueiredo, P. and Lemieux, L., 2015. Electrophysiological correlates of the BOLD signal for EEG-informed fMRI. *Human brain mapping*, *36*(1), pp.391-414.

Murta, T., Hu, L., Tierney, T.M., Chaudhary, U.J., Walker, M.C., Carmichael, D.W., Figueiredo, P. and Lemieux, L., 2016. A study of the electro-haemodynamic coupling using simultaneously acquired intracranial EEG and fMRI data in humans. *NeuroImage*, *142*, pp.371-380.

Murta, T., Chaudhary, U.J., Tierney, T.M., Dias, A., Leite, M., Carmichael, D.W., Figueiredo, P. and Lemieux, L., 2017. Phase–amplitude coupling and the BOLD signal: a simultaneous intracranial EEG (icEEG)-fMRI study in humans performing a finger-tapping task. *Neuroimage*, *146*, pp.438-451.

Noachtar, S. and Rémi, J., 2009. The role of EEG in epilepsy: a critical review. *Epilepsy & Behavior*, *15*(1), pp.22-33.

Niedermeyer, E. and da Silva, F.L. eds., 2005. *Electroencephalography: basic principles, clinical applications, and related fields*. Lippincott Williams & Wilkins.

Ogawa, S., Lee, T.M., Kay, A.R. and Tank, D.W., 1990. Brain magnetic resonance imaging with contrast dependent on blood oxygenation. *Proceedings of the National Academy of Sciences*, *87*(24), pp.9868-9872.

Olejniczak, P., 2006. Neurophysiologic basis of EEG. *Journal of clinical neurophysiology*, *23*(3), pp.186-189.

Ossadtchi, A., Baillet, S., Mosher, J.C., Thyerlei, D., Sutherling, W. and Leahy, R.M., 2004. Automated interictal spike detection and source localization in magnetoencephalography using independent components analysis and spatio-temporal clustering. *Clinical Neurophysiology*, *115*(3), pp.508-522.

Palmini, A., Gambardella, A., Andermann, F., Dubeau, F., da Costa, J.C., Olivier, A., Tampieri, D., Gloor, P., Quesney, F., Andermann, E. and Paglioli, E., 1995. Intrinsic epileptogenicity of human dysplastic cortex as suggested by corticography and surgical results. *Annals of neurology*, *37*(4), pp.476-487.

Pedreira, C., Vaudano, A.E., Thornton, R.C., Chaudhary, U.J., Vulliemoz, S., Laufs, H., Rodionov, R., Carmichael, D.W., Lhatoo, S.D., Guye, M. and Quiroga, R.Q., 2014. Classification of EEG abnormalities in partial epilepsy with simultaneous EEG–fMRI recordings. *Neuroimage*, *99*, pp.461-476.

Pittau, F., Dubeau, F. and Gotman, J., 2012. Contribution of EEG/fMRI to the definition of the epileptic focus. *Neurology*, *78*(19), pp.1479-1487.

Pittau, F., Fahoum, F., Zelmann, R., Dubeau, F. and Gotman, J., 2013. Negative BOLD response to interictal epileptic discharges in focal epilepsy. *Brain topography*, *26*(4), pp.627-640.

Quiroga, R.Q., Nadasdy, Z. and Ben-Shaul, Y., 2004. Unsupervised spike detection and sorting with wavelets and superparamagnetic clustering. *Neural computation*, *16*(8), pp.1661-1687.

Quiroga, R.Q., Reddy, L., Kreiman, G., Koch, C. and Fried, I., 2005. Invariant visual representation by single neurons in the human brain. *Nature*, *435*(7045), pp.1102-1107.

Quiroga, R.Q., 2007. Spike sorting. *Scholarpedia*, *2*(12), p.3583.

Quiroga, R.Q., Kraskov, A., Koch, C. and Fried, I., 2009. Explicit encoding of multimodal percepts by single neurons in the human brain. *Current Biology*, *19*(15), pp.1308-1313.

Radhakrishnan, K., So, E.L., Silbert, P.L., Jack, C.R., Cascino, G.D., Sharbrough, F.W. and O'brien, P.C., 1998. Predictors of outcome of anterior temporal lobectomy for intractable epilepsy A multivariate study. *Neurology*, *51*(2), pp.465-471.

Raichle, M.E., MacLeod, A.M., Snyder, A.Z., Powers, W.J., Gusnard, D.A. and Shulman, G.L., 2001. A default mode of brain function. *Proceedings of the National Academy of Sciences*, *98*(2), pp.676-682.

Rey, H.G., Pedreira, C. and Quiroga, R.Q., 2015. Past, present and future of spike sorting techniques. *Brain research bulletin*, *119*, pp.106-117.

Rosa, M.J., Kilner, J., Blankenburg, F., Josephs, O. and Penny, W., 2010. Estimating the transfer function from neuronal activity to BOLD using simultaneous EEG-fMRI. *Neuroimage*, *49*(2), pp.1496-1509.

Rosati, A., Aghakhani, Y., Bernasconi, A., Olivier, A., Andermann, F., Gotman, J. and Dubeau, F., 2003. Intractable temporal lobe epilepsy with rare spikes is less severe than with frequent spikes. *Neurology*, *60*(8), pp.1290-1295.

Rosenow, F., Klein, K.M. and Hamer, H.M., 2015. Non-invasive EEG evaluation in epilepsy diagnosis. *Expert review of neurotherapeutics*, *15*(4), pp.425-444.

Rutishauser, U., Schuman, E.M. and Mamelak, A.N., 2006. Online detection and sorting of extracellularly recorded action potentials in human medial temporal lobe recordings, in vivo. *Journal of neuroscience methods*, *154*(1), pp.204-224.

Salek-Haddadi, A., Diehl, B., Hamandi, K., Merschhemke, M., Liston, A., Friston, K., Duncan, J.S., Fish, D.R. and Lemieux, L., 2006. Hemodynamic correlates of epileptiform discharges: an EEG-fMRI study of 63 patients with focal epilepsy. *Brain research*, *1088*(1), pp.148-166.

Sander, J.W., 2003. The epidemiology of epilepsy revisited. *Current opinion in neurology*, *16*(2), pp.165-170.

Scherg, M., Ille, N., Weckesser, D., Ebert, A., Ostendorf, A., Boppel, T., Schubert, S., Larsson, P.G., Henning, O. and Bast, T., 2012. Fast evaluation of interictal spikes in long-term EEG by hyper-clustering. *Epilepsia*, *53*(7), pp.1196-1204.

Schulz, R., Lüders, H.O., Hoppe, M., Tuxhorn, I., May, T. and Ebner, A., 2000. Interictal EEG and ictal scalp EEG propagation are highly predictive of surgical outcome in mesial temporal lobe epilepsy. *Epilepsia*, *41*(5), pp.564-570.

Sharma, N.K., Pedreira, C., Centeno, M., Chaudhary, U.J., Wehner, T., França, L.G., Yadee, T., Murta, T., Leite, M., Vos, S.B., Ourselin, S, Diehl, B. and Lemieux, L., 2017. A novel scheme for the validation of an automated classification method for epileptic spikes by comparison with multiple observers. *Clinical Neurophysiology*, *128*(7), pp.1246-1254.

Singh, K. and Xie, M., 2008. Bootstrap: a statistical method. *Unpublished manuscript, Rutgers University, USA. Retrieved from http://www. stat. rutgers. edu/home/mxie/RCPapers/bootstrap. pdf*.

Sirven, J.I., Malamut, B.L., Liporace, J.D., O'Connor, M.J. and Sperling, M.R., 1997. Outcome after temporal lobectomy in bilateral temporal lobe epilepsy. *Annals of neurology*, *42*(6), pp.873-878.

Skrandies, W., 1990. Global field power and topographic similarity. *Brain topography*, *3*(1), pp.137-141.

Smith, S.M., Fox, P.T., Miller, K.L., Glahn, D.C., Fox, P.M., Mackay, C.E., Filippini, N., Watkins, K.E., Toro, R., Laird, A.R. and Beckmann, C.F., 2009. Correspondence of the brain's

functional architecture during activation and rest. *Proceedings of the National Academy of Sciences*, *106*(31), pp.13040-13045.

So, N., Gloor, P., Quesney, L.F., Jones-Gotman, M., Olivier, A. and Andermann, F., 1989. Depth electrode investigations in patients with bitemporal epileptiform abnormalities. *Annals of neurology*, *25*(5), pp.423-431.

Spencer, D., Nguyen, D.K. and Sivaraju, A., 2009. Invasive EEG in presurgical evaluation of epilepsy. *The Treatment of Epilepsy, Third Edition*, pp.767-798.

Spencer, D., Nguyen, D.K. and Sivaraju, A., 2015. Invasive EEG in presurgical evaluation of epilepsy. *The Treatment of Epilepsy, Fourth Edition*, pp.733-755.

Tao, J.X., Ray, A., Hawes-Ebersole, S. and Ebersole, J.S., 2005. Intracranial EEG substrates of scalp EEG interictal spikes. *Epilepsia*, *46*(5), pp.669-676.

Thornton, R., Laufs, H., Rodionov, R., Cannadathu, S., Carmichael, D.W., Vulliemoz, S., Salek-Haddadi, A., McEvoy, A.W., Smith, S.M., Lhatoo, S. and Elwes, R.D., 2010. EEG correlated functional MRI and postoperative outcome in focal epilepsy. *Journal of Neurology, Neurosurgery & Psychiatry*, *81*(8), pp.922-927.

Thornton, R., Vulliemoz, S., Rodionov, R., Carmichael, D.W., Chaudhary, U.J., Diehl, B., Laufs, H., Vollmar, C., McEvoy, A.W., Walker, M.C. and Bartolomei, F., 2011. Epileptic networks in focal cortical dysplasia revealed using electroencephalography–functional magnetic resonance imaging. *Annals of neurology*, *70*(5), pp.822-837.

Tierney, T.M., Weiss-Croft, L.J., Centeno, M., Shamshiri, E.A., Perani, S., Baldeweg, T., Clark, C.A. and Carmichael, D.W., 2016. FIACH: A biophysical model for automatic retrospective noise control in fMRI. *NeuroImage*, *124*, pp.1009-1020.

Todorova, S., Sadtler, P., Batista, A., Chase, S. and Ventura, V., 2014. To sort or not to sort: the impact of spike-sorting on neural decoding performance. *Journal of neural engineering*, *11*(5), p.056005.

Turkdogan, D., Duchowny, M., Resnick, T. and Jayakar, P., 2005. Subdural EEG patterns in children with taylor-type cortical dysplasia: comparison with nondysplastic lesions. *Journal of clinical neurophysiology*, *22*(1), pp.37-42.

Vadlamudi, L., So, E.L., Worrell, G.A., Mosewich, R.K., Cascino, G.D., Meyer, F.B. and Lesnick, T.G., 2004. Factors underlying scalp-EEG interictal epileptiform discharges in intractable frontal lobe epilepsy. *Epileptic disorders*, *6*(2), pp.89-95.

Valenti, P., Cazamajou, E., Scarpettini, M., Aizemberg, A., Silva, W. and Kochen, S., 2006. Automatic detection of interictal spikes using data mining models. *Journal of neuroscience methods*, *150*(1), pp.105-110.

Van Hese, P., Vanrumste, B., Hallez, H., Carroll, G.J., Vonck, K., Jones, R.D., Bones, P.J., D'Asseler, Y. and Lemahieu, I., 2008. Detection of focal epileptiform events in the EEG by spatio-temporal dipole clustering. *Clinical Neurophysiology*, *119*(8), pp.1756-1770.

Vulliemoz, S., Thornton, R., Rodionov, R., Carmichael, D.W., Guye, M., Lhatoo, S., McEvoy, A.W., Spinelli, L., Michel, C.M., Duncan, J.S. and Lemieux, L., 2009. The spatio-temporal mapping of epileptic networks: combination of EEG–fMRI and EEG source imaging. *Neuroimage*, *46*(3), pp.834-843.

Vulliemoz, S., Carmichael, D.W., Rosenkranz, K., Diehl, B., Rodionov, R., Walker, M.C., McEvoy, A.W. and Lemieux, L., 2011. Simultaneous intracranial EEG and fMRI of interictal epileptic discharges in humans. *Neuroimage*, *54*(1), pp.182-190.

Widdess-Walsh, P., Jeha, L., Nair, D., Kotagal, P., Bingaman, W. and Najm, I., 2007. Subdural electrode analysis in focal cortical dysplasia Predictors of surgical outcome. *Neurology*, *69*(7), pp.660-667.

Wilke, M., 2012. An alternative approach towards assessing and accounting for individual motion in fMRI timeseries. *Neuroimage*, *59*(3), pp.2062-2072.

Wilson, S.B., Turner, C.A., Emerson, R.G. and Scheuer, M.L., 1999. Spike detection II: automatic, perception-based detection and clustering. *Clinical neurophysiology*, *110*(3), pp.404-411.

Yadav, R., Shah, A.K., Loeb, J.A., Swamy, M.N.S. and Agarwal, R., 2011, August. A novel unsupervised spike sorting algorithm for intracranial EEG. In *Engineering in Medicine and Biology Society, EMBC, 2011 Annual International Conference of the IEEE* (pp. 7545-7548). IEEE.

Zijlmans, M., Huiskamp, G., Hersevoort, M., Seppenwoolde, J.H., van Huffelen, A.C. and Leijten, F.S., 2007. EEG-fMRI in the preoperative work-up for epilepsy surgery. *Brain*, *130*(9), pp.2343-2353.

Zijlmans, M., Huiskamp, G.M., van Huffelen, A.C., Spetgens, W.P. and Leijten, F.S., 2008. Detection of temporal lobe spikes: comparing nasopharyngeal, cheek and anterior temporal electrodes to simultaneous subdural recordings. *Clinical Neurophysiology*, *119*(8), pp.1771-1777.

Appendix A

This appendix contains the following results from chapter 5: the case reports and classification results for patient JR, MB and GC. The classification overlap results for all patients and the inter-rater agreement.

A.M –Determining a threshold of similarity between two classifications

Two classifications with perfect agreement have a *VI* value 0. In order to determine a threshold of similarity between two classifications, we generated random classifications for 50 artificial observers, as follows:

1. We established a possible maximum and minimum number of classes per dataset based on an initial evaluation of the clinical EEG report from the five patients involved in this study.
2. The number of classes assigned to each artificial observer was chosen using a random number from a uniform distribution within the range determined in 1.
3. For each of the 100 IEDs a class was assigned randomly from a uniform distribution.
4. The variation of information for each possible pair of artificial classifiers was calculated.
5. Two classifications were considered similar if their *VI* value was more than 2 SD below the mean *VI* value obtained from this random sample.

A.CR - Case Reports

Patient JR

WC identified 4 classes, H2 identified 9 classes and H3 and H4 identified 7 classes; all 4 classifiers had a non-IED class (see table 2). The numbers of events assigned to the non-IED class were 12 (WC), 25 (H2), 28 (H3) and 21 (H4) (see see Appendix A – table A1).

WC Class A

Forty-four IEDs were assigned to class WC_A and involved channels G4 and G5 which is identical to classes H2_A and H4_A, and involved 50% of the channels in H3_A (see Appendix A table A1). The visual similarity between these classes was further reflected in the classification overlap where WC_A agreed the most with H2_A (57%), H3_A (82%) and H4_A (53%) (see Appendix A – table A2).

WC Class B

Eleven IEDs were assigned to class WC_B and involved the same channels as WC_A but are distinguished by their amplitudes ($|A| < |B|$). Similar to WC_A, the channels involved in WC_B were identical to those for class H2_A, and involved 50% of the

channels in H3_A (see Appendix A table A1). The visual similarity between classes was further reflected in the classification overlap where WC_B agreed the most with H2_A (55%) and H3_A (82%). Although WC_B involved the same channels as H4_A, WC_B only had the second highest agreement with H4_A (36%) (see Appendix A table A2).

WC Class C

Thirty-three IEDs were assigned to class WC_C and involved channels G13 G21 G22 DP2 and DP3 which is identical to H4_C (see Appendix A table A1). The visual similarity between these classes was further reflected in the classification overlap and WC_C agreed the most with H4_C (39%) (see Appendix A table A2).

Visual comparison and classification overlap revealed that classes H2_C, _D, _E, _F, _G, _H, H3_B, _C, _D, _E, _F, H4_D, _E, _F did not correspond to any WC class.

Patient MB

WC identified six classes, H2 and H3 identified seven classes and H4 identified six classes; all 4 classifiers had a non-IED class (see table 2). The numbers of events assigned to a non-IED class were 24 (WC), 43 (H2), 11 (H3) and 6 (H4) (see Appendix A table A1).

WC Class A

Thirty-seven IEDs were assigned to class WC_A and involved channel LAH1. The channels involved in this class were identical to those in H2_C, H3_E and involved 50% of the channels involved in H4_A (see Appendix A table A1). This visual similarity was further illustrated in the classification overlap where class WC_A agreed the most with H3_E (100%) and H4_A (86%). Although WC_B involved the same channels as H2_C, WC_B agreed the most with the non-IED class for H2 (89%) (see Appendix A table A5).

WC Class B

Eighteen IEDs were assigned to class WC_B and involved channels RA1 and RA2 with a negative polarity. The channels involved in this class were identical to H2_B, H3_A and H4_D (see Appendix A table A1). This visual similarity was further illustrated in the classification overlap where WC_B agreed the most with H2_A (89%), H3_A (83%) and H4_D (94%) (see Appendix A table A5).

WC Class C

Nine IEDs were assigned to class WC_C and involved channels LAH1 LPH1. The channels involved in this class were identical to H3_C and H4_B and one of these

channels was present in H2_C (see Appendix A table A1). This visual similarity was further illustrated in the classification overlap where WC_C agreed the most with H3_C (56%) and H4_B (67%) (see Appendix A table A5). Although there was a visual similarity between WC_C and H2_C, WC only had the second highest agreement with H2_C (33%); the highest agreement was with the non-IED class (56%) (see Appendix A table A5).

WC Class D

Eight IEDs were assigned to class WC_D and involved the channels RA1 RA2 and RH1. Two out of three channels involved in this class were present in H2_A and B, H3_A and H4_D (see Appendix A table A1). This visual similarity was reflected in the classification overlap where WC_D agreed the most with H2_A (89%), H3_A (63%) and H4_D (100%) (see Appendix A table A5). Although the number of channels involved in WC_D was identical to H4_E, there was no classification overlap between these classes (see Appendix A table A5).

WC Class E

Four IEDs were assigned to class WC_E and involved the same channels as WC_B (RA1 RA2) but were distinguished due to the difference in polarity; WC_E had a negative polarity. Only EEG reviewer H2 did the same and this was shown in the visual similarity between WC_E and H2_B (see Appendix A table A1). This visual similarity is reflected in the classification overlap where WC_E agreed the most with H2_B (100%) (see Appendix A table A5).

The visual comparison and classification overlap indicated that WC classes did not correspond to the three classes H2_D, E and F, three classes H3 _B,D and F, nor H4 C.

Patient GC

WC identified three classes, H2 identified five classes, H3 identified four classes and H4 identified six classes. None of the classifiers had a non-IED class (see Appendix A table A1).

WC Class A

Sixty-three IEDs were assigned to class WC_A and involved the channels GA1 GA2 GA10 GA18. The channels involved in this class were identical to H2_A, H3_A and H4_B (see Appendix A table A1). This was reflected in the classification overlap where WC_A

agreed the most with H2_A (86%), H3_A (90%) and H4_B (48%) (see Appendix A table A6).

WC Class B

Sixteen IEDs were assigned to class WC_B and involved the channel SPBT4. The channel involved in this class was identical to H2_C, H3_B and H4_D (see Appendix A table A1). This was reflected in the classification overlap where WC_C agreed the most with H2_C (94%), H3_B (82%) and H4_D (75%) (see Appendix A table A6).

WC Class C

Twenty-one IEDs were assigned to class WC_C and involved the channels GA1 GA2 GA9 GA10 GA11 GA18 SPBT5 SPBT6. The channels involved in this class were identical to those for H2_B, H3_D and H4_C (see Appendix A table A1). This was reflected in the classification overlap where WC_C agreed the most with H2_B (76%), H3_D (90%) and H4_C (86%) (see Appendix A table A6).

The visual comparison and classification overlap indicated that WC classes did not correspond to 1) two H2 classes (D and E) 2) one H3_(C) 3) three H4 classes (A, E and F).

Table A 1| Summary of the classes and the channels for each class assigned by WC, H2, H3 and H4 for patient JR, MB and GC

EEG classifier / Patient	WC			H2			H3			H4		
	Class	Channels	Number	Class	Channels	Number	Class	Channels	Number	Class	Channels	Number
JR	A	G4 G5 low amp	44	A	G4-5	33	A	G4 G5 G12 G13	48	A	G4-5	30
	B	G4 G5 high amp	11	B	G4 5 21 22 29 30	19	B	G12 G13	9	B	G4 G5 G12 G13 G21 G22 G29 G30	23
	C	G13 G21 G22 DP2 DP3	33	C	G23 24	5	C	G23 G24	1	C	G13 G21 G22, DP2, DP3	16
	NS		12	D	G21 22	8	D	G21 G22	2	D	G21 G22 G23	8
				E	G14-22	7	E	G4 G5-7 G12 G13 G21 G22 G29 G30	7	E	G20	1
				F	G20	1	F	G13 G20 G21 G22	5	F	G24 G25 G31	1
				G	GA1-2	1	NS		28	NS		21
				H	DP2-DP3 G13 G20-23 G29 34-38 46-48	1						
				NS		25						
MB	A	LAH1	37	A	RA1 RA2 (-ve)	25	A	RA1 RA2	21	A	LAH1-2	35
	B	RA1 RA2 (-ve)	18	B	RA1 RA2 (+ve)	10	B	RA2	8	B	LAH1 LPH1	14
	C	LAH1 LPH1	9	C	LAH1	10	C	LAH1 LPH1	8	C	LPH1	7
	D	RA 1 RA2 RH1	8	D	LPH1(-ve)	3	D	LPH2	3	D	RA1-2	36
	E	RA1 RA2 (+ve)	4	E	LPH1(+ve)	8	E	LAH1	43	E	RA1-2 RH1	2
	NS		24	F	RH1	1	F	LAH2	6	NS		6
				NS		43	NS		11			
GC	A	GA1 GA2 GA10 GA18	63	A	GA1 2 10 18	59	A	GA1 2 10 18	59	A	GA1 2 9 10 17 18	29
	B	SPBT4	16	B	GA1-2 GA9 10 11 18 SPBT5-6	22	B	SPBT4	13	B	GA1 2 10 18	30
	C	GA1 GA2 GA9 GA10 GA11 GA18 SPBT5 SPBT6	21	C	SPBT4	15	C	SPBT4 SAT3 4	3	C	GA1 2 9 10 11 18 SPBT5-6	25
				D	SPBT5-6	2	D	GA 1 2 9 10 11 18 SPBT5-6	25	D	SPBT4	12
				E	GA17-18	2				E	SPBT4 SAT3-4 DH1 DH2	3
										F	SPBT5-6	1

Table A2| Classification overlap (%) between WC classes and classes assigned by H2 [A], H3 [B] and H4 [C] for patient JR. Note: Percentages highlighted in red show the maximum overlap

[A]

WC/H2	A_G4_5	B_G4_5_21_22_29_30	C_G23_24	NS	D_G21_22	E_G14_22	F_G20	G_GA1_2	H_DP2_3_G13_G20_23 G29_G34_38_G46_48
A_G4_5_lowamp	56.82	25.00	2.27	13.64	2.27	0.00	0.00	0.00	0.00
B_G4_5_highamp	54.55	36.36	0.00	9.09	0.00	0.00	0.00	0.00	0.00
C_G13_G21_G22_DP2_3	3.03	12.12	12.12	30.30	18.18	18.18	3.03	0.00	3.03
NS	8.33	0.00	0.00	66.67	8.33	8.33	0.00	8.33	0.00

[B]

WC/H3	A_G4_5_G12_13	B_G12_13	C_G23_24	NS	D_G21_22	E_G4_5_6_7_G12_13_G21_22_ G29_G30	F_G13_G20_21_22
A_G4_5_lowamp	81.82	2.27	0.00	11.36	0.00	4.55	0.00
B_G4_5_highamp	81.82	9.09	0.00	0.00	0.00	9.09	0.00
C_G13_G21_G22_DP2_3	6.06	18.18	3.03	42.42	6.06	9.09	15.15
NS	8.33	8.33	0.00	75.00	0.00	8.33	0.00

[C]

WC/H4	A_G4_5	B_G4_5_G12_13_G21_22_G29_30	C_G13_G21_G22_DP2_3	NS	D_G21_22_23	E_G20	F_G24_25_G31
A_G4_5_lowamp	52.27	36.36	2.27	6.82	2.27	0.00	0.00
B_G4_5_highamp	36.36	45.45	0.00	18.18	0.00	0.00	0.00
C_G13_G21_G22_DP2_3	3.03	3.03	39.39	33.33	15.15	3.03	3.03
NS	16.67	8.33	16.67	41.67	16.67	0.00	0.00

Table A3| Classification overlap between WC classes and classes assigned by H2 [A], H3 [B] and H4 [C] for patient IH. Note: Percentages highlighted in red show the maximum overlap

[A]

WC/H2	A_DA4_5	NS
A_DA4_5	70.59	29.41
B_DA4_5_GA51	88.00	12.00
NS	54.17	45.83

[B]

WC/H3	A_DA4_5	NS
A_DA4_5	94.12	5.88
B_DA4_5_GA51	100.00	0.00
NS	45.83	54.17

[C]

WC/H4	A_DA4_5	B_DA4_5_GA51_52	C_DA4_5_GA43_GA51	D_GA51_52	NS
A_DA4_5	78.43	7.84	9.80	0.00	3.92
B_DA4_5_GA51	4.00	48.00	48.00	0.00	0.00
NS	16.67	8.33	20.83	4.17	50.00

Table A4| Classification overlap between WC classes and classes assigned by H2[A], H3 [B] and H4 [C] for patient BS. Note: Percentages highlighted in red show the maximum overlap

[A]

WC/H2	A_PSMA2_3	B_ASMA1_2_PSMA2_3	C_PC1_5
A_PSMA2_3	79.49	17.95	2.56
B_ASMA1_2_PSMA2_3	9.84	90.16	0.00

[B]

WC/H3	B_PSMA2_3	A_ASMA1_2_PSMA2_3	C_PC1_5
A_PSMA2_3	64.10	33.33	2.56
B_ASMA1_2_PSMA2_3	4.92	95.08	0.00

[C]

WC/H4	A_PSMA2_3	A_ASMA1_2_PSMA2_3	C_PC1_5
A_PSMA2_3	64.10	33.33	2.56
B_ASMA1_2_PSMA2_3	9.84	90.16	0.00

Table A5| Classification overlap between WC classes and classes assigned by H2 [A], H3 [B] and H4 [C] for patient MB. Note: Percentages highlighted in red show the maximum overlap

[A]

WC/H2	C_LAH1	A_RA1_2(-ve)	D_LPH1(-ve)	F_RH1	B_RA1_2(+ve)	E_LPH1(+ve)	NS
A_LAH1	8.11	0.00	0.00	0.00	0.00	2.70	**89.19**
B_RA1_2(-ve)	0.00	**88.89**	0.00	0.00	5.56	0.00	5.56
C_LAH1_LPH1	33.33	0.00	0.00	0.00	0.00	11.11	**55.56**
D_RA1_2_RH1	0.00	**87.50**	0.00	0.00	12.50	0.00	0.00
E_RA1_2(+ve)	0.00	0.00	0.00	0.00	**100.00**	0.00	0.00
NS	16.67	8.33	12.50	4.17	16.67	**25.00**	16.67

[B]

WC/H3	E_LAH1	A_RA1_2	C_LAH1_LPH1	F_LAH2	B_RA2	D_LPH2	NS
A_LAH1	**100.00**	0.00	0.00	0.00	0.00	0.00	0.00
B_RA1_2(-ve)	0.00	**83.33**	0.00	0.00	0.00	0.00	16.67
C_LAH1_LPH1	33.33	0.00	**55.56**	0.00	0.00	0.00	11.11
D_RA1_2_RH1	0.00	**62.50**	0.00	0.00	0.00	0.00	37.50
E_RA1_2(+ve)	0.00	0.00	0.00	0.00	**100.00**	0.00	0.00
NS	12.50	4.17	12.50	**25.00**	16.67	12.50	16.67

[C]

WC/H4	A_LAH1_2	D_RA1_2	B_LAH1_LPH1	E_RA1_2_RH1	C_LPH1	NS
A_LAH1	**86.49**	0.00	0.00	0.00	0.00	13.51
B_RA1_2(-ve)	0.00	**94.44**	0.00	0.00	0.00	5.56
C_LAH1_LPH1	0.00	0.00	**66.67**	0.00	33.33	0.00
D_RA1_2_RH1	0.00	**100.00**	0.00	0.00	0.00	0.00
E_RA1_2(+ve)	0.00	**75.00**	0.00	25.00	0.00	0.00
NS	12.50	**33.33**	33.33	4.17	16.67	0.00

Table A6| Classification overlap (%) between WC classes and classes assigned by H2 [A], H3 [B] and H4 [C] for patient GC. Note: Percentages highlighted in red show the maximum overlap

[A]

WC/H2	A_GA1_GA2_GA10_GA18	C_SPBT4	B_GA1_2_GA9_GA10_GA11_GA18_SPBT5_6	D_SPBT5_6	E_GA17_18
A_GA1_GA2_GA10_GA18	85.71	0.00	9.52	1.59	3.17
B_SPBT4	0.00	93.75	0.00	6.25	0.00
C_GA1_2_GA9_GA10_GA11_GA18_SPBT5_6	23.81	0.00	76.19	0.00	0.00

[B]

WC/H3	A_GA1_GA2_GA10_GA18	B_SPBT4	D_GA1_2_GA9_GA10_GA11_GA18_SPBT5_6	C_SPBT4_SAT3_4
A_GA1_GA2_GA10_GA18	90.48	0.00	9.52	0.00
B_SPBT4	0.00	81.25	0.00	18.75
C_GA1_2_GA9_GA10_GA11_GA18_SPBT5_6	9.52	0.00	90.48	0.00

[C]

WC/H4	B_GA1_GA2_GA10_GA18	D_SPBT4	C_GA1_2_GA9_GA10_GA11_GA18_SPBT5_6	A_GA1_GA2_GA9_GA10_GA17_GA18	E_SPBT4_SAT3_4_DH1_2	F_SPBT5_6
A_GA1_GA2_GA10_GA18	47.62	0.00	11.11	41.27	0.00	0.00
B_SPBT4	0.00	75.00	0.00	0.00	18.75	6.25
C_GA1_2_GA9_GA10_GA11_GA18_SPBT5_6	0.00	0.00	85.71	14.29	0.00	0.00

Table A7| Summary of the inter-rater agreement for all H pairs. Note: Kappa values in bold indicate a good (k>0.4) inter-rater agreement. N: number of IEDs marked by both classifiers within a pair, k: the Cohen's Kappa value

	H2-H3		H2-H4		H3-H4	
Patient	N	κ	N	κ	N	κ
JR	62	**0.41**	68	**0.493**	63	0.329
IH	58	0.207	73	**0.567**	67	**0.412**
BS	100	**1.00**	100	**1.00**	100	**1.00**
MB	49	-0.078	56	0.11	83	-0.084
GC	100	**1.00**	100	**1.00**	100	**1.00**
Mean		**0.51**		**0.63**		**0.53**

Appendix B

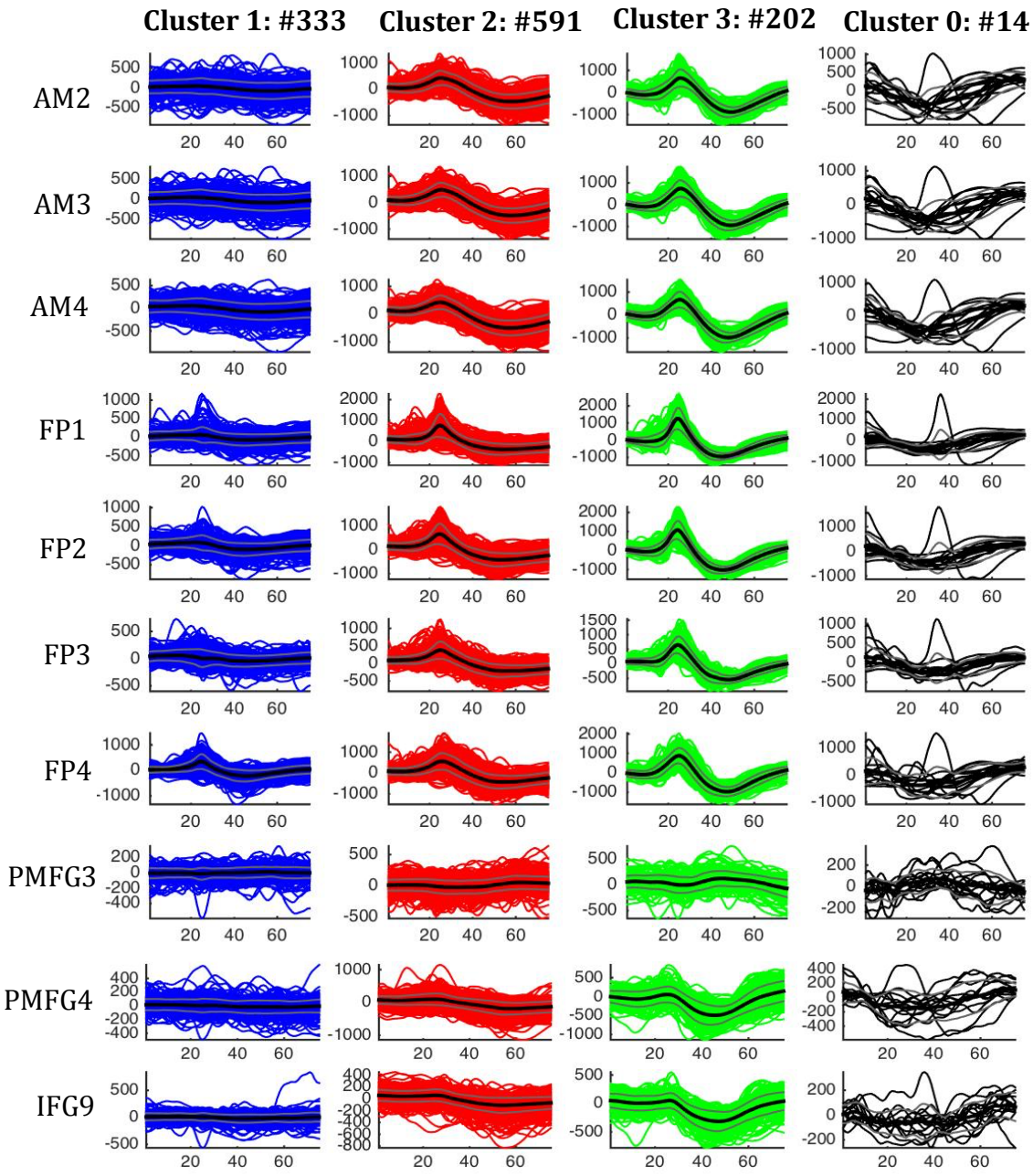

Figure B- 1| WC classification for patient SH. Cluster 1 and 2 are IZ1 spikes and cluster 3 is IZ2 spikes. Cluster 0 are events that were not assigned a class

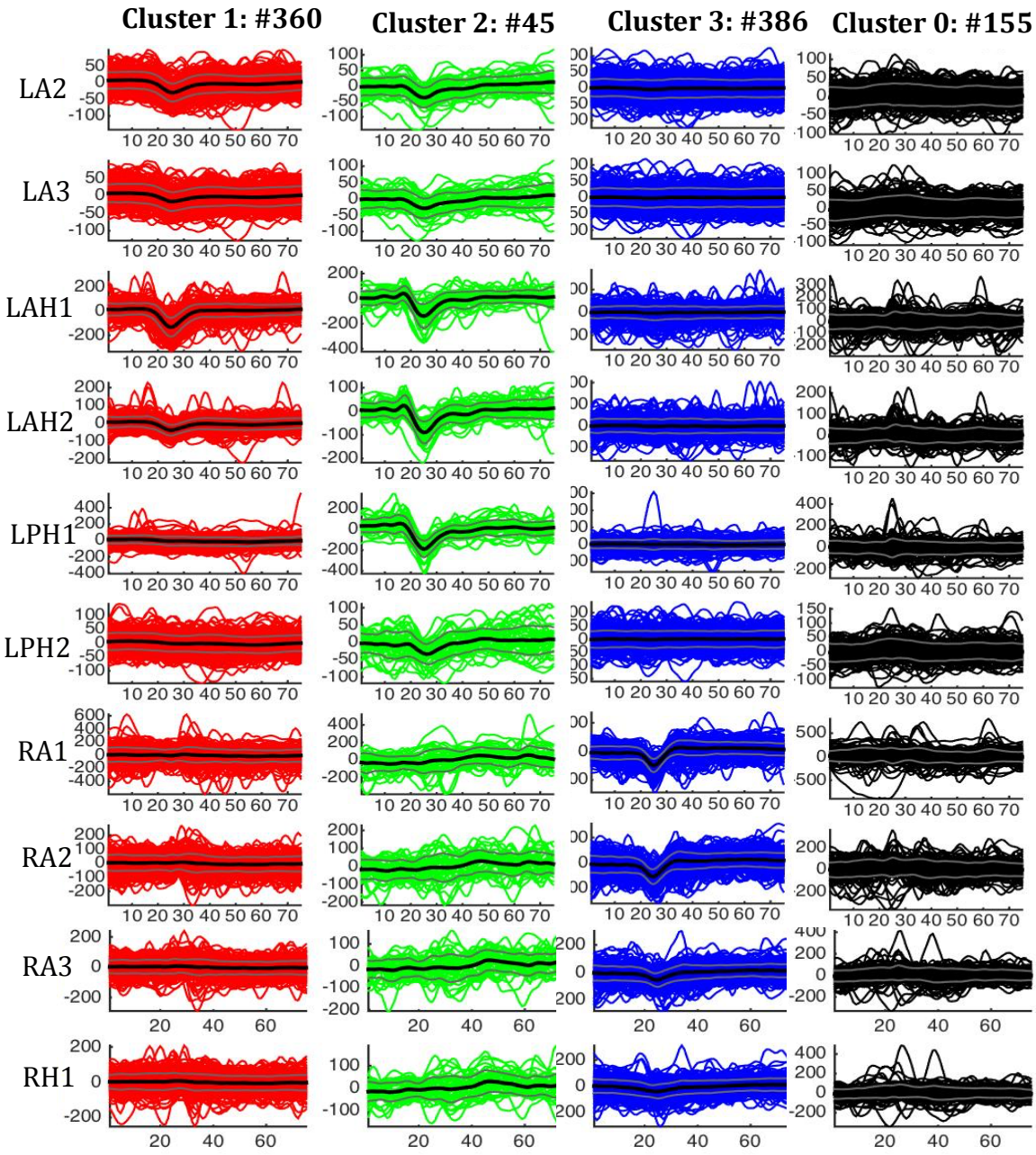

Figure B- 2| WC classification for patient MB. Cluster 1 and 2 are IZ1 spikes and cluster 3 is an IZ2 spike. Cluster 0 are the events that were not assigned a class.

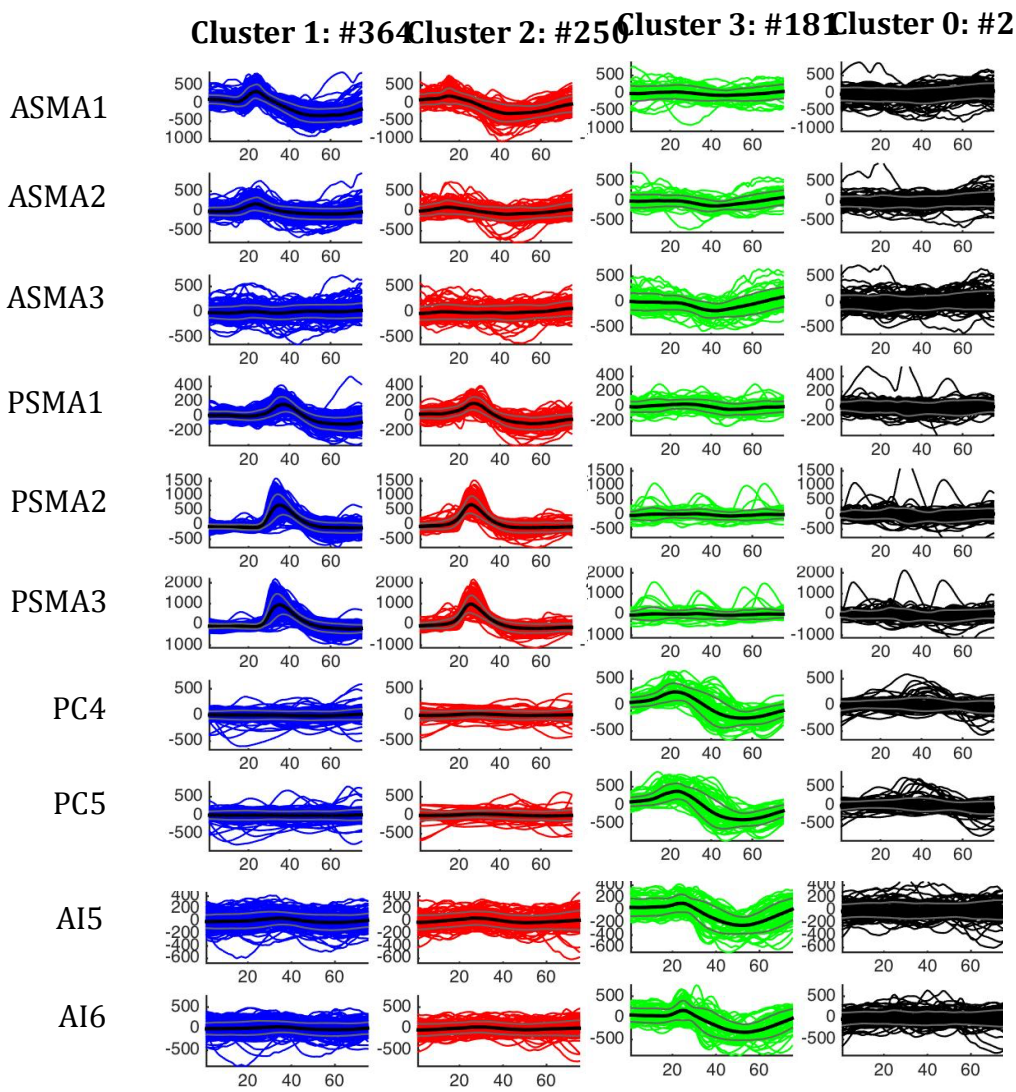

Figure B- 3| WC classification for patient BS. Cluster 1 and 2 are IZ1 spikes and cluster 3 is an IZ2 spike. Cluster 0 are the events that were not assigned a class.

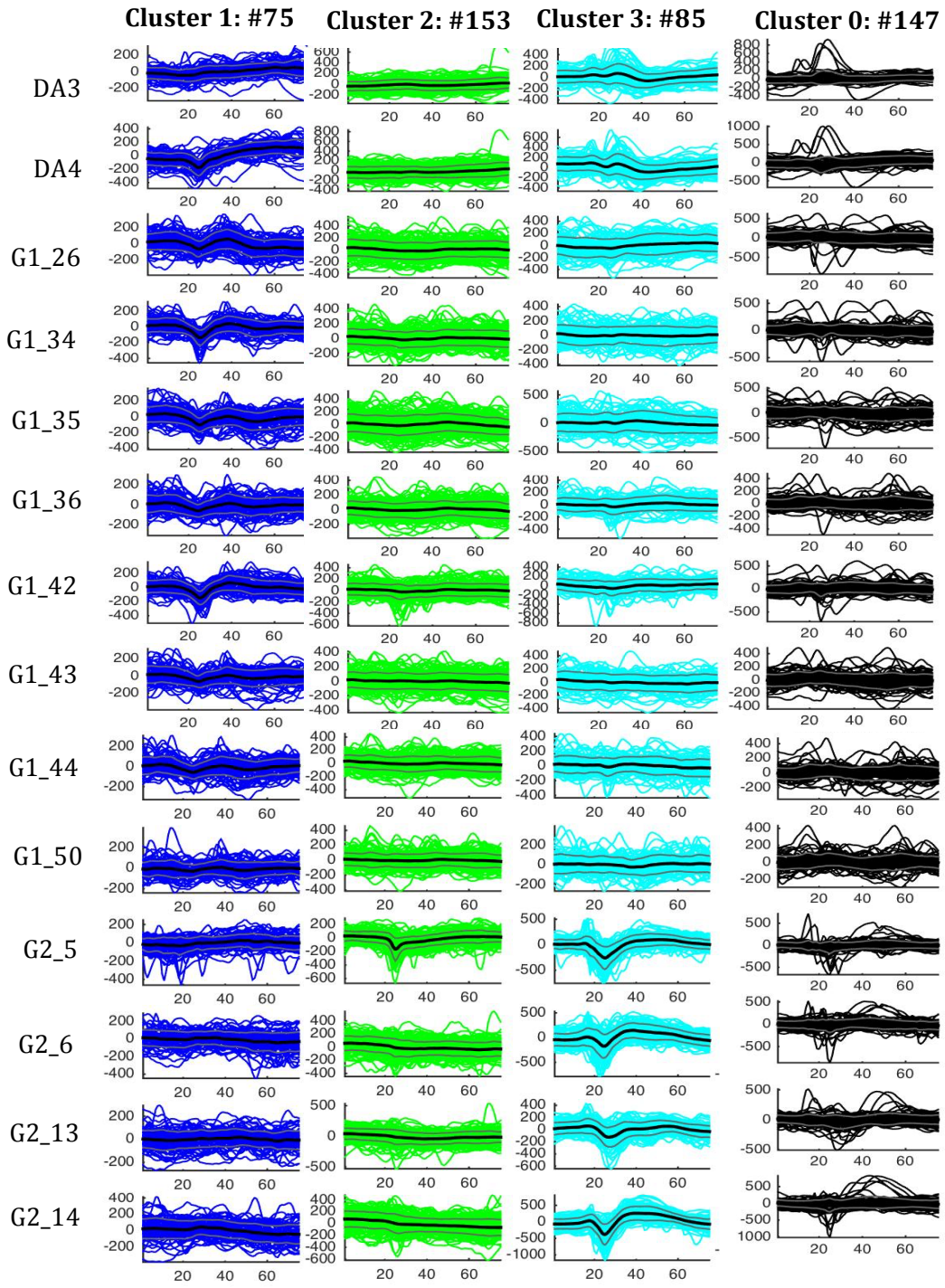

Figure B- 4| WC classification for patient HD. Cluster 1 was an IZ1 spike. Cluster 2 and 3 were IZ2 spikes. Cluster 0 are events that were not assigned a class.

Table B1| Summary of all classes obtained from visual and automated classification for all patients

	Visual Classification			EEG pattern						WC Classification			EEG pattern				
Patient	IED Class	Number	Total IEDs	SED	CED	PFA	IZ	IED Field Distribution	Patient	IED Class	Number	Total IEDs	SED	CED	PFA	IZ	IED Field Distribution
JR	G4,5	70	590	*			1	Focal	JR	G23	127	488	*			1	Focal
	G12-15	30		*			1	Focal		G4_5_13_21_29_DP2_3	131		*			1	Regional
	G4-6 + G12,13 +G22-24 + G28-30	60		*			1	Regional		G4_5_29	78		*			1	NC
	G12-15 + G21-24 + DP2-4	218		*			1	Regional		G13_20_21_DP2_3	152		*			1	Focal
	G4-8 +G12-15 + G20-24 + G28-30 + DP2-4	212		*			1	Widespread	IH	D4_5	498	760		*		1	Focal
IH	DA3-6	423	892		*		1	Focal		D4_5_GA50_51_52	106		*			1	Regional
	DA4,5 + GA51	261		*			1	Focal		D4_5_GA51	156		*			1	Focal
	DA2-6 + GA49-54	208		*			1	Regional	HD	DA3_4	770	1083		*		1	Focal
HD	DA3, 4	770	1035		*		1	Focal		DA3_4_G1	75		*			1	Focal
	DA3, 4 + G1 18,27,35,43	265		*			1	Regional		G2_5	153		*			2	Focal
	G2 6,14	195		*			2	Focal		G2_5_6_14_15	85		*			2	Focal
MB	LAH1, 2 + LPH1, 2 + LA3,4	60	1216	*			1	Regional	MB	RA1_2	549	1062	*			2	Focal
	LAH1-2	359		*			1	Focal		LA2_LAH1_2	360		*			1	Focal
	LA3-4	57		*			1	Focal		LAH1_2_LPH1	112		*			1	Focal
	LPH1-2	96		*			1	Focal		RA1-2 RH1 LH1-2-LPH1 (only poly)	41		*			2	NC
	RA1, 2 + RH1,2	634		*			2	Focal	SH	FP4	333	1126	*			1	Focal
	RA1, 2 + RAH1,2 +LAH2,3 + LPH2,3	10		*			2	NC		AM2-4 + FP1-4	591		*			1	Regional
SH	FP2-4	142	1140	*			1	Focal		AM2-4 + FP1-4 + PMFG 3-4 + IFG9	202		*			2	NC
	FP2-4 + AM2-4	81		*			1	Regional	BS	ASMA1-2 + PSMA 2-3	364	795	*			1	Focal
	AM2-4 + FP1-4 + PMFG3-6 + IFG9-11	203		*			2	NC		PSMA 2-3	250		*			1	Focal
	AM1-4 + FP3-4 + AM1-14 + ASMA2-5 + PMFG3-10 + IFG5-10	296		*			2	NC		PC4-5 + AI5-6	181		*			2	NC
	FP1-4 + AM1-6 + AM1-14 + FOF1-10 + ASMA2-	418		*			2	NC	CB	SF5-7 + GB4-7	68	277	*			1	NC

	7 + PMFG4-12 + IFG5-11																
BS	PSMA1-3	211	1033	*			1	Focal		SF6_7	177		*			1	Focal
	ASMA1-3	46		*			1	Focal		SF8	32		*			1	Focal
	ASMA1-3 + PSMA1-3	476		*			1	Regional	JN	D2_3_4	2481	3246		*		1	Focal
	PC5,6	150		*			2	Focal		G38-39-40-46-47	256		*			1	Regional
	PC5,6 + AI5,6	150		*			2	NC		D1_3_4 G37-38-39	184		*			1	Regional
CB	SF5-7	168	755	*			1	Focal		D1_3_4	75		*			1	Focal
	GB4-6 + 14-16	90		*			1	Regional		G45-46	128		*			1	Focal
	GC5-16	474		*			1	Regional		D1_3_4 G22_23_29_30_31_37_38	66		*			1	Regional
	SF5-7 + GB5-8 + GC5, 10,11,12,15,16	23		*			1	NC		D1_3_4 G22_23_30_31_38_39_40	56				*	1	Widespread
JN	D1	43	3567	*			1	Focal									
	D2	2481			*		1	Focal									
	G23	83		*			1	Focal									
	G31	72		*			1	Focal									
	G36	209		*			1	Focal									
	G38	226		*			1	Focal									
	G44	140		*			1	Focal									
	G45	127		*			1	Focal									
	G47	124		*			1	Focal									
	D1_3_4 G22_23_30_31_38_39_40	62				*	1	Widespread									

Table B2| GLM1: IcEEG and IED-related BOLD summary for IZ1spikes for all patients

			Summary of BOLD in EZ				
Patient	**IED Class**	**Concordance**	**No. of Voxels in EZ**	**Max z-score in EZ**	**HRF sign of peak change**	**GM location**	**BOLD in other location(s)**
JR	G4,5	Y	19	4.21	neg	R H	R Cer, P=t, O, P T, S Par L IFG
	G12-15	Y	51	4.9	neg	M O	R SMA, M Par, S Par, IFG, P T, I Par, R T pole L IFG, P T
	G4-6 + G12, 13 +G22-24 + G28-30	Y	9	4.19	neg	L IFG	R Cer, S Par, IFG, H L, H, C, P-T
	G12-15 + G21-24 + DP2-4	Y*	32	5.01	neg	---	L SMA, P-T, IFG R S Par
	G4-8 +G12-15 + G20-24 + G28-30 + DP2-4	Y*	91	4.5	pos	---	R SFG, P-T, O, H, IFG L, O
IH	DA3-6	Y	34	4.05	pos	R P-T	R I Par, IFG, H, O, MFG P CC L T pole, O, P-T, H, S Par
	DA4, 5 + GA51	N	-	-		L M O	R M Par, T pole L H, P-T, M PFC, M Par
	DA2-6 + GA49-54	Y	8	4.21	neg	R I Par	R F-T, H, P T, T pole L P T
HD	DA3, 4 (770)	N	-	-		R O	R P T, P CC L Thal
	DA3, 4 + G1 18,27,35,43 (265)	Y*	29	4.67		---	---
MB	LAH1, 2 + LPH1, 2 + LA3,4	Y	133	4.83	pos	L O	R IFG, SFG, MFG, P T, O, I Par, S Par L IFG, SFG, I Par, P T, SMA, P CC, M O
	LH1-2	Y	330	5.2	pos	L O	R, IFG, PFC, H, O, S Par, I Par, M Par L MFG, M Par, SMA, S Par, CC, PFC
	LA3-4	N	-	-		R SFG	R MFG, H, F-T, Cer, M Par, L IFG, S Par
	LP1-2	N	-	-		L OFC	---
SH	FP2-4	Y	27	3.98	neg	R M O	R H, MFG, O, Thal, A CC, IFG, I Par, S Par, L, H, T pole, S Par, T pole, MFG, IFG, P T

	FP2-4 + AM2-4	N	-	-		R M O	R M O, I Par, M Par, MFG, Cer, SFG L M O, OFC, M Par
BS	PSMA1-3	Y	21	4.01	neg	L OFC	L MFG
	ASMA1-3	Y	231	6.11	neg	R IFG	R I Par, P T L T pole, S Par, IFG, MFG
	ASMA1-3 + PSMA1-3	Y	32	3.8	pos	R F-T	R M Par L O, P T, F-T, M O
CB	SF5-7	N	-	-		L P T	R P T, OFC, P CC
	GB4-6 + 14-16	Y	5	3.51	pos	L M O	R OFC, IFG, P T, M O, S Par, MFG, SFG, A CC SMA L P T, M P
	GC5-16	Y	7	3.55	neg	R OFC	R I Par, Thal, SFG, CC L T pole, P T
	SF5-7 + GB5-8 + GC5,10,11,12,15,16	Y	6	3.28	neg	L M O	R IFG, M Par, O L S Par, M O, SMA, IFG
JN	D1	Y	124	3.88	neg	R IFG	R M O, SFG, MFG, P T
	D2	Y*	200	5.19	pos	---	R T pole, O L IFG, I Par, P T, SMA, Thal, O
	G23	Y	56	5	neg	R IFG	R PFC, SFG, SMA, OFC, M O, P T, I Par L O, MFG, OFC
	G31	Y	6	3.5	pos	R P T	R M PFC L I Par, OFC, S Par
	G36	Y	122	5.09	pos	R IFG	R M O, T Pole L IFG, S Par, SMA, IFG, I par, S par, thal
	G38	Y*	451	5.37	neg	---	R PFC, MFG, SMA, SFG L, IFG, PFC, I Par, M Par, CC
	G44	N	-	-		L MFG	R H, P CC L P T, F-T
	G45	Y	46	4.16	pos	R M PFC	R M O, IFG L, I Par, H, P T, F-T, SFG, I Par
	G47	N	-	-		L PFC	R MFG, OFC L I Par, M Par, T pole, IFG

Abbreviations| L, left; R, right; H, Hippocampus; A, anterior; P, posterior; Par, parietal; P-T, parieto-temporal; Cer, Cerebellum; O, occipital; SMA, supplementary motor area; IFG, inferior frontal gyrus; MFG, middle frontal gyrus; SFG, superior frontal gyrus; M, mesial; CC, cingulate cortex; PFC, prefrontal cortex; S, superior; I, inferior; T, temporal; T-O temporo-occipital; F-T, fronto-temporal; C, caudate; Thal, Thalamus; OFC, orbitofrontal cortex; GM, global maximum; * = BOLD cluster in EZ is the global maximum

Table B3| GLM2: IcEEG and IED-related BOLD summary for IZ1spikes for all patients

			Summary of BOLD in EZ				
Patient	**IED Class**	**Concordance**	**No. of Voxels in EZ**	**Max z-score in EZ**	**HRF sign of peak change**	**GM location**	**BOLD in other location(s)**
JR	G23	Y	180	5.79	neg	R O	R Par L F Pole, T-P, O
	G4_5_21_29_DP2-3	Y	10	3.82	pos	L P T	R T, O
	G4_5_29	Y*	19	4.05	pos	---	R T, MFG
	G13_20_21_DP2-3	Y	7	3.95	pos	L H	R H, O L, O, P T
IH	D4_5	Y	5	3.56	neg	R P T	R H, SFG, OFC, F Pole L T pole, SFG, Thal, S Par
	D4_5_GA49_51	N	-	-	-	L H	R F-T, S Par L H, P T
	D4_5_GA51	Y	9	3.72	pos	R A P	R SMA, T-P, thal, F pole, T pole L P T, IFG
HD	DA3_4	N	-	-	-	P CC	R S Par, F Pole L thal
	DA3_4_G1	N	-	-	-	L P T	R H, S Par L O
MB	LA2_LH1_2	Y	5	3.54	pos	CC	R M Par, MFG, OFC L MFG, IFG, Par, P CC, O
	LH1_2_LP1	Y*	21	4.54	pos	---	R A Par L OFC, M Par, O, SMA, A Par, P CC
SH	FP4	Y	269	5.63	pos	R O	R H, P T, S Par, O, I Par, MFG L IFG, S Par, A T
	AM2-4 + FP1-4	Y	155	4.46	pos	L S Par	R H, P-T, M Par, SFG, T Pole L I Par, T pole, MFG, H, PFC, SFG, IFG
BS	ASMA1-2 + PSMA 2-3	Y	130	4.75	neg	L F pole	R F pole, O, SFG, T, S Par, H, L M Par, MFG, P T, F-T
	PSMA2-3	Y	9	3.59	neg	R P T	L F-T, I Par, SFG
CB	SF5-7 + GB4-7	Y	26	4.02	pos	L O	R O, S Par, SFG, IFG L, F-T, SMA, IFG
	SF6_7	Y	39	4.03	neg	R S Par	R I Par, T-O, SFG, MFG, I Par, T pole, H L PFC, F-T
	SF8	Y	12	3.81	pos	R T pole	R MFG, IFG L S Par, F-T, O P CC

JN	D2_3_4	Y*	180	5.6	pos	---	R F-T, O, A CC, F pole L, T-P, S Par, M Par, P T
	G38-39-40-46-47	Y*	40	4.26	pos	---	R O L OFC, O, M Par
	D1_3_4 G37-38-39	Y	595	5.64	neg	R S Par	R F pole, IFG, SFG, T pole, H, P CC, SMA L F-T, IFG, T pole, T-O
	D1_3_4	Y*	22	4	pos	---	R S Par L M Par, OFC
	G45-46	N	-	-	-	L S Par	R OFC, F-T L M Par, F-T, CC, SMA
	D1_3_4 G22_23_29_30_31_37_38	Y	613	5.39	neg	R F-T	R P T, L T-P, M Par, MFG, SFG

Abbreviations| L, left; R, right; H, Hippocampus; A, anterior; P, posterior; Par, parietal; P-T, parieto-temporal; Cer, Cerebellum; O, occipital; SMA, supplementary motor area; IFG, inferior frontal gyrus; MFG, middle frontal gyrus; SFG, superior frontal gyrus; M, mesial; CC, cingulate cortex; PFC, prefrontal cortex; S, superior; I, inferior; T, temporal; T-O temporo-occipital; F-T, fronto-temporal; C, caudate; Thal, Thalamus; OFC, orbitofrontal cortex; GM, global maximum; * = BOLD cluster in EZ is the global

Table B- 4| GLM2: IcEEG and IED-related BOLD summary for IZ2 spikes and fast activity

		Summary of BOLD in EZ			
Patient	**IED Class**	**BOLD in area of resection**	**No. of Voxels Activated in EZ**	**Max z-score in EZ**	**HRF sign of peak change**
HD	G2_5	Y(GM)	11	4	neg
	G2_5_6_14_15	N	-	-	-
MB	RA1_2	Y	5	3.61	neg
	RA1-2 RH1 LH1-2-LP1	Y	18	3.99	pos
SH	AM2-4 + FP1-4 + PMFG 3-4 + IFG9	Y(GM)	330	5.68	neg
BS	PC4-5 + AI5-6	Y	242	6.47	neg
JN	fastactivity D1_3_4 G22_23_30_31_38_39_40	Y(GM)	487		pos

Table B- 5| GLM1: IcEEG and IED-related BOLD summary for IZ2 spikes and fast activity

		Summary of BOLD in EZ			
Patient	**IED Class**	**BOLD in area of resection**	**No. of Voxels Activated in EZ**	**Max z-score in EZ**	**HRF sign of peak change**
HD	G2 6,14	Y	25	4.06	neg
MB	RA1,2 + RH1,2	N	-	-	
	RA1,2 + RAH1,2 +LAH2,3 + LPH2,3	N			
SH	AM2-4 + FP1-4 + PMFG3-6 + IFG9-11	Y	20	3.53	pos
	AM1-4 + FP3-4 + ASMA2-5 + PMFG3-10 + IFG5-10	Y(GM)	200	5.22	pos
	FP1-4 + AM1-6 + FOF1-10 + ASMA2-7 + PMFG4-12 + IFG5-11	N	-	-	
BS	PC4,5	Y	20	3.85	neg
	PC4,5 + AI5,6	Y	23	3.71	neg
JN	fastactivity D1_3_4 G22_23_30_31_38_39_40	Y(GM)			pos